Journal of Inorganic Biochemistry 103 (2009) 1702–1710

Contents lists available at ScienceDirect

Journal of Inorganic Biochemistry

journal homepage: www.elsevier.com/locate/jinorgbio

Studies on the formation of a complex of Cu(II) with sodium 1,4-dihydroxy-9,10-anthraquinone-2-sulphonate – An analogue of the core unit of anthracycline anticancer drugs and its interaction with calf thymus DNA

Partha Sarathi Guin [a,b,2], Saurabh Das [b,1], P.C. Mandal [a,*]

[a] Chemical Sciences Division, Saha Institute of Nuclear Physics, 1/AF-Bidhannagar, Kolkata 700064, India
[b] Department of Chemistry, Jadavpur University, Raja S.C. Mullick Road, Kolkata 700032, India

ARTICLE INFO

Article history:
Received 18 July 2009
Received in revised form 19 September 2009
Accepted 23 September 2009
Available online 29 September 2009

Keywords:
Cu(II)
$NaQSH_2$
Stoichiometry
Stability constant
SEM
MS
Cyclic voltammetry
Calf thymus DNA
Binding parameters

ABSTRACT

Copper(II) forms a complex with sodium 1,4-dihydroxy-9,10-anthraquinone-2-sulphonate (sodium quinizarin-2-sulphonate, $NaQSH_2$), an analogue of the core unit of anthracycline antibiotics used in the treatment of cancer. The 1:2 metal–ligand complex is formed in aqueous solution at neutral and acidic pH while in alkaline pH both 1:1 and 1:2 species are formed. The effective stability constant of the 1:2 metal–ligand complex is 9.64×10^{16} while that of the 1:1 metal–ligand complex is 9.4×10^{9}. The 1:2 complex $Cu(NaQSH)_2(H_2O)_2$ was synthesized and characterized by different techniques in solid state and in solution. The complex $Cu(NaQSH)_2(H_2O)_2$ interacts with calf thymus DNA which was studied by fluorescence spectroscopy. The binding constant and site size for the interaction with DNA were determined.

1. Introduction

Anthracycline drugs adriamycin (doxorubicin), daunorubicin, carminomycin and nogalamycin are the most important therapeutic agents used in the treatment of acute leukemia, malignant lymphomas, solid tumors, particularly in case of breast cancer [1,2]. Studies [3–5] show, by forming strong intercalation complexes with DNA and in some cases by degrading DNA [6,7], anthracyclines inhibit DNA replication and RNA transcription [8]. However, their cardiotoxic property [9–12] binds the limit of their use. Cardiotoxicity is associated with several electron transfer processes involving the respiratory chain. The quinone moiety present in these drugs after one electron reduction becomes semiquinone, which plays a major role in determining toxicities of these drugs in cellular systems [13,14]. Complex formation with metal ions decrease toxicity of these drugs and this has been a route to modify the quinone moiety, which is the seat of all chemical reactions. A number of metal complexes of anthracyclines have been tried for treatment of cancer and their use has aroused a growing interest on the role of metal ions in such compounds [3,5,15,16]. Since metal ions are good binding agents for cellular target DNA, complex formation would result in better DNA targeting by such molecules, at the same time lead to the formation of a less cardiotoxic compound [3,17].

Previous studies have shown metal ions Cu(II), Ni(II), Fe(III), Al(III), Pd(II) and Tb(III) form complexes with adriamycin, daunorubicin and a few of their analogues [1–3,15–28]. Depending upon the pH of the reaction media Cu(II) forms both 1:1 and 1:2 complexes with adriamycin and daunorubicin simultaneously or separately [15,17,19]. It has been seen that in alkaline media 1:1 Cu(II)-complexes are in the form of a long chain polymer [4,18,19]. However, structural information on metal anthracycline or metal-dihydroxy anthraquinone (the core unit of such anthracyclines) is still lacking due to inherent difficulties in obtaining suitable single crystal for X-ray diffraction studies. Only crystal structures of a few free anthracyclines [29–31] and only one metal complex of terbium(III) with sodium 1,4-dihydroxy-9,10-anthraquinone-2-sulphonate (sodium quinizarin-2-sulphonate) are

* Corresponding author. Tel.: +91 33 23375345; fax: +91 33 23374637.
E-mail addresses: dasrsv@yahoo.in (S. Das), pc.mandal@saha.ac.in (P.C. Mandal).
[1] Tel.: +91 33 24146643; fax: +91 33 24146223.
[2] Present address: Department of Chemistry, Shibpur Dinobundhoo Institution (College), 412/1 G. T. Road (South), Howrah 711 102, WB, India.

0162-0134/$ - see front matter © 2009 Elsevier Inc. All rights reserved.
doi:10.1016/j.jinorgbio.2009.09.020

reported [28]. We tried in the past to understand the chemistry involved at the anthraquinone site of these drug molecules [32–35] and have now made an attempt using sodium 1,4-dihydroxy-9,10-anthraquinone-2-sulphonate, having similar binding sites to adriamycin and daunorubicin. Furthermore, sodium 1,4-dihydroxy-9,10-anthraquinone-2-sulphonate and its 1:2 Cu(II) complex are soluble in water and may find use under physiological conditions which is important for drug action. We recently showed that sodium 1,4-dihydroxy-9,10-anthraquinone-2-sulphonate has similar electrochemical behavior in aqueous and non aqueous solvent like that of other anthracycline antibiotics [36]. The reduction in the formation of superoxide by the formation of metal complexes of anthracyclines was verified by our group using 1,2-dihydroxy-9,10-anthraquinone and its Cu(II), Ni(II) and Fe(III) complexes in similar enzymatic studies [32,37]. Therefore, anthraquinone systems mimic anthracyclines, a fact that encourages us to look for more similarity in biochemical behavior using sodium 1,4-dihydroxy-9,10-anthraquinone-2-sulphonate and its Cu(II) complex.

The investigation of drug-DNA interaction is important to understand molecular mechanisms of drug action and designing specific DNA-targeted drugs. Fluorescence method was used to analyze binding of the compound to calf thymus DNA that enabled us to calculate the binding constant and site size. A model study such as this is also able to predict the role played by different chemical units such as the sugar [38] present with the side chain of anthracyclines in binding to DNA.

2. Experimental

2.1. Materials

The compound 1,4-dihydroxy-9,10-anthraquinone (96%) was purchased from Sigma Aldrich, USA, and purified by recrystalization from an ethanol–water mixture. Sodium 1,4-dihydroxy-9,10-anthraquinone-2-sulphonate was prepared by sulphonation of 1,4-dihydroxy-9,10-anthraquinone with aqueous sodium sulphite in presence of cupric oxide [24]. The compound thus obtained was recrystalized from an ethanol–water mixture. Elemental analysis was carried out on 2400 SERIES II CHN ANALYSER, Perkin–Elmer. Elemental analysis showed contents of C and H as 49.20 and 2.01 wt.%, respectively (calcd. C: 49.12% and H: 2.05%). ^{1}H NMR of the prepared compound was done in D_2O solvent on a Bruker Avance 300 NMR spectrometer using Tetramethyl Silane (TMS) as internal standard. The response of phenolic-OH protons were obtained at the characteristic region of 4.76–4.57 ppm. Aromatic protons were obtained at 7.46, 7.67, 7.88 ppm (figure not shown).

The quinone moiety being sensitive to light solutions were prepared just before experiment and kept in the dark. Concentrations of experimental solutions used were of the order of 10^{-5} M. Analytical grade $CuSO_4{\cdot}5H_2O$ was used to prepare standard Cu(II) solutions. Analytical grade Hepes buffer (N-2-hydroxyethylpiperazine-N-2-ethane-sulphonic acid, 0.02 M) (Specrochem Pvt. Ltd., India) and Britton Robinson buffer (0.02 M) were used to maintain pH. Sodium chloride of analytical grade was used to maintain ionic strength. All other reagents used were of AR grade. Microprocessor pH/ION Meter (pMX 3000) was used for checking pH values of solutions. All solutions were prepared in triple distilled water.

2.2. Methods

The p*K* values of sodium 1,4-dihydroxy-9,10-anthraquinone-2-sulphonate were determined by spectrometric titration. The solution of sodium 1,4-dihydroxy-9,10-anthraquinone-2-sulphonate was slowly titrated with 0.01 M NaOH keeping its concentration unchanged. Complex formation of Cu(II) with the ligand sodium 1,4-dihydroxy-9,10-anthraquinone-2-sulphonate was monitored using absorption and fluorescence spectroscopy. UV–Visible (UV–Vis) spectroscopic studies were carried out using a spectrophotometer (model UNICAM UV 500). A pair of 10×10 mm path length quartz cuvette was used for absorption experiments. Fluorescence spectroscopic measurements were carried out using a fluorimeter (model JOBIN YVON Fluoro Max 3). A 10×10 mm fluorescence cuvette was used for measurements. Scanning electron microscopy (SEM) imaging was done using FEI Quanta 200F Schottky field emission gun (FEG) microscopy. To avoid charging, imaging was done in low vacuum mode at 0.64 Torr operated at 10 kV. Magnetic moment was measured on a vibratory sample magnetometer. FTIR analysis was performed on a Perkin–Elmer RX-I spectrophotometer. The spectra of KBr pellets were recorded in the range 400–4000 cm^{-1}. Mass spectrum was recorded on Micromass Q-Tof micro™, Waters Corporation. Cyclic voltammetry experiments were carried out using the conventional three-electrode system at 25 °C. The temperature was maintained at 25 °C using a circulating water bath. A platinum electrode of surface area 0.1257 cm^2 served as the working electrode, a platinum wire acted as the counter electrode while Ag/AgCl in saturated KCl was the reference electrode. Experiments were done using *EG* & *G* Potentiostat Model 263A. All experimental solutions were degassed for 30 min with high- purity argon gas before any voltammetry experiment was done. Highly polymerized calf thymus DNA (CT DNA) was purchased from Sisco Research Laboratories Pvt. Ltd., India and after dissolution in buffer purity was checked from the absorbance ratio A_{260}/A_{280}. For all the solutions the absorption ratio was in the range $1.8 < A_{260}/A_{280} < 1.9$. Therefore, no further deproteinization of the DNA was required. Concentration of DNA in terms of nucleotide was determined taking $\varepsilon_{260} = 6600\ M^{-1}cm^{-1}$ per base for calf thymus DNA. In all the experiments, DNA concentration has been expressed in terms of base.

3. Results and discussions

3.1. p*K* values of sodium 1,4-dihydroxy-9,10-anthraquinone-2-sulphonate

Absorption spectra of sodium 1,4-dihydroxy-9,10-anthraquinone-2-sulphonate at various pH values were recorded. It was found that after pH 7.0 the intensity of the peak of the molecule at 465 nm decreased and a new peak at 580 nm appeared whose intensity increases with an increase in pH. Change in absorbance at 580 nm indicates release of the first phenolic proton in the pH range 8–10 while the second phenolic proton is released in the pH range 11–13.

Sodium 1,4-dihydroxy-9,10-anthraquinone-2-sulphonate ($NaQSH_2$) exists in aqueous solution in three distinct forms depending on the pH of the solution. At acidic and neutral pH, the solution is yellowish orange, it is blue violet in dilute alkali and deep blue in strongly alkaline solution representing neutral ($NaQSH_2$), anionic ($NaQSH^-$) and dianionic ($NaQS^{2-}$) states, respectively.

$$NaQSH_2 \rightleftharpoons H^+ + NaQSH^-$$

$$K_1 = \frac{[H^+][NaQSH^-]}{[NaQSH_2]} \quad (1)$$

$$NaQSH^- \rightleftharpoons H^+ + NaQS^{2-}$$

$$K_2 = \frac{[H^+][NaQS^{2-}]}{[NaQSH^-]} \quad (2)$$

Proton dissociation constants K_1 and K_2, were calculated from the change in absorbance of the compound at 580 nm in the pH range 3–13. The observed absorbance, A_{obs}, at 580 nm would be given by

$$A_{obs} = \frac{A_1}{1 + 10^{(pH-pK_1)} + 10^{(pH-pK_2)}} + \frac{A_2}{1 + 10^{(pK_1-pH)} + 10^{(pH-pK_2)}} + \frac{A_3}{1 + 10^{(pK_1-pH)} + 10^{(pK_2-pH)}} \quad (3)$$

where A_1, A_2 and A_3 are the absorbances corresponding to the forms $NaQSH_2$, $NaQSH^-$ and $NaQS^{2-}$, respectively. The measured absorbance at 580 nm versus pH was fitted according to Eq. (3), shown in Fig. 1A. The evaluated pK values are $pK_1 = 9.29 \pm 0.10$ and $pK_2 = 12.14 \pm 0.10$ which are in good agreement with those determined earlier [39].

3.2. Stoichiometry of metal–ligand complexes formed at different pH by different techniques

The absorption spectra of sodium 1,4-dihydroxy-9,10-anthraquinone-2-sulphonate at neutral pH in absence and presence of different amounts of Cu(II) is shown in Fig. 2. From Fig. 2, it is clear that when $CuSO_4$ was added to a solution of the ligand sodium 1,4-dihydroxy-9,10-anthraquinone-2-sulphonate at neutral pH two new peaks at 320 and 560 nm appeared while intensity of ligand peaks at 252 and 465 nm decreased. There are clearly three isosbestic points at 260, 390 and 525 nm. The two peaks at 320 nm and 560 nm are characteristic absorption peaks of the metal complex. The peak at 320 nm is due to a strong charge transfer band that develops in the complex while the one at 560 nm (17857 cm^{-1}) corresponds to d–d transition. The ligand absorption at this wavelength (560 nm) is almost negligible being evident from the spectra obtained for the solution containing only the ligand. This lends support to the fact that the peak at 560 nm is exclusively due to complex formation. As the metal ion concentration increases the peak at this wavelength also increases. In order to determine stoichiometry of the copper complex in solution, a mole-ratio study was performed. Keeping ligand concentration fixed metal concentration was varied from a ratio of 0.15 to 1.25 and vice versa and the absorbance was measured at 560 nm. In the mole-ratio plots two lines were obtained, the intersection of which determines the stoichiometry of the complex in aqueous solution. Fig. 3 (fixed ligand concentration) and Fig. S1 (fixed metal concentration) [Supplementary information data] suggests that the stoichiometry of the complex in solution for metal to ligand is 1:2 at neutral pH.

To determine stoichiometry of complex formation at neutral pH fluorescence spectra of sodium 1,4-dihydroxy-9,10-anthraquinone-2-sulphonate in absence and presence of different amounts of copper(II) were recorded following an excitation at 480 nm. The emission spectrum exhibits a maxima at 590 nm with a shoulder at 545 nm (Fig. S2). From fluorescence study it was found as metal concentration increases in these metal–ligand mixtures

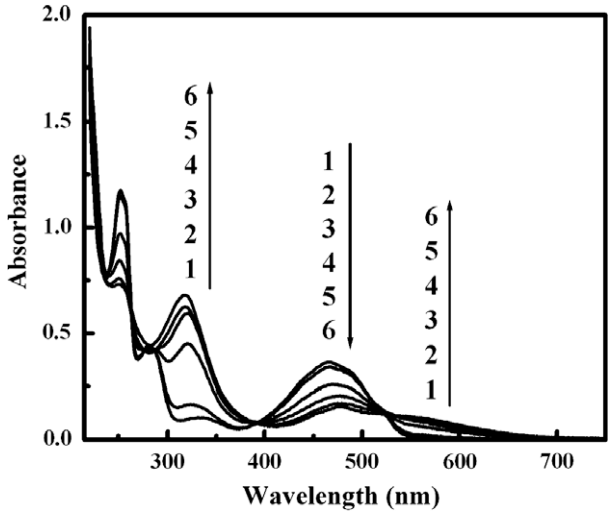

Fig. 2. Absorption spectra of $NaQSH_2$ at different $[Cu^{2+}]/[NaQSH_2]$ ratios: 0.0 (1), 0.25 (2), 0.50 (3), 0.75 (4), 1.00 (5) and 1.25 (6) at a fixed ligand concentration at neutral pH. $[NaQSH_2]$ = 40 μM, [NaCl] = 10 mM, 25 °C.

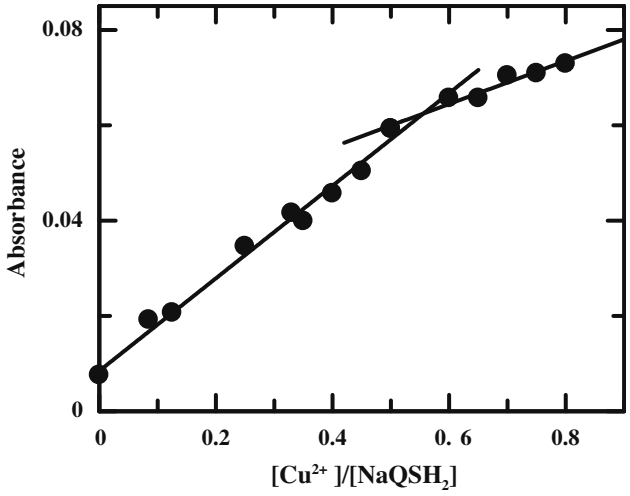

Fig. 3. Mole-ratio plot of absorbance of $[Cu^{2+}]/[NaQSH_2]$ at a fixed ligand concentration at neutral pH; $[NaQSH_2]$ = 40 μM, [NaCl] = 10 mM, 25 °C.

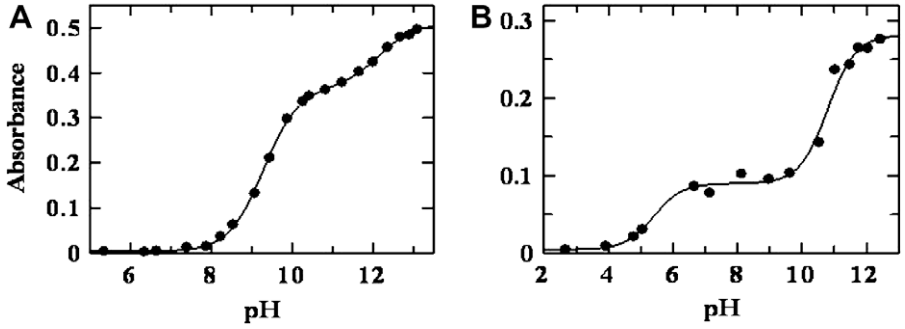

Fig. 1. (A): Spectrophotometric titration of $NaQSH_2$, shown by the variation of absorbance at 580 nm; $[NaQSH_2]$ = 40 μM, [NaCl] = 10 mM, 25 °C; (B): spectrophotometric titration of $NaQSH_2$ in presence of Cu^{2+} as shown by the variation of absorbance at 560 nm; $[NaQSH_2]$ = 40 μM, $[Cu^{2+}]$ = 20 μM, [NaCl] = 10 mM, 25 °C.

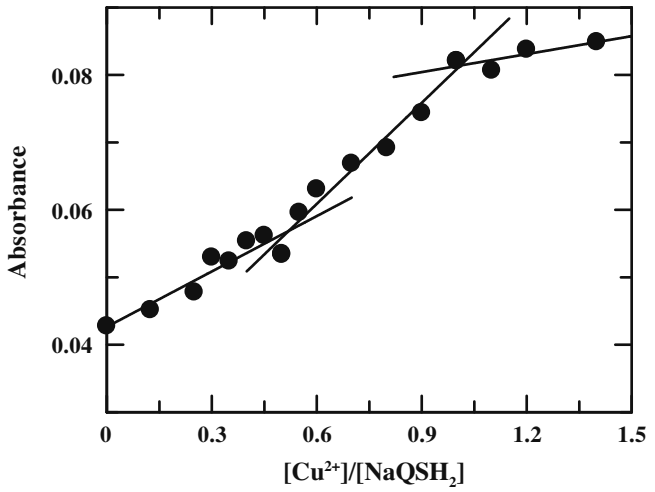

Fig. 4. Mole-ratio plot of absorbance of $[Cu^{2+}]/[NaQSH_2]$ at a fixed ligand concentration at pH 8.5. $[NaQSH_2]$ = 40 μM, [NaCl] = 10 mM, 25 °C.

quenching of fluorescence also increases (Fig. S2). Fluorescence emission intensity at 590 nm decreases as mole-ratio increases with a clear intersection at metal to ligand ratio 1:2 (Fig. S3). Hence fluorescence study also suggests 1:2 metal–ligand complex formation at neutral pH.

To find out whether there is a dependence of pH on the stoichiometry of the complex formed in solution, Cu(II)–ligand complex formations were carried out at different pH (acidic and alkaline). Similar to neutral pH, in acidic and alkaline solutions absorbance was measured at 560 nm and plotted against mole-ratio of reactants. The mole-ratio plots at acidic (pH 6.0) and alkaline pH (pH 8.5) are shown in Figs. S4 and 4, respectively. The plots clearly indicate a 1:2 metal–ligand complex formation at acidic pH and formation of both 1:2 and 1:1 metal–ligand complexes at alkaline pH.

3.3. Determination of formation constants of metal–ligand complexes

In order to determine the formation constants of Cu(II)–$NaQSH_2$ complexes, metal ion and ligand were taken in the molar ratio 1:2 and spectrometric titration was carried out. At first the 1:2 metal to ligand mixture was acidified to pH 3.1 and it was slowly titrated with 0.01 M NaOH keeping metal and ligand concentrations fixed and absorption spectra at various pH values were taken. In such titration it was found that the intensity of the peak at 560 nm gradually increases with an increase in pH, which thereafter becomes constant and a plateau is reached in the pH range 6.7–8.5. Further increase in pH causes an increase in absorbance at that wavelength (Fig. 1B). The absorbance A_{obs} at 560 nm of $NaQSH_2$ in presence of Cu(II) at different pH values were fitted according to Eq. (3) (Fig. 1B). In this case A_1, A_2 and A_3 refer to absorbance of $NaQSH_2$, $NaQSH^-$ and $NaQS^{2-}$, respectively in presence of Cu(II). Fitting the experimental data according to Eq. (3) we obtained values for $pK_1 = 5.40 \pm 0.10$ and $pK_2 = 10.79 \pm 0.10$.

The formation constants β_{II}^* and β_{II} for the 1:2 complex can be described as follows:

$$Cu^{2+} + 2NaQSH_2 \rightleftharpoons Cu(NaQSH)_2 + 2H^+ \quad (4)$$

$$\beta_{II}^* = \frac{[Cu(NaQSH)_2][H^+]^2}{[Cu^{2+}][NaQSH_2]^2} \quad (5)$$

$$Cu^{2+} + 2NaQSH^- \rightleftharpoons Cu(NaQSH)_2 \quad (6)$$

$$\beta_{II} = \frac{[Cu(NaQSH)_2]}{[Cu^{2+}][NaQSH^-]^2} \quad (7)$$

From Eqs. (1), (5), and (7) formation constant β_{II} can be deduced as

$$\beta_{II} = \frac{\beta_{II}^*}{K_1^2} \quad (8)$$

where K_1 is the equilibrium constant for the dissociation of the first proton of $NaQSH_2$ molecule as shown in Eq. (1).

The formation constants β_I^* and β_I for the 1:1 complex can be shown as follows:

$$Cu^{2+} + NaQS^{2-} \rightleftharpoons Cu(NaQS) \quad (9)$$

$$\beta_I = \frac{[Cu(NaQS)]}{[Cu^{2+}][NaQS^{2-}]} \quad (10)$$

$$Cu^{2+} + Cu(NaQSH)_2 \rightleftharpoons 2Cu(NaQS) + 2H^+ \quad (11)$$

$$\beta_I^* = \frac{[Cu(NaQS)]^2[H^+]^2}{[Cu^{2+}][Cu(NaQSH)_2]} \quad (12)$$

Using Eqs. (1), (2), (5), (7), (10), and (12), β_I can be derived as

$$\beta_I = \frac{\sqrt{\beta_I^*\beta_{II}^*}}{K_1K_2} \quad (13)$$

The formation constants β_I^* and β_{II}^* of the 1:1 and 1:2 Cu(II)–$NaQSH_2$ complex were determined from the above spectrometric titration. The formation constants β_I and β_{II} of 1:1 and 1:2 complexes could then be calculated using Eqs. (8) and (13) and they were found to be 9.4×10^9 and 9.64×10^{16}, respectively. The stability constants obtained above for the 1:1 and 1:2 species bear a very close similarity with 1:1 and 1:2 Cu(II)–adriamycin complexes that are $(1.8 \pm 0.7) \times 10^{12}$ and $(4.6 \pm 1.1) \times 10^{16}$, respectively [16] thus indicating similarity in chemical behavior between the metal complexes of Cu(II) formed with the anthracycline drugs and anthraquinones.

3.4. Analysis of the 1:1 Cu(II)–$NaQSH_2$ complex

During the entire investigation on the interaction of sodium 1,4-dihydroxy-9,10-anthraquinone-2-sulphonate with Cu(II), formation of a 1:1 metal–ligand polymeric specie formed a part of the study. When various concentrations of Cu(II) and ligand were used either to prepare the 1:2 complex or to study different physicochemical parameters a very common feature, particularly at alkaline pH has been the tendency of the metal ion and the ligand to form a polymeric specie. The substance that is formed gradually separates out from the solution as a long chain sticky mass. This phenomenon has been prominent at pH beyond 7.5. However, when the concentration of Cu(II) and the ligand is very small ($\sim 10^{-6}$ M) then upon approaching alkaline pH the complex, $Cu(NaQSH)_2$ changes composition from 1:2 to 1:1 and in such a case the new substance remains in solution and does not form a precipitate. The newly formed specie has the probable composition $[Cu_2(NaQS)_2]$ or $[Cu(NaQS)]_2$. We feel strongly that this same specie $Cu_2(NaQS)_2$ or $[Cu(NaQS)]_2$ at higher concentrations of Cu(II) and ligand $NaQSH_2$ is able to form larger aggregates of Cu(NaQS) linked to each other generating $[Cu(NaQS)]_n$ thus creating a polymer but having 1:1 stoichiometry. The polymeric complex of Cu(II) with doubly deprotonated ligand ($NaQS^{2-}$) at alkaline pH were obtained in solid state. This complex is insoluble both in water and in ethanol. The polymeric compound was obtained as a blackish residue. This was washed with water and methanol and dried in air. Scanning electron microscopy (SEM), elemental analysis

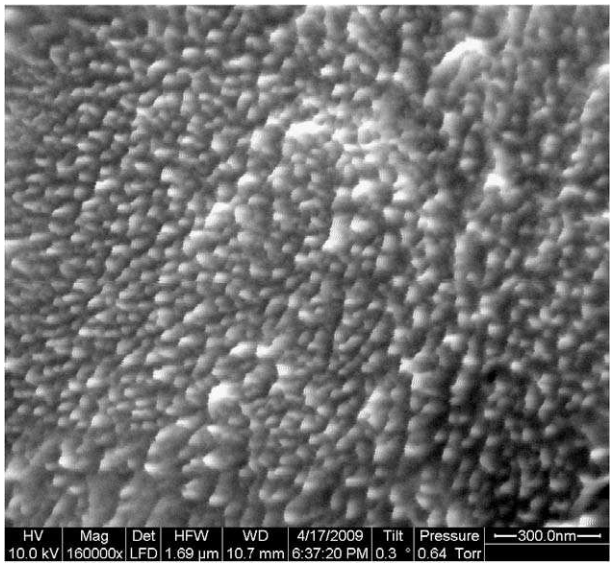

Fig. 5. Scanning electron microscopy (SEM) image of solid 1:1 polymeric specie.

and IR spectroscopy were performed to analyze this complex. At higher magnification (160,000×) SEM image (Fig. 5) of the polymeric compound reveals ball like structure of it having diameter 30 ± 5 nm which is probably due to coiling up of a long polymer chain. Therefore, SEM study clearly shows that the insoluble compound is a polymer.

Elemental analysis of the polymeric substance, provides data for C = 38.53%, H = 2.29%, other elements = 59.18%. The theoretically determined values based on the structural aspect $[Cu(NaQS)(H_2O)_2]_n$ where Cu(NaQS) is the repeat unit gives C = 38.14%, H = 2.27%, other elements = 59.59%. It therefore, clearly indicates that there is a good agreement between experimental results and that of the theoretical structure $[Cu(NaQS)]_n$ with two water molecules per Cu(II).

Fiallo and Gurnier-Suillerot have established that Pd(II) forms a 1:1 complex with adriamycin where both the dimeric specie and the polymeric specie are possible [5]. As copper and palladium are diagonal elements it is seen that tetra coordinated Cu(II) and Pd(II) ions have almost comparable radius, $r_{Cu(II)}$ = 71 pm and $r_{Pd(II)}$ = 78 pm [40]. Therefore, from the standpoint of ionic potential it can be said that Cu(II) would form an identical 1:1 complex with sodium 1,4-dihydroxy-9,10-anthraquinone-2-sulphonate as that formed by Pd(II) with adriamycin.

Similar polymeric species were observed for the studies of Cu(II) with adriamycin, anthraquinones and naphthoquinones at alkaline pH [18,19,25,41,42]. Therefore, by the same analogy it can be said that the complex formed in our study is polymeric in nature. Comparing the structure of the polymeric species of Cu(II) with doubly deprotonated adriamycin ligand [18] and doubly deprotonated 1,4-dihydroxy-9,10-anthraquinone [40] ligand the structure of the polymeric compound can be proposed to be as shown in Scheme 1.

3.5. Preparation and analysis of 1:2 Cu(II)–$NaQSH_2$ complex

The solid 1:2 Cu(II) complex was prepared by mixing $Cu(OH)_2$ and sodium 1,4-dihydroxy-9,10-anthraquinone-2-sulphonate in molar ratio 1:2 in an aqueous medium at neutral pH. The mixture was refluxed for 4 h and the volume was reduced. This was dried in air to obtain a blackish violet mass. The red copper complex was extracted with methanol from the blackish violet mass and precipitated by slow evaporation in air. It was then filtered and recrystallized from a methanol–water mixture. Elemental analysis was carried out using a 2400 SERIES II CHN ANALYSER, Perkin–Elmer. Results indicate that, contents of C and H as 42.06% and 2.09 wt.%, respectively. Theoretical values for carbon and hydrogen based on the composition $Cu(NaQSH)_2(H_2O)_2$ is C: 42.19%, H: 2.05%.

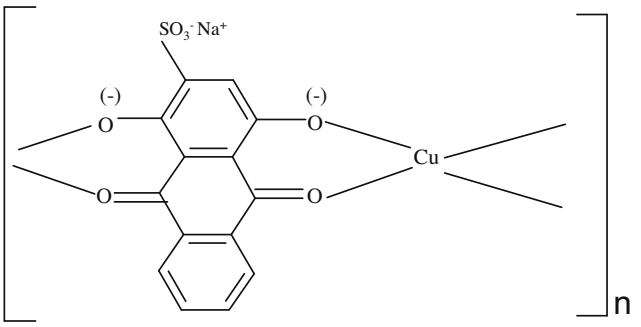

Scheme 1. Proposed structure of 1:1 Cu(II)–$NaQSH_2$ polymeric specie.

Estimations of copper in the 1:2 complex was carried out by methods described in the literature [43]. Experimentally obtained data indicates presence of Cu(II) in the complex as (7.98 ± 0.1)%. Based on the structure $Cu(NaQSH)_2(H_2O)_2$, Cu(II) theoretically should be 8.13%. A magnetic study performed on the prepared solid complex provides molar magnetic susceptibility 1.225×10^{-3} CGS unit from which the magnetic moment (μ) of the complex was found to be 1.736 BM indicating the complex to be paramagnetic due to one unpaired electron.

To find out the crystal structure of the above complex several methods to grow a single crystal were carried out extensively using different solvent compositions and techniques. The method used in the reported crystal structure of terbium(III) complex of sodium 1,4-dihydroxy-9,10-anthraquinone-2-sulphonate [28] was also followed. However, all attempts failed to obtain a crystal for the above said 1:2 species. This is in accordance with the nature of anthracyclines and anthraquinones as they do not form single crystals with metal ions [28]. The planarity of the anthraquinone moiety may be a possible reason as to why such compounds do not easily form crystals that can be collected and mounted on a X-ray diffractometer for systematic analysis. Therefore, a crystal structure of our Cu(II) complex with sodium 1,4-dihydroxy-9,10-anthraquinone-2-sulphonate was not achieved. However, efforts are still on in this regard. Not obtaining the crystal, being a disadvantage in our case made us all the more cautious in our experiments that help in determining structure like IR spectroscopy and mass spectra. These were done several times from different crop of prepared material and the results obtained were reproducible.

3.6. Analysis of IR spectra of the ligand and the 1:2 complex

The IR spectrum of the compound sodium 1,4-dihydroxy-9,10-anthraquinone-2-sulphonate shows peaks at 3560 cm^{-1}, 2924 cm^{-1} and 2852 cm^{-1}, which are characteristic of O–H stretching and therefore indicates the presence of O–H groups on the anthraquinone (Fig. S5). In the IR spectrum of the Cu(II) complex (Fig. S6) the peak at 3560 cm^{-1} for the quinone becomes a broad band (3461 cm^{-1}) indicating a sharp deformation of the O–H group. The fact that the peak in this region did not completely disappear indicates that the other O–H on the quinone is present unaltered as in the compound $NaQSH_2$. Another reason for the presence of the broad nature of the peak in the complex is attributed to the presence of water molecules in the co-ordination sites of the metal (detected by Thermo Gravimetric Analysis, TGA). The

peaks obtained for the quinone (Fig. S5) at 2924 cm^{-1} and 2852 cm^{-1} were drastically reduced in the complex. In the IR spectra of the quinone (Fig. S5), a characteristic peak for the carbonyl stretching is seen at 1745 cm^{-1} which disappears in the Cu(II) complex (Fig. S6) indicating that the quinone participates in binding the metal ion. The peaks obtained at 1624 cm^{-1} and 1583 cm^{-1} in the IR spectra of the quinone (Fig. S5) may be attributed to C=O stretching due to carbonyl and C=C stretching due to double bonds, respectively or a combination of both. This region in the IR spectra of the Cu(II) complex (Fig. S6) undergoes a distinct change in the sense that the sharp peaks obtained for the free quinone change to broad bands in the complex further indicating participation of the oxygen of the carbonyl in binding the metal ion leading to change in the bond types in the immediate vicinity of the carbonyl. The peaks obtained in the region from 1425 cm^{-1} to 1055 cm^{-1} in the IR spectrum of the ligand (quinone) is attributed to combinations of O–H bending and C–H bending modes. The nature of the peaks in this region is somewhat different in the Cu(II) complex. What is noteworthy is that the peaks at 1220 cm^{-1} and 1055 cm^{-1} are strikingly similar in the spectrum of the free quinone and that of the complex of the quinone with Cu(II).

From elemental analysis, infra-red spectrum and other physicochemical studies performed in solution it can be said that the formed complex of Cu(II) is $Cu(NaQSH)_2(H_2O)_2$.

3.7. Analysis of IR spectra of the 1:1 polymer specie

The region for O–H stretching is completely flat in the IR spectrum (Fig. S7) of the polymer indicating that both the phenolic –O–H groups of $NaQSH_2$ are completely deprotonated and linked to metal ions as $NaQS^{2-}$. The region appears as a very broad band indicating the presence of H_2O either loosely coordinated to the metal ion or present in the vicinity of Cu(II) due to charge-dipole or dipole–dipole interaction.

The characteristic peak for carbonyl stretching seen at 1745 cm^{-1} for $NaQSH_2$ (Fig. S5) is absent in the IR spectrum of the polymer clearly indicating that like the 1:2 complex the 1:1 polymeric form is also formed by involvement of the carbonyl. The most prominent change however is seen in the region 1630 cm^{-1} to 1540 cm^{-1} where the response is due to C=O stretching and C=C stretching. In the IR spectrum of the polymer (Fig. S7) this region is different from both the IR spectra of $NaQSH_2$ (Fig. S5) and that for 1:2 metal–ligand complex, $Cu(NaQSH)_2(H_2O)_2$, (Fig. S6), clearly indicating that the bonding in the 1:1 complex (polymeric form) is different. In fact, a new peak appears at 1539 cm^{-1} (Fig. S7) while the existing peaks at 1624 cm^{-1} and 1583 cm^{-1} almost disappear.

Another striking feature of the IR spectrum (Fig. S7) of the polymer (1:1 species) is that the region from 1220 cm^{-1} to 1055 cm^{-1} which were strikingly similar for $NaQSH_2$ and $Cu(NaQSH)_2(H_2O)_2$ undergoes a drastic change. The two intense peaks at 1220 cm^{-1} and 1055 cm^{-1} undergoes modifications which is accompanied by the formation of a broad peak at 1211 cm^{-1} and the appearance of a new peak at 1001 cm^{-1} very close to the reduced 1053 cm^{-1} response (Fig. S7). The nature of the IR response at 1220 cm^{-1} and 1055 cm^{-1} being similar for $NaQSH_2$ and 1:2 complex, $Cu(NaQSH)_2(H_2O)_2$ actually indicates that the 1:2 complex, $Cu(NaQSH)_2(H_2O)_2$ and the ligand $NaQSH_2$ are similar to each other with respect to the non bonded quinone and the phenolic O–H group. That the IR response in this region is different for the 1:1 specie actually indicates that the mode of binding in 1:1 complex is quite different from that of the 1:2 complex $Cu(NaQSH)_2(H_2O)_2$ or the ligand $NaQSH_2$ and further indicates that in the 1:1 complex both the quinone units of a single ligand $NaQS^{2-}$ are involved in coordinating the metal ions.

3.8. Analysis of the mass spectra of the 1:2 complex

The mass spectrum obtained for the 1:2 Cu(II) complex (Fig. S8) provides good evidence for the stoichiometry of the formed complex which match to a very good extent with the information obtained from other methods of analysis. Considering that the Cu(II) complex has the form $Cu(NaQSH)_2(H_2O)_2$, the mass spectra of the complex was analyzed.

For the Cu(II) complex, no molecular ion or protonated molecular ion is detected at the expected value m/z = 781 or 783 (considering isotopic distribution for Cu). A clear signal but not so intense at m/z = 751.54 (calculated m/z = 751.04 or 752.04) corresponds to the fragment obtained from the complex after one Na ion and approximately 7 or 8 hydrogen atoms have departed. A comparatively more intense signal is seen at m/z = 729.4 (calculated m/z = 729.04 or 730.04) which corresponds to a fragment generated by the loss of Na^+, a molecule of water and approximately 11 hydrogen atoms from the parent complex molecule. A still stronger signal at 707.41 (calculated m/z = 707.04) is probably due to the moiety obtained by the loss of Na^+, two molecules of water and an O–H group from the complex. Loss of two Na^+ and approximately 4 hydrogens from the complex generates a moiety with two units of charge (m/z calculated = 365.52). This is detected as the most intense signal in the mass spectrum and is seen at m/z = 365.2 thus indicating that the above species is the most abundant in the process of fragmentation of the Cu(II) complex during the mass spectral analysis. Two comparatively less intense signals are detected at m/z = 301.29 (calculated m/z = 301.52) which corresponds to a fragment that is generated from the complex due to loss of 2 Na^+, 2 molecules of H_2O and 6 atoms of oxygen from the two sulphonate groups present (one on each ligand).

3.9. Electrochemical behavior of $Cu(NaQSH)_2(H_2O)_2$ in dimethyl formamide solvent

The electrochemical behavior of the compound in dimethyl formamide solvent was studied using cyclic voltammetry (Fig. 6). A control study with free 0.128 mM $CuSO_4$ in dimethyl formamide was studied under same experimental conditions. The control study showed no reduction or oxidation peak. The compound $Cu(NaQSH)_2(H_2O)_2$ was reduced reversibly by one electron showing only one reduction peak at −580 mV versus Ag/AgCl in saturated KCl. The formal reduction potential was −530 mV versus

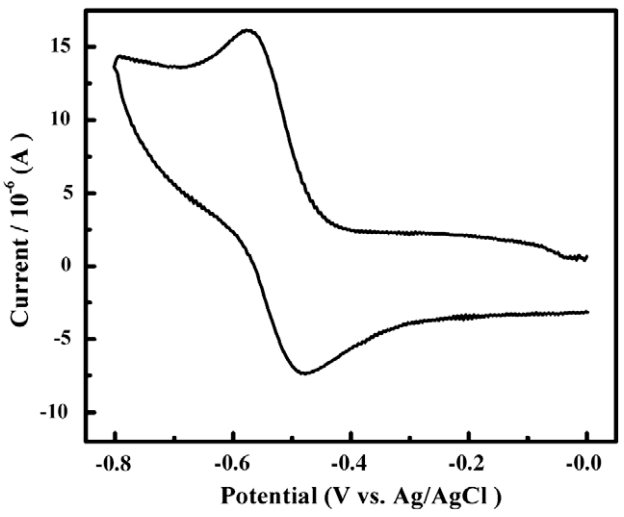

Fig. 6. Cyclic voltammogram of 0.128 mM of $Cu(NaQSH)_2(H_2O)_2$ complex in dimethyl formamide. Scan Rate: 200 mV s^{-1}.

Ag/AgCl in saturated KCl. This is completely different from the ligand sodium 1,4-dihydroxy-9,10-anthraquinone-2-sulphonate in the same solvent where the ligand undergoes successive two one- electron reduction steps forming semiquinone and quinone dianion, respectively [36].

3.10. Interaction of $[Cu(NaQSH)_2(H_2O)_2]$ to CT DNA: fluorescence spectroscopic studies to determine binding parameters

To see whether the compound, $Cu(Na)_2(H_2O)_2$, interacts with calf thymus DNA the compound solution at physiological pH was titrated with increasing amount of calf thymus DNA keeping the concentration of the compound unchanged. For this purpose separate solutions were made containing constant concentration of complex and different concentrations of CT DNA. The fluorescence spectra of $Cu(NaQSH)_2(H_2O)_2$ in presence of different amount of calf thymus DNA was recorded following an excitation at 480 nm. The emission spectrum exhibits a maximum at 590 nm. From Fig. 7, it is clear that fluorescence emission intensity was decreased gradually with increasing amount of DNA, showing that the fluorescence of $Cu(NaQSH)_2(H_2O)_2$ was efficiently quenched upon binding to DNA.

The fluorescence quenching constant (K_{SV}) was evaluated using the Stern–Volmer Eq. (14) [44]:

$$\frac{F_0}{F} = 1 + K_{SV}C_D \tag{14}$$

where F_0 and F are the fluorescence intensities in the absence and presence of DNA, respectively, K_{SV} is the Stern–Volmer quenching constant, which is a measure of the efficiency of quenching by DNA. From the titration data F_0/F values were determined and plotted against DNA concentration (Fig. S9). K_{SV} was obtained from the slope of the linear line and was found to be $5.2 \times 10^2\ M^{-1}$. The Stern–Volmer plot is linear, indicating that only one type of quenching process occurs, either static or dynamic quenching [45,46].

The binding isotherms were analyzed using non-linear curve fitting method. To do so, the following compound–DNA equilibrium was considered [47]:

$$L + D \rightleftharpoons LD \tag{15}$$

$$K_d = \frac{[L][D]}{[LD]} \tag{16}$$

where L represents $[Cu(NaQSH)_2(H_2O)_2]$ and D represents CT DNA. Apparent dissociation constant ($K_d = 1/K_{app}$, where K_{app} is the apparent binding constant) was determined using non-linear curve fitting analysis (Eqs. (17) and (18)) based on such equilibrium. All experimental points for binding isotherms were fitted by least-square analysis;

$$K_d = \frac{\left[C_0 - \left(\frac{\Delta F}{\Delta F_{max}}\right)C_0\right]\left[C_D - \left(\frac{\Delta F}{\Delta F_{max}}\right)C_0\right]}{\left(\frac{\Delta F}{\Delta F_{max}}\right)C_0} \tag{17}$$

$$C_0\left(\frac{\Delta F}{\Delta F_{max}}\right)^2 - (C_0 + C_D + K_d)\left(\frac{\Delta F}{\Delta F_{max}}\right) + C_D = 0 \tag{18}$$

where, ΔF is the change in fluorescence emission intensity of $Cu(NaQSH)_2(H_2O)_2$ at 590 nm (λ_{ex} = 480 nm) for each point of titration curve, ΔF_{max} is the same parameter when the Cu(II)-complex is totally bound to CT DNA, C_D is the concentration of CT DNA and C_0 is the initial concentration of $Cu(NaQSH)_2(H_2O)_2$. Double reciprocal plot (Fig. S10) was used for determination of ΔF_{max} and K_d using Eq. (19):

$$\frac{1}{\Delta F} = \frac{1}{\Delta F_{max}} + \frac{K_d}{\Delta F_{max}(C_D - C_0)} \tag{19}$$

This approach is based on the assumption that fluorescence is linearly proportional to the concentration of $Cu(NaQSH)_2(H_2O)_2$. Here, the concentration of the $Cu(NaQSH)_2(H_2O)_2$ was 10 μM and for construction of this plot DNA concentration was kept around 90-fold greater than that of $Cu(NaQSH)_2(H_2O)_2$.

Binding stoichiometry or the binding site size was determined from the point of intersection of two straight lines obtained from the least-square fit plot of normalized increase of $\Delta F/\Delta F_{max}$ against the ratio of input concentration of DNA in bases and $Cu(NaQSH)_2(H_2O)_2$. Two straight lines were drawn by considering points below saturation and after saturation, respectively.

Fig. 8 shows the binding isotherms of $Cu(NaQSH)_2(H_2O)_2$ with CT DNA. The binding constant was calculated using Eqs. (17) and (18) as described above. The apparent binding constant obtained is$1.43 \times 10^3\ M^{-1}$. The apparent binding constant obtained from double reciprocal plot following Eq. (19) (Fig. S10) is $1.45 \times 10^3\ M^{-1}$. It indicates that the apparent binding constant obtained from two different techniques is similar. The normalized increase of $\Delta F/\Delta F_{max}$ as a function of mole-ratio of DNA to $Cu(NaQSH)_2(H_2O)_2$.

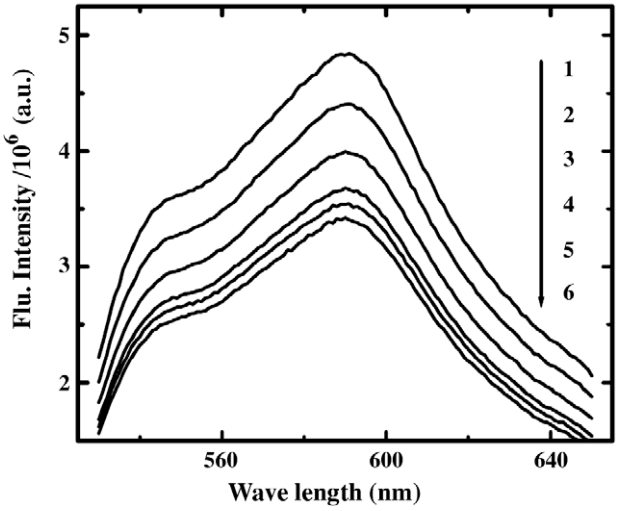

Fig. 7. Fluorescence spectra of 10 μM $Cu(NaQSH)_2(H_2O)_2$ in absence (1) and presence of different CT DNA concentrations: 140.8 μM (2), 355.0 μM (3),563.2 μM (4), 704.0 μM (5) and 844.8 μM (6); pH = 7.4, [NaCl] = 500 mM, 25 °C.

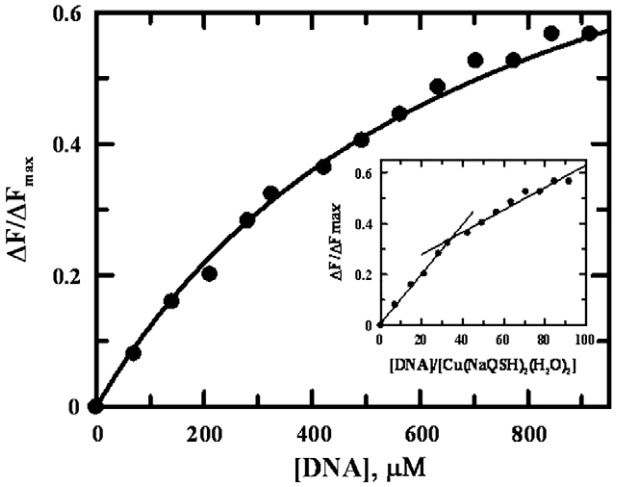

Fig. 8. Binding isotherm of $Cu(NaQSH)_2(H_2O)_2$ and calf thymus DNA and corresponding non-linear fit; $[Cu(NaQSH)_2(H_2O)_2]$ = 10 μM, pH = 7.4, [NaCl] = 500 mM, 25 °C. Inset: plot of normalized increase of fluorescence emission intensity as a function of mole-ratio of calf thymus DNA to $Cu(NaQSH)_2(H_2O)_2$.

$(H_2O)_2$ was plotted (inset of Fig. 8). The breakpoint of the two straight lines drawn considering points below and above saturation gives the stoichiometry or the binding site size (n) (inset of Fig. 8). For 1:2 Cu(II) complex of sodium 1,4-dihydroxy-9,10-anthraquinone-2-sulphonate, $Cu(NaQSH)_2(H_2O)_2$, the 'n' value is 32 bases i.e. 16 base pairs. We have found in a recent investigation that sodium 1,4-dihydroxy-9,10-anthraquinone-2-sulphonate intercalates into DNA base pairs and the 'n' value for it interacting alone with CT DNA is 16 bases i.e. 8 base pairs [48]. Therefore, the binding site size of the copper complex with CT DNA is just double the binding site size of sodium 1,4-dihydroxy-9,10-anthraquinone-2-sulphonate with CT DNA, further corroborating formation of a 1:2 complex between Cu(II) and sodium 1,4-dihydroxy-9,10-anthraquinone-2-sulphonate. Since the copper(II) ion is very small in size therefore, it may be said that the dimension of the complex is double to that of the ligand (sodium 1,4-dihydroxy-9,10-anthraquinone-2-sulphonate) supporting such a ratio (16:8) for binding site size in base pairs indicating a mode of intercalation for the complex where the open end of one quinone bound to Cu(II) intercalates first followed by Cu(II) which is followed by the other quinone linked to Cu(II). Knowing n, the intrinsic binding constant K, i.e. ($K_{app} \times n$), obtained as ($1.43 \times 10^3\ M^{-1} \times 32$) i.e. $4.58 \times 10^4\ M^{-1}$ is 1.33 times greater than that found for the interaction of sodium 1,4-dihydroxy-9,10-anthraquinone-2-sulphonate with CT DNA [48]. Introduction of a metal ion brings about better targeting of DNA [3] and this study is actually able to show this.

It should be mentioned here that interaction of anthracyclines with CT DNA were reported earlier and shown to have overall binding constant values in the range $(1.9–3.3) \times 10^5\ M^{-1}$ at pH 7.4 [49]. From the data, it is seen that anthracyclines with one sugar unit have lower binding constant values suggested in the range and as the number of sugar unit increases the binding constant values also increase being on the higher side of the range. Adriamycin and daunorubicin with one sugar in their structure has binding constant values $2.7 \times 10^5\ M^{-1}$ and $1.7 \times 10^5\ M^{-1}$, respectively while 4′-o-tetrahydropyrannyladriamycin having two sugar units in its structure was shown to have a value of $3.3 \times 10^5\ M^{-1}$. Just as this is true, it was also shown [49] in the same study an anthracycline aclacinomycin having three sugar units in the structure has a binding constant value of $1.94 \times 10^5\ M^{-1}$ which is lower than that of adriamycin [49] which could be because as number of sugar units increase beyond two, steric hindrance may become a dominant factor in binding. Our chosen molecule (sodium 1,4-dihydroxy-9,10-anthraquinone-2-sulphonate) and its Cu(II) complex are different from anthracyclines in the fact that they do not possess sugar units in their structure i.e. the compounds used are actually anthracycline drugs minus the sugar. Sodium 1,4-dihydroxy-9,10-anthraquinone-2-sulphonate binds calf thymus DNA with a binding constant $3.44 \times 10^4\ M^{-1}$ [48] which is weaker than that known for anthracyclines with CT DNA [30] suggesting some role for the sugar units in anthracyclines binding DNA. Complex formation with Cu(II) increases binding constant value by 1.33 times that of sodium 1,4-dihydroxy-9,10-anthraquinone-2-sulphonate and this study therefore is an indication that complexes of hydroxy-9,10-anthraquinones is a route to better DNA targeting that can be used to match the values reported for anthracyclines in clinical trials.

4. Conclusions

Cu(II) forms 1:2 metal–ligand complex with sodium 1,4-dihydroxy-9,10-anthraquinone-2-sulphonate at neutral and acidic pH while both 1:1 and 1:2 complexes are formed at alkaline pH. The elemental analysis is in excellent agreement with that calculated on the basis of the stoichiometry proposed. The same composition is also supported by mass spectrum. The formation constants β_I and β_{II} of 1:1 and 1:2 Cu(II) complexes of sodium 1,4-dihydroxy-9,10-anthraquinone-2-sulphonate being 9.4×10^9 and 9.64×10^{16}, respectively has close similarity with stability constant values obtained for Cu(II) with adriamycin and daunorubicin. This indicates similar modes of binding and therefore keeps open the possibility of using sodium1,4-dihydroxy-9,10-anthraquinone-2-sulphonate, if found to have similar biochemical activity, in the treatment of cancer in the near future. A DNA interaction study performed revealed that the Cu(II) complex of sodium 1,4-dihydroxy-9,10-anthraquinone-2-sulphonate interacts with calf thymus DNA at physiological pH. Binding site size and intrinsic binding constant K ($4.58 \times 10^4\ M^{-1}$) that were evaluated revealed the complex possesses a higher binding constant than the binding constant of sodium 1,4-dihydroxy-9,10-anthraquinone-2-sulphonate with DNA.

5. Abbreviations

$NaQSH_2$, sodium 1,4-dihydroxy-9,10-anthraquinone-2-sulphonate; CT DNA, calf thymus DNA; TMS, tetramethylsilane; SEM, scanning electron microscopy; UV–Vis, UV–Visible.

Acknowledgments

One of the authors, P.S.G., gratefully acknowledges Council of Scientific & Industrial Research, New Delhi, India, for a Senior Research Fellowship. The authors are grateful to Prof. Samiran Mitra, Department of Chemistry, Jadavpur University for his help in IR experiments and to Prof. Subrata Mukhopadhyay, Department of Chemistry, Jadavpur University for kindly providing D_2O required for NMR spectroscopy. The authors are also grateful to Prof. Tapas Chini and Mr. Souvik Banerjee of Surface Physics Division, Saha Institute of Nuclear Physics, Kolkata, India for their help in SEM experiments. PCM wish to thank Intramural MMDDA project at SINP for financial support.

Appendix A. Supplementary material

Supplementary data associated with this article can be found, in the online version, at doi:10.1016/j.jinorgbio.2009.09.020.

References

[1] J.G. Hardman, A.G. Gilman, L.E. Limbird, Goodman and Gilman's the Pharmacological Basis of Therapeutics, ninth ed., McGraw-Hill Companies, 1996.
[2] F. Arcamone, S. Penco, Anthracycline and Anthracycline-based Anticancer Agents, Elsevier, Amsterdam, 1988.
[3] H. Beraldo, A. Gurnier-Suillerot, L. Tosi, F. Lavelle, Biochemistry 24 (1985) 284–289.
[4] P.K. Dutta, J.A. Hutt, Biochemistry 25 (1986) 691–695.
[5] M.M.L. Fiallo, A. Gurnier-Suillerot, Biochemistry 25 (1986) 924–930.
[6] J.W. Lown, S.-K. Sim, K.C. Matjumdar, R. Chang, Biochem. Biophys. Res. Commun. 76 (1977) 705–710.
[7] E. Feinstein, E. Canaani, L.M. Weiner, Biochemistry 32 (1991) 13156–13161.
[8] A. DiMarco, F. Zunnio, R. Silverstrini, C. Gambarucci, R.A. Gambetta, Biochem. Pharmacol. 20 (1971) 1323–1328.
[9] E. Bachmann, E. Weber, G. Zbinder, Agents Actions 5 (1975) 383–393.
[10] V.J. Ferrans, Cancer Treat. Rep. 62 (1978) 955–961.
[11] D. Barasch, O. Zipori, I. Ringel, I. Ginsburg, A. Samuni, J. Katzhendler, Eur. J. Med. Chem. 34 (1999) 597–615.
[12] A. Di Marco, M. Gaetani, P. Orezzi, B. Scarpinato, R. Silvestrini, M. Soladati, T. Dasdia, L. Valentini, Nature 201 (1964) 706–707.
[13] A. Kumbhar, S. Padhye, D. Ross, Biometals 9 (1996) 235–240.
[14] A. Bartoszek, Acta Biochim. Pol. 49 (2002) 323–331.
[15] R. Kiraly, B. Martin, Inorg. Chim. Acta 67 (1982) 13–18.
[16] P.M. May, G.K. Williams, D.R. Williams, Inorg. Chim. Acta 46 (1980) 221–228.
[17] M. Feng, Y. Yang, P. He, Y. Fang, Spectrochim. Acta Part A 56 (2000) 581–587.
[18] F.T. Greenaway, J.C. Dabrowiak, J. Inorg. Biochem. 16 (1982) 91–107.
[19] H. Beraldo, A. Garnier-Suillerot, L. Tosi, Inorg. Chem. 22 (1983) 4117–4124.

[20] E. Pereira, M.M.L. Fiallo, A. Garnier-Suillerot, T. Kiss, H. Kozlowski, J. Chem. Soc. Dalton Trans. (1993) 455–459.
[21] M.M.L. Fiallo, A. Gurnier-Suillerot, Biochim. Biophys. Acta 840 (1985) 91–98.
[22] S.S. Massoud, R.B. Jordan, Inorg. Chem. 30 (1991) 4851–4856.
[23] M.J. Maroney, R.O. Day, T. Psyris, L.M. Fleury, J. Whitehead, Inorg. Chem. 28 (1989) 173–175.
[24] P.G. Marshall, J. Chem. Soc. (1931) 3206–3207.
[25] H.W. Coble, H.F. Holtzclaw, J. Inorg. Nucl. Chem. 36 (1974) 1049–1053.
[26] P. Yang, H. Wang, F. Gao, B. Yang, J. Inorg. Biochem. 62 (1996) 137–145.
[27] M. Kadarkaraisamy, D. Mukjerjee, C.C. Soh, A.G. Sykes, Polyhedron 26 (2007) 4085–4092.
[28] M.D. Vaira, P. Orioli, F. Piccioli, B. Bruni, L. Messori, Inorg. Chem. 42 (2003) 3157–3159.
[29] F. Arcamone, G. Cassinelli, F.D. Matteo, S. Forenza, M.C. Ripamonti, G. Rivola, A. Vigevani, J. Clardy, T. McCabe, J. Am. Chem. Soc. 102 (1980) 1462–1463.
[30] S.K. Arora, J. Biomol. Struct. Dyn. 3 (1985) 377–385.
[31] D.A. Berkowitz, S. Danishefski, G.K. Schulte, J. Am. Chem. Soc. 114 (1992) 4518–4529.
[32] S. Das, A. Saha, P.C. Mandal, Talanta 43 (1996) 95–102.
[33] S. Das, P.C. Mandal, M.C. Rath, T. Mukherjee, Res. Chem. Intermed. 25 (1999) 379–391.
[34] S. Das, A. Bhattacharya, P.C. Mandal, M.C. Rath, T. Mukherjee, Radiat. Phys. Chem. 65 (2002) 93–100.
[35] S. Das, A. Saha, P.C. Mandal, Environ. Health Perspect. 105 (1997) 1459–1462.
[36] P.S. Guin, S. Das, P.C. Mandal, Int. J. Electrochem. Sci. 3 (2008) 1016–1028.
[37] S. Das, A. Saha, P.C. Mandal, J. Radioanal. Nucl. Chem. 196 (1996) 57–63.
[38] W. Priebe, Molecules 5 (2000) 299–301.
[39] T. Mukherjee, E.J. Land, A.J. Swallow, J. Chem. Soc., Faraday Trans. 1 84 (1988) 2855–2873.
[40] R.D. Shannon, Acta Crystallogr. A32 (1976) 751–757.
[41] R.S. Bottei, J.T. Fangman, J. Inorg. Nucl. Chem. 28 (1966) 1259–1264.
[42] R.S. Bottei, P.S. Gerace, J. Inorg. Nucl. Chem. 23 (1961) 245–251.
[43] A.I. Vogel, Solvent extraction, in: G.H. Jeffery, J. Bassett, J. Mendham, R.C. Denney (Eds.), Textbook of Quantitative Chemical analysis, fifth ed., ELBS/Longman, Great Britain, 1989, pp. 178–182.
[44] A.M. Pyle, J.P. Rehmann, R. Meshoyrer, C.V. Kumar, N.J. Turro, J.K. Barton, J. Am. Chem. Soc. 111 (1989) 3051–3058.
[45] J.R. Lakowicz, Principles of Fluorescence Spectroscopy, Kluwer Academic, New York, 1999. pp. 239–240.
[46] W. Zhong, J.S. Yu, W.L. Huang, K.Y. Ni, Y.Q. Liang, Biopolymers 62 (2001) 315–323.
[47] S. Chakraborti, B. Bhattacharyya, D. Dasgupta, J. Phys. Chem. B 106 (2002) 6947–6953.
[48] P.S. Guin, S. Das, P.C. Mandal, J. Phys. Org. Chem. (2009), doi:10.1002/poc.1624.
[49] F. Frezard, A. Garnier-Suillerot, Biochim. Biophys. Acta 1036 (1990) 121–127.

RSC Advances

PAPER

View Article Online
View Journal | View Issue

Cite this: *RSC Adv.*, 2014, **4**, 59344

Synthesis, crystal structure, DNA interaction and *in vitro* anticancer activity of a Cu(II) complex of purpurin: dual poison for human DNA topoisomerase I and II†

Piyal Das,[a] Chetan Kumar Jain,[bd] Sanjoy K. Dey,[c] Rajat Saha,[c] Abhishek Dutta Chowdhury,[a] Susanta Roychoudhury,[b] Sanjay Kumar,[c] Hemanta Kumar Majumder[d] and Saurabh Das*[a]

Although generation of reactive oxygen species (ROS) by anthracycline anticancer drugs is essential for anti-tumor activity, they make these drugs cardiotoxic. Metal–anthracyclines that generate relatively fewer ROS are however, effective antitumor agents. Purpurin (LH_3), a hydroxy-9,10-anthraquinone, closely resembles doxorubicin, an established anthracycline drug. This molecule was chosen to study the extent to which simpler analogues are effective. A Cu(II) complex of LH_3 [$Cu^{(II)}$–$(LH_2)_2$] was synthesized to mimic the metal–anthracycline complexes. The crystal structure of [$Cu^{(II)}$–$(LH_2)_2$] was determined by Rietveld refinement of PXRD data using an appropriate structural model developed on the basis of spectroscopic data. This is the first report on the crystal structure of any hydroxy-9,10-anthraquinone with a 3d-transition metal ion. The bond lengths and bond angles obtained by structural refinement corroborate those calculated by the DFT method. DNA binding of the complex was slightly better than purpurin. However, more importantly, unlike purpurin, binding constant values did not decrease with increasing pH of the medium. DNA relaxation assays show $Cu^{(II)}$–$(LH_2)_2$ as a novel potent dual inhibitor of human DNA topoisomerase I and topoisomerase II enzymes. $Cu^{(II)}$–$(LH_2)_2$ stabilizes covalent topoisomerase–DNA adducts both *in vitro* and within cancer cells. The cleavage assay keeps the complex well ahead of LH_3 with regard to efficacy. These results paralleled those of cell growth inhibition and showed that the complex was more effective in killing ALL MOLT-4 cells than LH_3, suggesting it targets topoisomerase enzymes within cells. The NADH dehydrogenase assay revealed further that the generation of superoxide was less in the case of the complex as compared to LH_3.

Received 15th July 2014
Accepted 24th October 2014

DOI: 10.1039/c4ra07127a

www.rsc.org/advances

1. Introduction

Anthracycline anticancer agents are currently in use in various forms of chemotherapy.[1] The two most well known drugs in this series, adriamycin (doxorubicin, DOX) and daunomycin are extensively used in breast cancer and acute lymphoblastic leukemia (ALL). These compounds function as DNA topoisomerase inhibitors.[1] DNA topoisomerases are essential nuclear enzymes found in cells that help to maintain DNA topology during processes like replication, transcription and recombination, ensuring the faithful segregation of chromosomes during cell division.[1–3] The nuclei of mammalian cells contain two principal types of DNA topoisomerases, DNA topoisomerase I (topo I) and DNA topoisomerase II (topo II), which are molecular targets for several anticancer drugs.[2,3] Topoisomerase inhibitors belong to two different classes. Class I inhibitors or topoisomerase poisons inhibit controlled strand rotation or the re-ligation step of the enzymatic reaction cycle forming enzyme linked DNA lesions that initiate cell cycle arrest, leading to apoptosis.[4] Class II inhibitors or catalytic topoisomerase inhibitors inhibit DNA binding or the DNA nicking step of the enzyme-reaction cycle.[5–8]

The major concern on the use of anthracyclines is their associated cardiotoxicity and life-threatening heart damage.[9–18] Studies on breast cancer itself reveal that ~27% of patients

[a]*Department of Chemistry, Jadavpur University, Kolkata-700032, India. E-mail: sdas@chemistry.jdvu.ac.in; Fax: +91-3324146223; Tel: +91-8902087756*

[b]*Cancer Biology & Inflammatory Disorder Division, Indian Institute of Chemical Biology, Kolkata-700032, India*

[c]*Department of Physics, Jadavpur University, Kolkata-700032, India. E-mail: kumars@phys.jdvu.ac.in*

[d]*Infectious Diseases and Immunology Division, Indian Institute of Chemical Biology, Kolkata-700032, India. E-mail: hkmajumder@iicb.res.in*

† Electronic supplementary information (ESI) available: Physicochemical experiments on complex formation in solution. Spectroscopic characterization (IR, Mass, EPR) of the complex. Table showing TDDFT calculation. Various plots for evaluation of binding parameters of LH_3 and $Cu^{(II)}$–$(LH_2)_2$ with CT DNA. CIF files of $Cu^{(II)}$–$(LH_2)_2$. CCDC 916875. For ESI and crystallographic data in CIF or other electronic format see DOI: 10.1039/c4ra07127a

suffer congestive heart failure later in life owing to anthracycline treatment.[19,20] Reports have indicated that reactive oxygen species (ROS) produced by anthracyclines are mainly responsible for cardiotoxicity and that the hydroxy-9,10-anthraquinone moiety present in these molecules is the site of generation of ROS.[1] At the same time, ROS is also essential for anticancer activity.[21,22] Hence, there is a need to have a proper balance in the generation of ROS such that it maintains its anticancer activity but is not cardiotoxic. Lowering ROS generation to appropriate levels could be one approach to minimize the side effects of these drugs and their analogues.

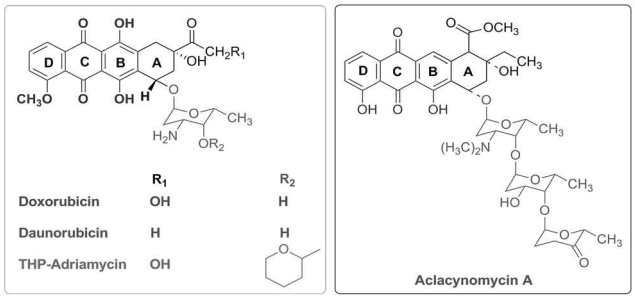

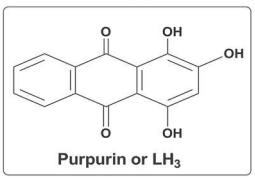

Recent studies on hydroxy-9,10-anthraquinones and their metal complexes have shown remarkable similarities with anthracyclines, particularly with regard to physicochemical attributes, electrochemical behavior and biophysical interactions.[23–25] The cardiotoxicity of anthracyclines was shown to decrease significantly when they form complexes with metal ions.[26,27] Complexes of Cu(II) with anthracyclines generate relatively small amounts of ROS but are effective anti-cancer agents.[26–29] With these facts in mind, our aim was to pick simple hydroxy-9,10-anthraquinones, prepare their complexes and compare them with similar complexes of anthracyclines.[30] Purpurin (1,2,4-trihydroxy-9,10-anthraquinone), which closely resembles DOX, was chosen and a Cu(II) complex was prepared. Results obtained with this complex were compared with Cu(II) complexes of DOX with regard to semiquinone formation, DNA interaction and action on DNA topoisomerase enzymes to realize its potential as an anticancer agent.[31]

2. Experimental

2.1 Synthesis of a Cu(II) complex of LH_3

Purpurin (LH_3) of ~96% purity was purchased from Sigma-Aldrich and further purified by re-crystallization from ethanol–water mixtures. The compound, being photosensitive, was stored in the dark. The complex was prepared by mixing $Cu(NO_3)_2 \cdot 3H_2O$ and LH_3 in the ratio 1 : 2 (metal to ligand stoichiometry was determined by the molar ratio method, ESI†). LH_3 (0.09 mmol) and $Cu(NO_3)_2 \cdot 3H_2O$ (0.045 mmol) were dissolved in a minimum volume of hot absolute ethanol and triple distilled water, respectively. The Cu(II) solution was added drop by drop to the yellowish-orange solution of LH_3 taken in a beaker, with continuous stirring with the help of a temperature-controlled magnetic stirrer. The intense yellowish-orange color of LH_3 changed almost immediately to dark brown upon addition of the aqueous Cu(II) solution. The solvent ratio was 2 : 1 ethanol–water. The reaction mixture was stirred for 2 hours at 40 °C. After 2 hours, it was kept overnight in the dark. A brown solid settled to the bottom of the beaker while the supernatant was yellow in color. The solution was filtered. The brown residue was washed with warm 10% ethanol solution. It was then purified from acetonitrile and dried in a vacuum desiccator. Utmost care was taken to prevent the formation of a polymeric 1 : 1 complex under alkaline conditions.[32] The pH of the medium was maintained at ~6.00 using sodium bicarbonate.

Yield: 68%. Analytical calculation (%) for $CuC_{28}H_{18}O_{12}$: C, 55.13; H, 2.95. Experimentally found: C, 54.81; H, 2.90. Cu(II) was estimated using the standard procedure.[33] Analytical calculation (%) 10.42, experimentally found 10.34. UV-Vis spectra: λ_{max} at 515 nm. MS (m/z): 630 $[M + Na]^+$.

2.2 X-ray powder diffraction measurements and crystal structure of $Cu^{(II)}$–$(LH_2)_2$

The X-ray powder diffraction data was collected on a Bruker D8 Advanced powder diffractometer using Cu-Kα radiation (λ = 1.5418 Å). The generator settings were 40 kV and 40 mA. The diffraction pattern was recorded at room temperature (21 °C) with step size 0.0199° (2θ) and a count time of 5 s per step over the 2θ range 5–80°. The X-ray powder diffraction pattern was indexed by NTREOR of EXPO 2009 package and the results indicate the sample crystallizes in a triclinic unit cell with a = 12.575 Å, b = 12.412 Å, c = 10.343 Å and $\alpha = 97.09°$, $\beta = 113.49°$, $\gamma = 62.38°$ [M(20) = 14, F(20) = 14(0.003767, 338)].[34] The statistical analysis of powder patterns using the FINDSPACE of EXPO 2009 software package indicates that the most probable space group is $P\bar{1}$. The structure was solved by a global optimization method in direct-space using a Monte Carlo based simulated annealing technique (in parallel tempering mode), as implemented in the program FOX with the help of an initial structural model developed on the basis of spectroscopic information (provided in ESI†).[35] The initial molecular geometry was optimized by MOPAC 2007 program and this optimized structural model was used as an input to the FOX program in order to obtain the atomic coordinates.[35,36] The atomic coordinates thus obtained from FOX were used as the starting model for Rietveld refinement carried out by the GSAS software package with EXPGUI interface.[37,38] The lattice parameters, background coefficients and profile parameters were refined. The background was described by the shifted Chebyshev function of the first kind with 24 points regularly distributed over the entire 2θ range. A fixed isotropic displacement parameter of 0.04 Å^2 for all non-hydrogen atoms and 0.06 Å^2 for hydrogen atoms was maintained. In the final stage of refinement, the preferred orientation correction was applied using the generalized spherical harmonic model of order 10.

2.3 Computational details

Full geometry optimizations were carried out at the (U)B3LYP levels using the density functional theory method with Gaussian 09 (revision A.02).[39–41] All elements were assigned by the LanL2DZ basis set with effective core potential.[42,43] Stationary-point calculations were carried out using the output coordinates from the geometry optimization calculations. GaussSum was used to calculate the fractional contributions of various groups to each molecular orbital.[44,45] No symmetry constraints were imposed during structural optimizations and the nature of the optimized structures and energy minima were defined by subsequent frequency calculations. Natural bond orbital analyses were performed using NBO 3.1 module of Gaussian 09 on optimized geometry.[46–49] All calculated structures were visualized with ChemCraft.[50]

2.4 Electrochemistry of $Cu^{(II)}$–$(LH_2)_2$

Cyclic voltammetry was performed on an EG & G Potentiostat Model 263A, Princeton Applied Research with power suite software for electrochemistry. Voltammograms were recorded using the three-electrode system. A glassy-carbon electrode of surface area 0.1256 cm^2 was the working electrode, Ag/AgCl, KCl (saturated) was the reference while a platinum wire served as the counter electrode. Electrochemical measurements were undertaken in a 50 ml electrochemical cell with dimethyl formamide (DMF) as the solvent and 0.1 (M) tetrabutylammonium bromide (TBAB) as the supporting electrolyte.[23,24] Before each cyclic voltammetry experiment, the solution was purged using high purity Argon for 40 minutes, while in between each scan the solution was purged with Argon for a further 5 minutes.

2.5 Interaction of LH_3 and $Cu^{(II)}$–$(LH_2)_2$ with CT DNA

2.5.1 By UV-Vis spectroscopy. Interaction was studied using a JASCO V-630 UV-Vis spectrophotometer. A pair of quartz cuvettes (STARNA Scientific Ltd.; 10 mm × 10 mm path length) was used. Separate aliquots, each containing a constant concentration (75 μM) of LH_3 or $Cu^{(II)}$–$(LH_2)_2$ and different concentrations of CT DNA were used at different pH. The concentration of CT DNA was gradually increased until saturation was reached. The total volume was kept constant at 2.0 ml using 15 mM Tris buffer and 120 mM NaCl. At the end of the titration, CT DNA was ~30 fold greater than the concentration of compounds used. Each experiment was repeated thrice. The binding constant and site size of the interaction was determined using standard equations.[23,24,33,51,52]

2.5.2 By fluorescence spectroscopy. The interaction was studied using a HITACHI S-7000 fluorescence spectrophotometer.[23,24,32] Solutions were excited at 515 nm and emission was measured at 582 nm at 298 K. The complex (75 μM) was taken in a fluorescence cuvette (10 mm × 10 mm path length) and titrated with increasing amounts of CT DNA. The total volume (2.0 ml) was constant using 15 mM Tris buffer (pH 7.4) and 120 mM NaCl. Here too, at the point of saturation, CT DNA was ~30 fold greater than the concentration of $Cu^{(II)}$–$(LH_2)_2$. The experiment was repeated thrice. The binding constant and the site size of the interaction was evaluated.

2.6 DNA relaxation assays for topoisomerase I and topoisomerase II enzymes

Recombinant human DNA topoisomerase I and human DNA topoisomerase II enzymes were purchased from TopoGEN Inc (Port Orange, Florida, USA). DNA relaxation assays for recombinant human DNA topoisomerase I and topoisomerase II enzymes were performed in the presence and absence of the compounds by briefly incubating 100 fmol of supercoiled pBS SK (+) DNA with 50 fmol of the enzyme in the reaction buffer provided with the enzymes. Dimethyl sulphoxide (DMSO) concentration was maintained at 1% (vehicle control). Camptothecin (CPT) and doxorubicin (DOX) were purchased from Sigma (St. Louis, MO, US) to be used as positive control drugs that stabilize covalent topoisomerase I-DNA complexes and covalent topoisomerase II-DNA complexes, respectively. The reactions were incubated at 37 °C for 30 minutes, loaded on 1% agarose gel and subjected to electrophoresis at 20 volts overnight. After completion of electrophoresis, gels were stained with 0.5 μg ml^{-1} ethidium bromide and viewed by Gel Doc 2000 (BioRad) under UV illumination. Relaxation was assessed by monitoring the decreased electrophoretic mobility of relaxed topoisomers of pBS SK (+) DNA.

2.7 DNA cleavage assay for topoisomerase I and topoisomerase II enzymes

DNA cleavage assay for topoisomerase I and topoisomerase II was performed in the presence or absence of the compounds by briefly incubating 100 fmol of supercoiled pBS (SK^+) DNA with 500 fmol of enzyme. For topoisomerase I, the reaction buffer contained 10 mM Tris-HCl (pH 7.5), 50 mM KCl, 5 mM $MgCl_2$, 0.1 mM EDTA and 15 μg ml^{-1} BSA while for topoisomerase II the assay was done in a mixture of the two reaction buffers provided with the enzyme. All reactions were performed in the presence of 400 μM *N*-acetyl cysteine (NAC) (Sigma) and 100 μM ascorbic acid (AA) (Sigma). Reactions were incubated at 37 °C for 30 minutes and stopped with 0.5% SDS. Enzymes were digested by proteinase K treatment. DMSO concentration was maintained at 1% (vehicle control). CPT and DOX were used as positive control drugs that stabilize covalent topoisomerase I-DNA complexes and covalent topoisomerase II–DNA complexes, respectively. Reactions were loaded on 1% agarose gel with 0.5 μg ml^{-1} ethidium bromide. Electrophoresis at 80 volts was carried out for 3 hours. After completion of electrophoresis, gels were viewed by Gel Doc 2000 (BioRad) under UV illumination.

2.8 Cell culture and cell viability assay

MOLT-4 cells were cultured in a RPMI medium (GIBCO, Invitrogen, Carlsbad, CA, US), supplemented with 10% fetal bovine serum (GIBCO), antibiotic mixture (1×) PSN (GIBCO) and gentamicin reagent solution (GIBCO). Cells were incubated in a humidified CO_2 incubator at 37 °C. Etoposide (ETO) was purchased from Sigma (St. Louis, MO, US) to be used as a

positive control drug along with CPT and DOX. These were dissolved in DMSO. MOLT-4 cells were seeded in 96 well plates for 24 hours before drug treatment. After 24 hours, the cells were treated with LH_3, $Cu^{(II)}$–$(LH_2)_2$ and the control compounds. DMSO concentration was less than 0.5%. After treatment for 72 hours cell viability was checked by 3-(4,5-dimethylthiazol-2-yl)-2,5-diphenyltetrazolium bromide (MTT) assay. Briefly, the cells were washed with 1× PBS and treated with MTT for 4 hours at 37 °C. The precipitates were dissolved in DMSO and the plates were analyzed on a Thermo MULTISKAN EX plate reader at 595 nm.

2.9 Immunoband depletion assay

For the immunoband depletion assay MOLT-4 cells were cultured in 35 mm dishes and treated with either 10 μM CPT or 10 μM DOX or 40 μM LH_3 or 20 μM $Cu^{(II)}$–$(LH_2)_2$. Cells were harvested at 0 hours, 4 hours, 8 hours and 12 hours. Equal amounts of protein were subjected to electrophoresis on SDS–poly acryl amide gel. The separated proteins were then transferred onto a nitrocellulose membrane and western blotting was performed using anti-topo I and anti-topo II antibodies (Santa Cruz Biotechnology, Inc. Santa Cruz, CA, USA).

2.10 NADH dehydrogenase assay

The enzyme assay was undertaken at 298 K with cytochrome c as an electron acceptor.[25,53] LH_3 and $Cu^{(II)}$–$(LH_2)_2$ were assayed for NADH-cytochrome c reductase activity, monitoring the reduction of cytochrome c at 550 nm. Tris buffer (pH ∼ 7.4), 80.0 μM cytochrome c, 160.0 μM NADH, 3.0 U per litre NADH dehydrogenase and test compounds were used. LH_3 and $Cu^{(II)}$–$(LH_2)_2$ concentrations were varied from 0 to 45.0 μM. The activity of NADH dehydrogenase is expressed in units, where one unit of activity reduces 1.0 μ mole oxidized cytochrome c per minute at 298 K. Formation of the superoxide radical anion catalyzed by LH_3 and $Cu^{(II)}$–$(LH_2)_2$ was measured from the reduction of cytochrome c inhibited by superoxide dismutase (SOD) (0 or 40.0 μg ml^{-1}) in the presence of NADH and NADH dehydrogenase.[25–27] The kinetics software of JASCO V-630 was utilized for the purpose.

3. Results and discussions

3.1 X-ray crystal structure description of $[C_{28}H_{14}O_{10}Cu]$

Structural analysis from PXRD data (Fig. 1a) indicates that the Cu(II) complex crystallizes in the $P\bar{1}$ space group. The ORTEP diagram for the complex is depicted in Fig. 1b. According to the refined structure obtained by analyzing the PXRD data, each asymmetric unit of the complex contains one Cu(II) ion, two monanionic LH_2^- units and two guest water molecules. Each Cu(II) center shows perfect square planar geometry with a coordination number of four. The coordination environment of Cu(II) is satisfied by two deprotonated phenolic –OH groups (O18 and O35) of two different LH_3 units and two carbonyl oxygen atoms (O19 and O34). The crystal structure obtained by Rietveld refinement of the PXRD data shows that all Cu–O bond distances vary in the range 1.847–1.884 Å and all *cisoid* and *transoid* angles vary in the range 87.2–92.9° and 179.86–179.89°, respectively. Two LH_3 units are inversely connected to the metal center; each monomeric unit is connected by supramolecular interactions leading to higher dimensions. The ORTEP diagram of the $Cu^{(II)}$–$(LH_2)_2$ complex (Fig. 1b) almost completely matches the DFT optimized structure (Fig. 1c). In the absence of a single crystal for systems such as this one, powder X-ray diffraction remains the only option to obtain a structure. In our case, the structure obtained from powder diffraction not only matched other experimental findings but was also in good agreement with DFT calculations. This is the first reported structure of a complex of any hydroxy-9,10-anthraquinone with a 3d-transition metal ion.[30] The final crystallographic data, structure refinement parameters, selected bond length and bond angles are summarized in Tables 1 and 2.

3.2 DFT study of $Cu^{(II)}$–$(LH_2)_2$ complex

Although the structure of $Cu^{(II)}$–$(LH_2)_2$ was obtained from powder X-ray diffraction data, a DFT study was carried out to check the formation of the complex and to predict certain physical and chemical properties. The MO composition of $Cu^{(II)}$–$(LH_2)_2$ from DFT calculations is provided in Table 1S.† The α-HOMOs and β-LUMOs are primarily composed of redox non-innocent quinone moieties of $Cu^{(II)}$–$(LH_2)_2$ that essentially make the paramagnetic copper centre a redox silent site (Fig. 1d–g). DFT calculations of $Cu^{(II)}$–$(LH_2)_2$ predict quinone based redox processes. Analysis of the spin density plot (Fig. 1h) predicts a mixed metal–ligand behavior of the paramagnetic copper center, which was experimentally verified in the EPR spectrum of the complex (ESI†). The TDDFT calculation revealed that electronic transitions obtained in the UV-Vis spectrum would be LLCT (Table 3). DFT computer predictions of $Cu^{(II)}$–$(LH_2)_2$ were in excellent agreement with the solved structure, with calculated bond lengths and angles being very close to those obtained through a computer model that provided a best fit for the experimental data (Fig. 1b, c, Tables 1 and 2).

3.3 Electrochemical behavior of $Cu^{(II)}$–$(LH_2)_2$ complex

The complex showed one-electron reduction in DMF (Fig. 2a) with a peak at −0.866 V (*vs.* Ag,AgCl/KCl saturated) and $E_{1/2}$ = −0.810 V was similar to an earlier report from our laboratory.[32] In the case of LH_3, we reported earlier that the molecule undergoes two-step one-electron reduction, forming a semiquinone that converts to a quinone di-anion.[23] The variation of cathodic peak current with square root of potential sweep rate according to the Randles equation (eqn (1)) was linear in the case of the complex (Fig. 2b), indicating that the reduction of $Cu^{(II)}$–$(LH_2)_2$ in DMF was diffusion controlled.[55,56]

$$i_{pc} = (2.69 \times 10^5) n^{3/2} D_0^{1/2} A C \nu^{1/2} \quad (1)$$

i_{pc} = cathodic peak current (A), n = total number of electrons involved, A = area of the electrode (cm^2), C = concentration (moles per cm^3), ν = scan rate (V s^{-1}). The diffusion coefficient (D_0) was calculated from the slope of the plot (Fig. 2b) and found

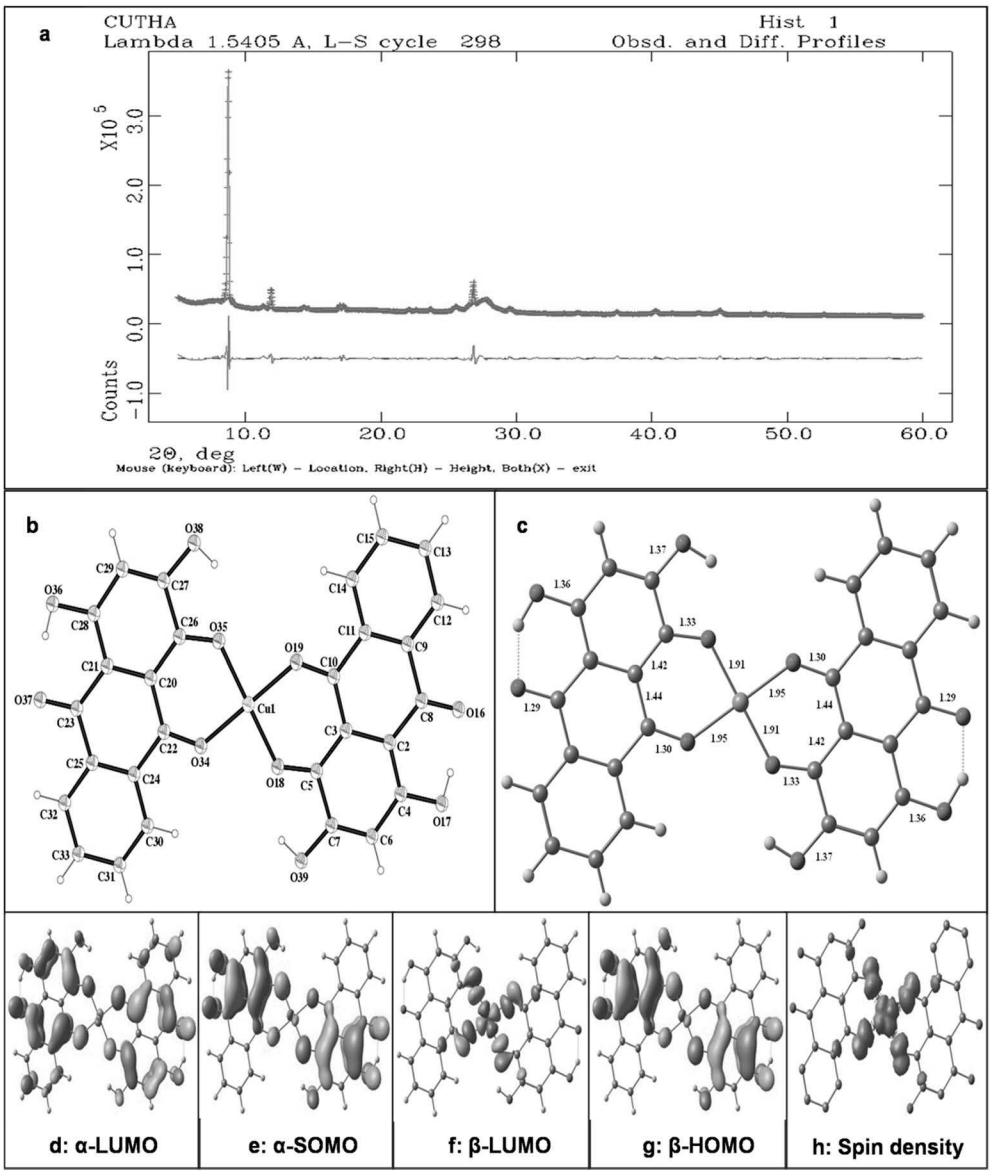

Fig. 1 (a) The final Rietveld plot, where the red curve denotes the experimental pattern, the green curve denotes the simulated pattern and the pink curve indicates the difference of these two patterns. (b) ORTEP diagram of the complex $Cu^{(II)}$–$(LH_2)_2$ (for clarity guest water molecules were omitted). Ellipsoids are drawn at 30% probability. (c) DFT optimized structure of $Cu^{(II)}$–$(LH_2)_2$ complex. (d) to (g) area pictorial representation of respective MO diagrams of the $Cu^{(II)}$–$(LH_2)_2$ complex. (h) Spin density plot of $Cu^{(II)}$–$(LH_2)_2$ complex.

to be 4.462×10^{-5} cm^2 s^{-1}. The ratio of peak currents at different potential sweep rates were calculated with the help of Nicholson's equation.[56,57]

$$i_{pa}/i_{pc} = \frac{(i_{pa})_0}{i_{pc}} + \frac{0.485 \times (i_{sp})_0}{i_{pc}} + 0.086 \qquad (2)$$

$(i_{sp})_0$ was the current at E_λ (switching potential) and $(i_{pa})_0$ was the uncorrected anodic peak current with respect to zero current (baseline). The experimental data in Table 4 shows that the ratio of peak currents (i_{pa}/i_{pc}) was unity at all scan rates. This indicates that the redox behavior of $Cu^{(II)}$–$(LH_2)_2$ in an aprotic solvent like DMF was completely reversible. Redox processes of the complex obtained from cyclic voltammetry studies corroborate the prediction made earlier from DFT calculations that redox processes would be quinone based. The Cu(II)/Cu(I) couple had a reduction potential of 0.55 V *vs.* Ag,AgCl/KCl (saturated) in an acetonitrile solvent.

3.4 Interaction of LH_3 with CT DNA by UV-Vis spectroscopy: the effect of pH

A detailed study on the interaction of LH_3 with CT DNA was reported earlier.[23] In that report, we showed that LH_3 is a DNA intercalator. Intrinsic binding constant and site size of the interaction was found to be $(4.51 \pm 0.20) \times 10^4$ M^{-1} and (5.21 ± 0.20) nucleotides, respectively.[23] In this study, an effort was made to show the manner in which the intrinsic binding

Table 1 Crystallographic data and refinement parameters obtained from PXRD data analysis

Formula	$C_{28}H_{10}CuO_{12}$
Formula weight	601.92
Crystal system	Triclinic
Space group	$P\bar{1}$
a/Å	12.6644(14)
b/Å	12.2799(10)
c/Å	10.4602(13)
α/°	97.155(11)
β/°	113.937(9)
γ/°	61.539(6)
V/Å^3	1302.34(18)
Z	2
ρ_{calc}/g cm^{-3}	1.494
Temperature/K	293
Radiation/Å	1.54184
2θ range/°	5–80
R_{wp}	0.0685
R_p	0.0429

constant for the interaction of LH_3 with DNA varied with pH at constant ionic strength of the medium. It was observed that as pH increased, the extent of interaction between the LH_3 and CT DNA decreased (Table 2S†), attributed to the generation of an anionic form of LH_3 at physiological pH.[58] With increasing pH, LH_2^- formed from LH_3 faced more repulsion from DNA, which was manifested in a decrease in binding constant values. Since LH_3 exists in two forms at physiological pH [6.65 to 8.35], hence binding of it to CT DNA at any pH in the specified range was a consequence of both.[58] To know the contribution of each and the impact that a change in pH has on the strength of interaction, the overall binding constant at each pH was treated according to the Henderson–Haselbach equation (eqn (3)).[58,59]

$$\mathrm{pH} = \mathrm{p}K_a + \log \frac{[D^-]}{[D_0]} \quad (3)$$

The impact of the negative charge on LH_2^- on the overall binding constant was determined by plotting K^* at five different pH values. Thus, the contribution of each form towards the overall binding constant was evaluated with the help of eqn (8) and (9). The overall binding constant could be defined as

$$K^* = \frac{[C_b]}{[C_f][\mathrm{DNA}]} \quad (4)$$

The change in absorbance of LH_3 upon binding enabled the determination of C_b and C_f (ESI†). [DNA] represents the total concentration of CT DNA. Since the overall binding constant at each pH was considered to be made up of two terms, K^0 and K^-, K^0 was defined as the overall binding constant of the neutral form $\left(K^0 = \frac{[C_b^0]}{[C_f^0][\mathrm{DNA}]}\right)$ while K^- was that due to the anionic form $\left(K^- = \frac{[C_b{}^-]}{[C_f{}^-][\mathrm{DNA}]}\right)$. The total bound and free forms of purpurin were

$$[C_b] = [C_b^0] + [C_b{}^-] \quad (5)$$

and

$$[C_f] = [C_f^0] + [C_f{}^-] \quad (6)$$

$$\mathrm{pH} = \mathrm{p}K_a + \log \frac{\left[C_f{}^-\right]}{\left[C_f^0\right]} \quad (7)$$

Table 2 Selected bond lengths and bond angles of $Cu^{(II)}$–$(LH_2)_2$ obtained by refinement of the PXRD pattern and those calculated by the DFT method

	Bond lengths (Å)	
Bonds	Obtained by refinement of the PXRD pattern	Calculated by the DFT method
Cu1–O18	1.8469	1.919
Cu1–O19	1.8839	1.954
Cu1–O34	1.8843	1.954
Cu1–O35	1.8467	1.919
	Bond angles (°)	
O18–Cu1–O19	92.89	90.02
O18–Cu1–O34	87.23	89.98
O18–Cu1–O35	179.88	179.98
O19–Cu1–O34	179.86	179.99
O19–Cu1–O35	87.00	89.98
O34–Cu1–O35	92.89	90.02
Cu1–O18–C5	126.23	127.75
Cu1–O19–C10	129.45	131.05
Cu1–O34–C22	129.44	131.05
Cu1–O35–C26	126.25	127.75

Table 3 TDDFT table of the $Cu^{(II)}$–$(LH_2)_2$ complex

Energy (eV)	Wavelength (nm)	f	Involved transition	Character
2.4741	501.13	0.3618	α HOMO−1 → α LUMO (0.57671)	Ligand (pπ) → ligand (pπ*)
3.2292	383.94	0.5022	β HOMO−6 → β-LUMO (0.70551)	Ligand (pπ) → ligand (pπ*)

Eqn (4) could then be written as

$$K^*(1 + 10^{pH-pK}) = K^0 + K^- \times 10^{pH-pK} \quad (8)$$

or

$$K^* = (K^0 + K^- \times 10^{pH-pK})/(1 + 10^{pH-pK}) \quad (9)$$

According to eqn (8), the plot of $K^*(1 + 10^{pH-pK})$ as a function of 10^{pH-pK} yields a straight line (Fig. 3a) with correlation coefficient 0.99. K^- was determined as the slope and K^0 as the intercept. The values were $(5.65 \pm 0.48) \times 10^6\ M^{-1}$ and $(2.41 \pm 0.04) \times 10^4\ M^{-1}$ for K^0 and K^-, respectively. The overall binding constants (K^*) were also plotted against pH according to eqn (9) (Fig. 3b) and values for K^0 and K^- were $(4.61 \pm 0.10) \times 10^6\ M^{-1}$ and $(2.69 \pm 0.07) \times 10^4\ M^{-1}$, respectively. Knowing the contributions of the neutral (K^0) and mono-anionic (K^-) forms of purpurin, one is now in a position to calculate K^* for purpurin binding to CT DNA at any pH. The results indicate that the negative charge on the anionic form of LH_3 (LH_2^-) holds the molecule back from interacting with CT DNA, which might have an impact on its overall potency.[58,60] If the generation of the negative charge on LH_3 is prevented then the overall binding constant (K^*) should increase allowing purpurin to have binding constants with CT DNA that are comparable to those reported for anthracyclines.[59] This is expected from a structure–function correlation that is today an important feature in understanding modern aspects in chemical biology.[60]

Table 4 Electrochemical properties of single step one-electron reduction of $Cu^{(II)}$–$(LH_2)_2$ in DMF

ν (V s^{-1})	i_{pa}/i_{pc}	$-E_{1/2}$ (V)
0.025	1.0500	0.817
0.050	1.0175	0.812
0.075	1.0283	0.804
0.100	1.1208	0.801
0.200	1.0536	0.805
0.300	1.0339	0.819
0.400	1.0641	0.809
0.500	1.0768	0.820
0.750	1.0414	0.818
1.000	1.0233	0.826

3.5 Interaction of $Cu^{(II)}$–$(LH_2)_2$ with CT DNA

3.5.1 By UV-Vis spectroscopy. $Cu^{(II)}$–$(LH_2)_2$ has a peak at 515 nm at physiological pH that gradually decreased in intensity on adding CT DNA. The spectra also show a slight blue shift by 4–7 nm (Fig. 3c). Interaction between the electronic states of the $Cu^{(II)}$–$(LH_2)_2$ chromophore and those of the DNA bases could be a reason for this hypsochromic shift.[23,24] These spectral features suggest that interaction between $Cu^{(II)}$–$(LH_2)_2$ and CT DNA was a case of intercalation through an ordered stacking of $Cu^{(II)}$–$(LH_2)_2$ between aromatic heterocyclic base pairs of the DNA helix.[23,24,32] π–π stacking and dipole–dipole interactions help to stabilize the [$Cu^{(II)}$–$(LH_2)_2$]–DNA adduct formed as a consequence of interaction between the electron-deficient quinones

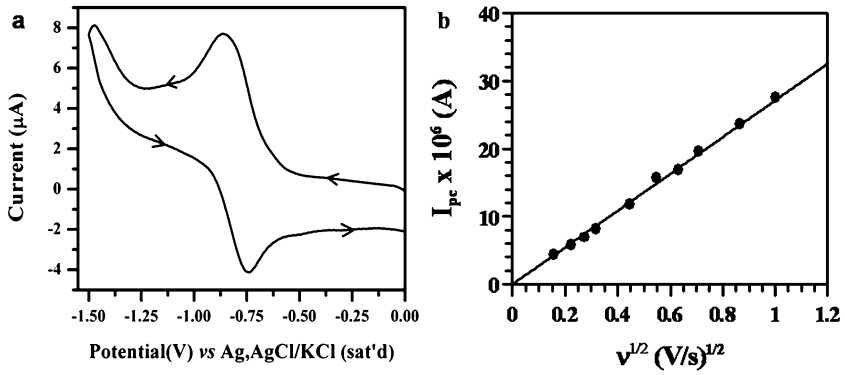

Fig. 2 (a) Cyclic voltammogram of 120 μM of $Cu^{(II)}$–$(LH_2)_2$ solution in DMF, recorded at 0.1 V s^{-1} potential sweep rate in 0.1 M TBAB as the supporting electrolyte, using the glassy carbon electrode (0.1256 cm^2) at 298 K. (b) Linear dependence of cathodic peak current on the square root of the potential sweep rate for the one step two electron reduction of $Cu^{(II)}$–$(LH_2)_2$ in DMF.

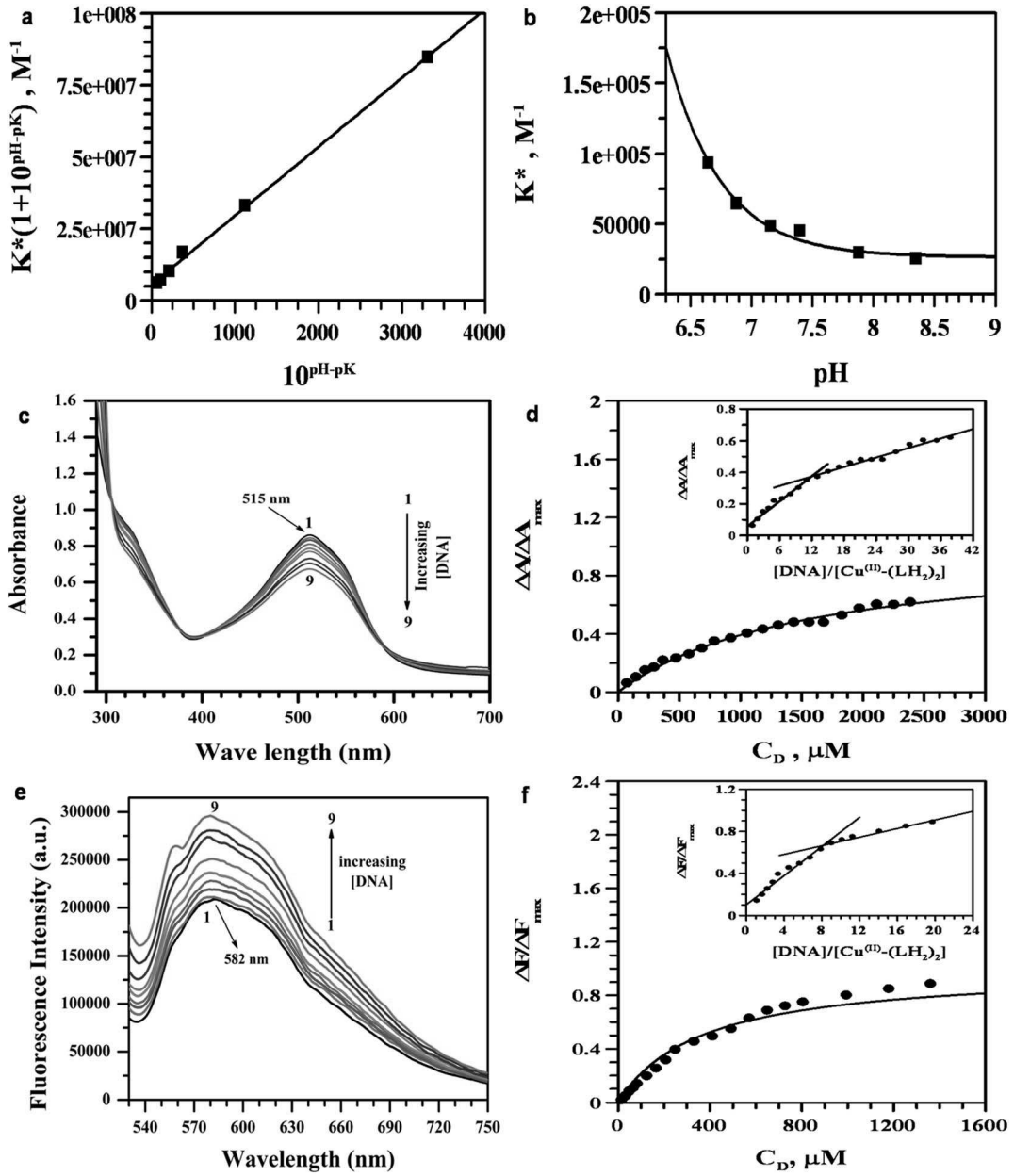

Fig. 3 (a and b) Dependence of intrinsic binding constants (K^*) for LH_3 interacting with CT DNA for a variation of pH in the medium. An average of all K^* values was considered for this plot. The solid line is the fitted data, which obeys eqn (8) [(a)] & eqn (9) [(b)]. [LH_3] = 75 μM; [NaCl] = 120 mM; [Tris buffer] = 15 mM; T = 298 K. (c) Absorbance spectrum showing interaction of $Cu^{(II)}$–$(LH_2)_2$ with CT DNA in the absence (1) and presence of (2) 296.83 μM, (3) 720.8729 μM, (4) 1218.027 μM, (5) 1682.03 μM, (6) 1974.56 μM, (7) 2523.05 μM, (8) 3027.66 μM, (9) 3493.46 μM CT DNA. (d) Binding isotherm for the spectrophotometric study of $Cu^{(II)}$–$(LH_2)_2$ with CT DNA and the corresponding non-linear fit. Inset, the mole ratio plot of the same; (e) Fluorescence spectrum of $Cu^{(II)}$–$(LH_2)_2$ interacting with CT DNA in the absence (1) and presence of (2) 15.50 μM, (3) 30.95 μM, (4) 77.14 μM, (5) 153.53 μM, (6) 304.04 μM, (7) 667.71 μM, (8) 1722.87 μM, (9) 2584.3 μM CT DNA. (f) Binding isotherm of fluorometric study of $Cu^{(II)}$–$(LH_2)_2$ with CT DNA and the corresponding non-linear fit. Inset, the mole ratio plot of the same; [$Cu^{(II)}$–$(LH_2)_2$] = 75 μM, [NaCl] = 120 mM; [Tris buffer] = 15 mM of pH 7.42; T = 298 K.

of $Cu^{(II)}$–$(LH_2)_2$ and electron-rich purine or pyrimidine bases of the DNA helix.[24]

The overall binding constant (K^*) was determined with the help of standard equations (ESI†) [shown in Fig. 3d, S7(a) and (b)†]. The results are summarized in Table 5. Under conditions of 1 : 1 compound–DNA adduct formation, the presence of excess CT DNA compared to $Cu^{(II)}$–$(LH_2)_2$, the Benesi–Hildebrand equation (eqn (10)) was used to determine K^*.[23,24,61]

$$\frac{A_0}{A - A_0} = \frac{\varepsilon_G}{\varepsilon_{H-G} - \varepsilon_G} + \frac{\varepsilon_G}{\varepsilon_{H-G} - \varepsilon_G} \frac{1}{K'[DNA]} \quad (10)$$

Table 5 Results of the binding parameters of $Cu^{(II)}$–$(LH_2)_2$ with CT DNA by spectroscopic techniques

Experiment	$K_{app} \times 10^{-3}$ (M^{-1}) from double-reciprocal plot	$K_{app} \times 10^{-3}$ (M^{-1}) from non-linear curve fitting	$K' \times 10^{-4}$ (M^{-1}) $= K_{app} \times n_b$	$K' \times 10^{-4}$ (M^{-1}) Scatchard plot	$K' \times 10^{-4}$ (M^{-1}) Benesi–Hildebrand double-reciprocal plot	n_b Scatchard plot
UV-Vis	3.55 ± 0.42	1.72 ± 0.50	3.84 ± 0.15	4.80 ± 0.20	1.60 ± 0.20	10.82 ± 0.20
Fluorimetry	5.23 ± 0.22	6.28 ± 0.30	4.49 ± 0.28	4.04 ± 0.33	—	8.58 ± 0.48

A_0 and A are absorbances of $Cu^{(II)}$–$(LH_2)_2$ in the absence and presence of CT DNA; ε_G and ε_{H-G} are absorption coefficients of $Cu^{(II)}$–$(LH_2)_2$ and its adduct with DNA, respectively. The plot of $A_0/(A - A_0)$ *versus* 1/[DNA] [Fig. S7(c)†] was linear. K* is reported in Table 5.

Upon complex formation, dissociation of the phenolic-OH at C_2 of LH_3 is retarded, with its pK value now being well beyond the physiological pH. As a result, formation of anionic species for $Cu^{(II)}$–$(LH_2)_2$ did not arise and we found that, at all pH values (in the physiological pH range), the complex not only had a higher binding constant compared to purpurin (LH_3), but more importantly the values remained constant over a considerable pH range.[60] This aspect has a lot of significance for cancer patients for whom fluctuations in body pH occurs.

3.5.2 By fluorescence spectroscopy. Interaction of $Cu^{(II)}$–$(LH_2)_2$ with CT DNA was followed at physiological pH by monitoring the increase in fluorescence upon adding CT DNA to a constant concentration of $Cu^{(II)}$–$(LH_2)_2$. An increase in fluorescence was an indication that the mode of interaction was intercalation, as observed earlier for LH_3.[23] The emission spectrum of $Cu^{(II)}$–$(LH_2)_2$ (Fig. 3e) exhibited a maximum at 582 nm, which was used to calculate the change in fluorescence (ΔF). Binding parameters for $Cu^{(II)}$–$(LH_2)_2$ with CT DNA were analyzed using the same equations as mentioned for the UV-Vis study. For the purpose of analysis, the change in fluorescence intensity (ΔF) was considered instead of ΔA (equations are provided in the ESI†). In the case of fluorescence, our approach was based on the assumption that fluorescence intensity was linearly proportional to the concentration of $Cu^{(II)}$–$(LH_2)_2$ bound to CT DNA. ΔF_{max} and K_{app} ($= K_d^{-1}$) were obtained from typical double reciprocal plots as the intercept and slope, respectively (Fig. S8(a)†). $\Delta F/\Delta F_{max}$ was plotted against concentration of CT DNA. Applying non-linear fitting, K_{app} ($= K_d^{-1}$) was obtained (Fig. 3f). Data obtained from fluorimetric titration of $Cu^{(II)}$–$(LH_2)_2$ with CT DNA was also analyzed according to Scatchard (Fig. S8(b)†).[62] The results are summarized in Table 5. The data obtained from fluorescence and UV-Vis studies corroborate each other.

3.6 *In vitro* activity of LH_3 and $Cu^{(II)}$–$(LH_2)_2$ on human topoisomerase enzymes

To check the inhibitory effects of LH_3 and $Cu^{(II)}$–$(LH_2)_2$ on human DNA topoisomerase I and human DNA topoisomerase II, DNA relaxation assays were performed using recombinant human DNA topoisomerase enzymes in the absence and presence of the compounds (Materials and Methods). The relaxation assay is based on the fact that supercoiled DNA molecules are relaxed by active topoisomerase enzymes, resulting in the formation of topoisomers of relaxed DNA molecules. These topoisomers migrate slowly compared to supercoiled plasmid DNA in agarose gel. Therefore, the activity of the enzymes may be checked by observing the gel bands for relaxed topoisomers. However, when the enzyme is inhibited, bands for the relaxed topoisomers do not appear on the gel. We found that $Cu^{(II)}$–$(LH_2)_2$ completely inhibited DNA topoisomerase I and DNA topoisomerase II relaxation activities at a concentration of 20 μM, while LH_3 had no effect at this concentration (Fig. 4a and b). We used established positive control inhibitors, CPT and DOX, for topoisomerase I and topoisomerase II enzymes, respectively. A kDNA decatenation assay was carried out for DNA topoisomerase II enzyme in the presence of LH_3 and $Cu^{(II)}$–$(LH_2)_2$. $Cu^{(II)}$–$(LH_2)_2$ inhibited the decatenation activity of DNA topoisomerase II enzyme at 20 μM, while LH_3 had no effect at this concentration (Fig. S9†). Therefore, our results suggest that $Cu^{(II)}$–$(LH_2)_2$ is a novel potent dual inhibitor of topoisomerase I and topoisomerase II enzymes *in vitro*, similarly to CPT and DOX. Thus $Cu^{(II)}$–$(LH_2)_2$ inhibit relaxation as well as decatenation activities of topoisomerase II enzymes.

3.7 *In vitro* stabilization of covalent cleavage complexes by LH_3 and $Cu^{(II)}$–$(LH_2)_2$

In order to find out the type of topoisomerase inhibitor that the complex is, plasmid cleavage assays were performed for topoisomerase I and topoisomerase II enzymes, as described in Materials and Methods. A plasmid cleavage assay is based on the stabilization of covalent complexes between the enzyme and DNA, which decreases mobility of DNA in agarose gel. This is because during complex formation DNA is nicked, and nicked plasmid DNA has a lower electrophoretic mobility than supercoiled plasmid DNA. Therefore, when an inhibitor is of type class I it would stabilize covalent complexes that could be observed on agarose gel. The concentration of LH_3 used was double (*i.e.* 40 μM) that of the complex [$Cu^{(II)}$–$(LH_2)_2$] (20 μM), in order to confirm the fact that the effect was due to the complex as a whole and not due to the free ligand. $Cu^{(II)}$–$(LH_2)_2$ stabilized the covalent enzyme–DNA complexes at 20 μM, while LH_3 had no effect on such complex formation, even when used at 40 μM. CPT, which stabilizes covalent topoisomerase I-DNA complexes was used as a positive control (Fig. 5a). We further checked the effect of LH_3 and $Cu^{(II)}$–$(LH_2)_2$ on topoisomerase II-DNA covalent complex formation and found that $Cu^{(II)}$–$(LH_2)_2$ completely stabilized the covalent topoisomerase II-DNA complex at 20 μM, while LH_3 had no effect, even when used at 40 μM. DOX was used as the positive control drug, since it is known to stabilize

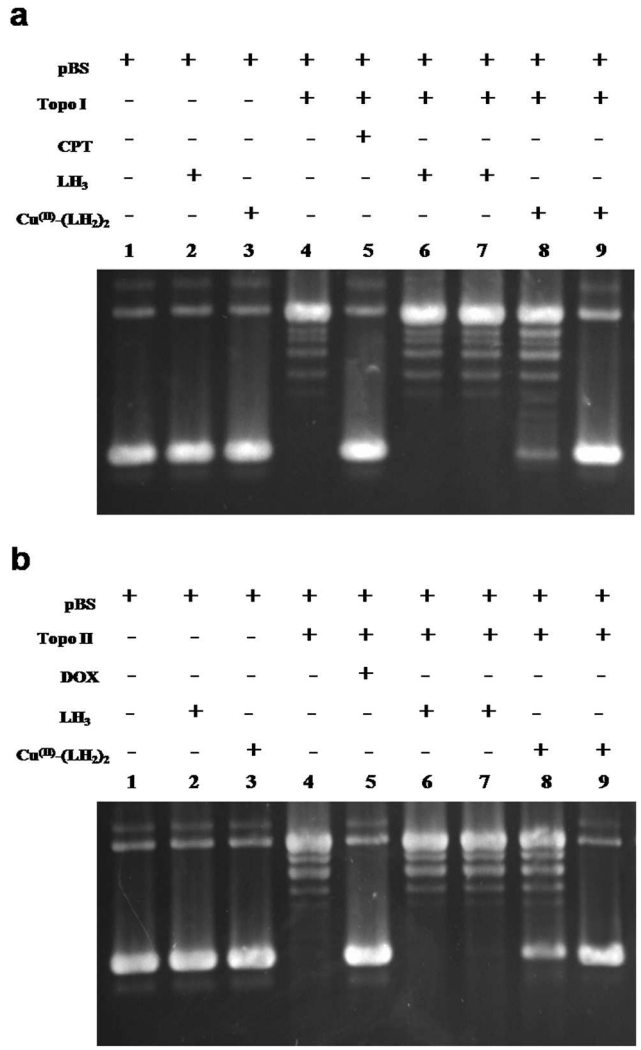

Fig. 4 DNA topoisomerase relaxation assays. (a) DNA topo I relaxation assay. Lane 1 is 100 fmol supercoiled pBS (SK^+) DNA; lane 2 is 100 fmol supercoiled pBS (SK^+) DNA with 40 μM LH_3; lane 3 is 100 fmol supercoiled pBS (SK^+) DNA with 40 μM $Cu^{(II)}$–$(LH_2)_2$; lane 4 is 100 fmol supercoiled pBS (SK^+) DNA with 50 fmol topoisomerase I enzyme; lane 5 is the same as lane 4 but with 10 μM CPT; lane 6 is the same as lane 4 but with 20 μM LH_3; lane 7 is the same as lane 4 but with 40 μM LH_3. Lane 8 is the same as lane 4 but with 10 μM $Cu^{(II)}$–$(LH_2)_2$; lane 9 is the same as lane 4 but with 20 μM $Cu^{(II)}$–$(LH_2)_2$. All the reactions were incubated at 37 °C for 30 minutes and analysed by agarose gel electrophoresis. (b) DNA topo II relaxation assay. Lane 1 is 100 fmol supercoiled pBS (SK^+) DNA; lane 2 is 100 fmol supercoiled pBS (SK^+) DNA with 40 μM LH_3; lane 3 is 100 fmol supercoiled pBS (SK^+) DNA with 40 μM $Cu^{(II)}$–$(LH_2)_2$; lane 4 is 100 fmol supercoiled pBS (SK^+) DNA with 50 fmol topoisomerase II enzyme; lane 5 is the same as lane 4 but with 10 μM DOX; lane 6 is the same as lane 4 but with 20 μM LH_3; lane 7 is the same as lane 4 but with 40 μM LH_3. Lane 8 is the same as lane 4 but with 10 μM $Cu^{(II)}$–$(LH_2)_2$; lane 9 is the same as lane 4 but with 20 μM $Cu^{(II)}$–$(LH_2)_2$. All the reactions were incubated at 37 °C for 30 minutes and analysed by agarose gel electrophoresis.

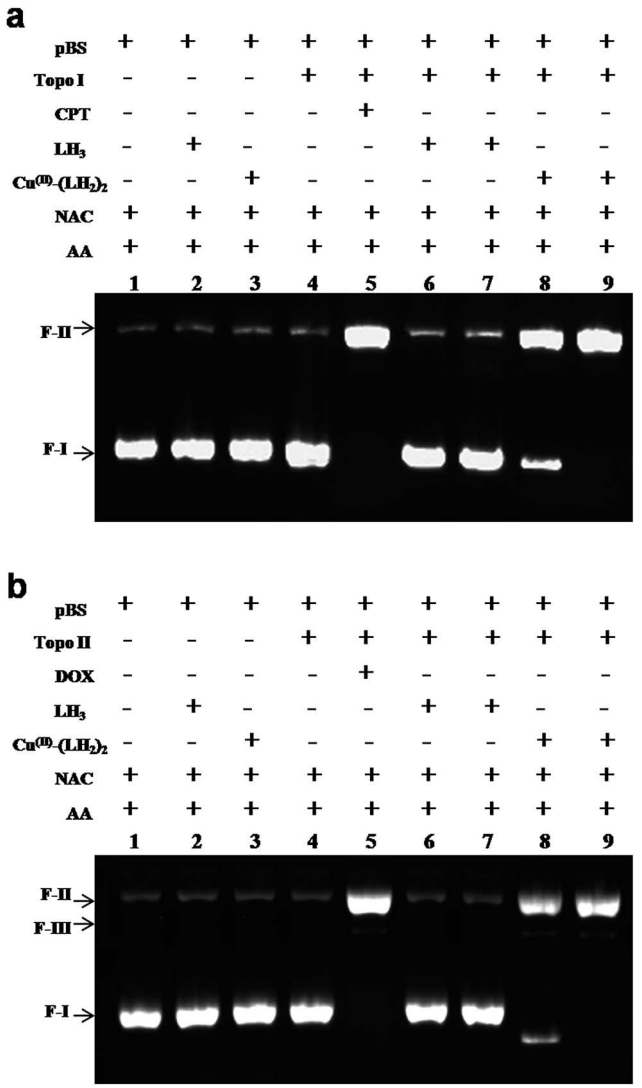

Fig. 5 Plasmid cleavage assays. (a) DNA topoisomerase I plasmid cleavage assay. All the cleavage assays were performed in the presence of NAC and ascorbic acid. Lane 1 is 100 fmol supercoiled pBS (SK^+) DNA; lane 2 is 100 fmol supercoiled pBS (SK^+) DNA with 40 μM LH_3; lane 3 is 100 fmol supercoiled pBS (SK^+) DNA with 40 μM $Cu^{(II)}$–$(LH_2)_2$; lane 4 is 100 fmol supercoiled pBS (SK^+) DNA with 500 fmol topoisomerase I enzyme; lane 5 is the same as lane 4 but with 10 μM CPT; lane 6 is the same as lane 4 but with 20 μM LH_3; lane 7 is the same as lane 4 but with 40 μM LH_3. Lane 8 is the same as lane 4 but with 10 μM $Cu^{(II)}$–$(LH_2)_2$; lane 9 is the same as lane 4 but with 20 μM $Cu^{(II)}$–$(LH_2)_2$. All the reactions were incubated at 37 °C for 30 minutes and stopped with 0.5% SDS. The enzyme was digested by proteinase K treatment and the reactions were analysed by agarose gel electrophoresis. (b) DNA topoisomerase II plasmid cleavage assay. Lane 1 is 100 fmol supercoiled pBS (SK^+) DNA; lane 2 is 100 fmol supercoiled pBS (SK^+) DNA with 40 μM LH_3; lane 3 is 100 fmol supercoiled pBS (SK^+) DNA with 40 μM $Cu^{(II)}$–$(LH_2)_2$; lane 4 is 100 fmol supercoiled pBS (SK^+) DNA with 500 fmol topoisomerase II enzyme; lane 5 is the same as lane 4 but with 10 μM DOX; lane 6 is the same as lane 4 but with 20 μM LH_3; lane 7 is the same as lane 4 but with 40 μM LH_3. Lane 8 is the same as lane 4 but with 10 μM $Cu^{(II)}$–$(LH_2)_2$; lane 9 is the same as lane 4 but with 20 μM $Cu^{(II)}$–$(LH_2)_2$. All the reactions were incubated at 37 °C for 30 minutes and stopped with 0.5% SDS. The enzyme was digested by proteinase K treatment and the reactions were analysed by agarose gel electrophoresis.

covalent topoisomerase II-DNA complexes (Fig. 5b). Since $Cu^{(II)}$–$(LH_2)_2$ generates ROS (although insignificant, discussed later), this could be responsible for DNA cleavage also. For this reason, cleavage assays were performed in the presence of NAC and AA,

which are well-recognized ROS scavengers.[63,64] With this result, one can now say that DNA cleavage was due to topoisomerase enzyme inactivation and not due to ROS generation (Fig. 5a and b). Together the results are interesting and allow us to speculate that $Cu^{(II)}$–$(LH_2)_2$ could be a novel poison (class I inhibitor) for topoisomerase I and topoisomerase II enzymes.

3.8 Effect of LH_3 and Cu(II)–$(LH_2)_2$ on viability of MOLT-4 cells

Since DOX and other topo II inhibitors like etoposide (ETO) are used in the treatment of ALL we checked the effects of LH_3 and $Cu^{(II)}$–$(LH_2)_2$ on acute lymphoblastic leukemia (ALL) MOLT-4 cells. MTT assays were performed with CPT (IC_{50} = 8.89 ± 0.19 μM), ETO (IC_{50} = 5.59 ± 0.23 μM) and DOX (IC_{50} = 5.25 ± 0.55 μM) (Fig. 6a). The same cell viability assay was also carried out for LH_3 and $Cu^{(II)}$–$(LH_2)_2$ on ALL MOLT-4 cells. We found that $Cu^{(II)}$–$(LH_2)_2$ kills MOLT-4 cells with an IC_{50} value of 18.59 ± 0.77 μM while the equivalent value for LH_3 was 26.35 ± 0.31 μM, suggesting that $Cu^{(II)}$–$(LH_2)_2$ was more potent than LH_3 (Fig. 6b). We suspect that enhanced cell killing by $Cu^{(II)}$–$(LH_2)_2$ was due to inhibition of the human DNA topoisomerase I and topoisomerase II enzymes present in the nucleus of MOLT-4 cells. Although IC_{50} for $Cu^{(II)}$–$(LH_2)_2$ in MOLT-4 cells was higher compared to CPT, ETO and DOX, since $Cu^{(II)}$–$(LH_2)_2$ produces relatively low ROS and exerts a novel dual inhibitory action on topoisomerase enzymes it could be developed as a useful and less costly alternative.

3.9 Intracellular stabilization of topoisomerase–DNA covalent complexes by $Cu^{(II)}$–$(LH_2)_2$

To check for intracellular stability of $Cu^{(II)}$–$(LH_2)_2$ and formation of intracellular enzyme–DNA complexes we performed topoisomerase I and topoisomerase II immunoband depletion assay (IDA). IDA is based on the fact that if a topoisomerase inhibitor stabilizes the covalent enzyme–DNA complex inside the cell then enzyme molecules become associated with chromatin and will not be detected in the immunoband of the enzyme. In such a situation, the immunoband for topoisomerases will be depleted in a time dependent manner. Our results for topoisomerase I and topoisomerase II immunoband depletion assays (Fig. 6c) clearly showed that $Cu^{(II)}$–$(LH_2)_2$ efficiently depletes the immunoband of both topoisomerase I and topoisomerase II after 12 hours of treatment with 20 μM $Cu^{(II)}$–$(LH_2)_2$. On the contrary, LH_3 did not deplete the immunoband after a similar 12 hour treatment with 40 μM (concentration of LH_3 used was double that of $Cu^{(II)}$–$(LH_2)_2$ in order to confirm that the effect was due to the complex and not the free ligand). These results indirectly indicate that $Cu^{(II)}$–$(LH_2)_2$ is stable inside the cellular environment and shows without any doubt that it efficiently inhibits topoisomerase I and topoisomerase II enzymes by stabilizing covalent enzyme–DNA complexes.

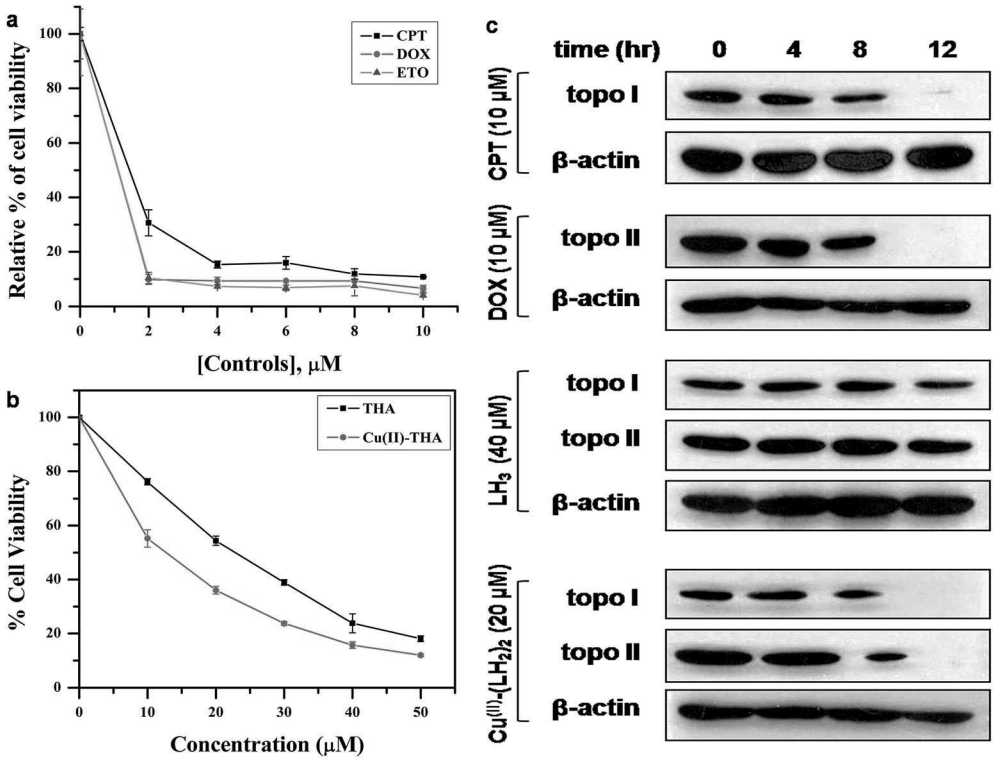

Fig. 6 (a) Plot showing effects of CPT, ETO and DOX on MOLT-4 cells. (b) Dose response curve for effects of LH_3 and $Cu^{(II)}$–$(LH_2)_2$ on MOLT-4 cells. In both cases, MOLT-4 cells were treated with the respective compounds for 72 hours and a MTT assay was performed. (c) Immuno band depletion assay. Cultured MOLT-4 Cells were treated with the indicated concentrations of the compounds and harvested at 0 hour, 4 hours, 8 hours and 12 hours post treatment. CPT (10 μM) and DOX (10 μM) were used as positive controls.

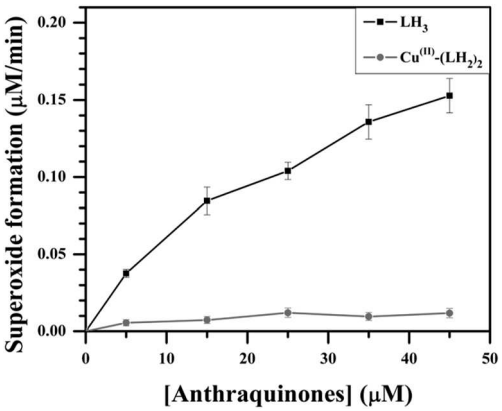

Fig. 7 Effect of LH_3 and $Cu^{(II)}$–$(LH_2)_2$ on superoxide formation by NADH dehydrogenase, determined spectrophotometrically by the rate of SOD-inhibitable cytochrome-c reduction at pH 7.4 Tris buffer; [SOD] = 40 μg ml^{-1}; [NADH] = 160 μM; [cytochrome c] = 80 μM; [NADH dehydrogenase] = 5 U per l.

3.10 NADH dehydrogenase assay of LH_3 and $Cu^{(II)}$–$(LH_2)_2$

Several studies have suggested that the aspect of cardiotoxicity associated with anthracycline anticancer drugs is related to the formation of reduced oxygen species like the superoxide radical anion.[1,10,11,16–18,26,27] It was shown earlier that metal complexes of anthracyclines generate less superoxide but are effective against tumors.[27] Keeping this in mind, we compared the generation of superoxide by LH_3 and $Cu^{(II)}$–$(LH_2)_2$ by measuring the reduction of cytochrome c inhibited by superoxide dismutase (SOD).[53] We found that on increasing the concentration of LH_3, the yield of $O_2^{-\bullet}$ increased (Fig. 7), suggesting that LH_3 catalyzed the flow of electrons from NADH to molecular oxygen through the enzyme NADH dehydrogenase. However, in the case of $Cu^{(II)}$–$(LH_2)_2$, the formation of $O_2^{-\bullet}$ decreased considerably (Fig. 7). In these reactions, the formation of superoxide ($O_2^{-\bullet}$) occurs when semiquinones are oxidized by molecular oxygen.[25–27] In the complex, the carbonyl at C_9 of LH_2^- is involved in coordinating Cu(II), leading to a substantial decrease in semiquinone formation. Only one carbonyl (C_{10}) on each LH_2^- is free to form semiquinones. Hence, much less semiquinone formation is expected for the complex. Moreover, owing to the presence of Cu(II) in the complex, the semiquinone formed quickly transfers its electron to the metal centre, leading to further decrease in its concentration.[54] This affects its interaction with molecular oxygen, leading to decreased $O_2^{-\bullet}$ formation.

4. Conclusions

A mononuclear complex of Cu(II) with LH_3 [$Cu^{(II)}$–$(LH_2)_2$] was prepared and characterized by physico-chemical and spectroscopic studies. Although a single crystal was not obtained, the structure was solved from X-ray powder diffraction data that was corroborated by a DFT study. Ours is the first reported crystal structure of any hydroxy-9,10-anthraquinone with a 3d-transition metal ion. Cyclic voltammetry of $Cu^{(II)}$–$(LH_2)_2$ in DMF showed one-electron reduction [$E_{1/2}$ = −0.810 V *vs.* Ag,AgCl/KCl (saturated)], which occurred at the quinone moiety of the ligand. The findings from cyclic voltammetry were corroborated by predictions from a DFT study that suggested redox processes would be quinone based. Physicochemical and electrochemical attributes of purpurin and its Cu(II) complex were similar to the anthracycline drug doxorubicin and its Cu(II) complex. The interaction of the complex with CT DNA suggests that, while in the case of purpurin the binding constant values decreased with increasing pH, complex formation could prevent this trend. For the complex, binding with CT DNA not only increased but remained constant over a wide range of pHs, improving the latter's applicability. *In vitro* DNA topoiomerase relaxation assays showed that [$Cu^{(II)}$–$(LH_2)_2$] was a dual poison for human DNA topoisomerase I and human DNA topoisomerase II enzymes, such as those known for CPT and DOX, which was a significant improvement following complex formation. DNA cleavage assays for topoisomerase I and topoisomerase II in the presence of the complex and known ROS scavengers revealed that DNA cleavage was due to the stabilization of the enzyme–DNA adduct and not due to ROS generation. With the help of ALL MOLT-4 cells, we could show that the complex inhibits topoisomerase I and topoisomerase II enzymes forming enzyme–DNA covalent complexes within the cells, as revealed by the results of the immunoband depletion assay. The NADH dehydrogenase assay performed for determining ROS generation by the compounds revealed that the generation of superoxide radicals by $Cu^{(II)}$–$(LH_2)_2$ was much lower than LH_3.

Since the complex was found to be more potent in killing ALL MOLT-4 cells than LH_3 and considering findings on DNA topoisomerase enzymes, it may be suggested that the complex targets topoisomerase I and topoisomerase II enzymes during anticancer activity. Findings from this study illustrate that $Cu^{(II)}$–$(LH_2)_2$ is a promising anticancer agent. Further understanding of the mode of action of the complex may rationally help to modify the chemical and biological properties to optimize anticancer activity.

Abbreviations

LH_3	Purpurin or 1,2,4-trihydroxy-9,10-anthraquinone
$Cu^{(II)}$–$(LH_2)_2$	Cu(II) complex of purpurin or LH_3
CT DNA	Calf thymus DNA
ROS	Reactive oxygen species
SOD	Superoxide dismutase
ETO	Etoposide
CPT	Camptothecin
DOX	Doxorubicin
NAC	*N*-Acetyl acetic acid
AA	Ascorbic acid

Acknowledgements

Financial support from DST, Govt. of West Bengal [794(Sanc.) 1(10) ST/P/S&T/9G-23/2013] in the form of a research project to

S. D. is gratefully acknowledged. P. D. expresses his gratitude to the University Grants Commision, Government of India for a research fellowship. C. K. J. also acknowledges the University Grants Commision, Government of India, for providing a research fellowship. S. D. offers his gratitude to Prof. Samita Basu, Head, CSD, SINP and former Head, Prof. Soumen Basak for allowing P. D. to carry out experiments on fluorescence and cyclic voltammetry. S. D. also wishes to thank Prof. Amitabha De and his student Ankan Dutta Chowdhury of CSD, SINP for their co-operation in carrying out cyclic voltammetry experiments.

References

1 G. Minotti, P. Menna, E. Salvatorelli, G. Cairo and L. Gianni, *Pharmacol. Rev.*, 2004, **56**, 185–229.
2 K. C. Chow, T. L. Macdonald and W. E. Ross, *Mol. Pharmacol.*, 1988, **34**, 467–473.
3 J. C. Wang, *Nat. Rev. Mol. Cell Biol.*, 2002, **3**, 430–440.
4 D. A. Koster, A. Crut, S. Shuman, M. Bjornsti and N. H. Dekker, *Cell*, 2010, **142**, 519–530.
5 Y. Pommier, *Chem. Rev.*, 2009, **109**, 2894–2902.
6 Y. Pommier, *Curr. Med. Chem.: Anti-Cancer Agents*, 2004, **5**, 429–434.
7 Y. Pommier, E. Leo, H. L. Zhang and C. Marchand, *Chem. Biol.*, 2010, **17**, 421–433.
8 Y. Pommier, *Nat. Rev. Cancer*, 2006, **6**, 789–802.
9 F. Arcamone and S. Penco, in *Anthracycline and Anthracenedione-Based Anticancer Agents*, ed. J. W. Lown, Elsevier, Amsterdam, 1988.
10 A. J. M. Ferreri, E. Campo, A. Ambrosetti, F. Ilariucci, J. F. Seymour, R. Willemze, G. Arrigoni, G. Rossi, A. Lopez-Guillermo, E. Berti, M. Eriksson, M. Federico, S. Cortelazzo, S. Govi, N. Frungillo, S. Dell'Oro, M. Lestani, S. Asioli, E. Pedrinis, M. Ungari, T. Motta, R. Rossi, T. Artusi, P. Iuzzolino, E. Zucca, F. Cavalli and M. Ponzoni, *Ann. Oncol.*, 2004, **15**, 1215–1221.
11 E. V. Barry, S. E. Lipshultz and S. E. Sallan, Anthracycline-induced cardiotoxicity: natural history, risk factors, and prevention, in *American Society of Clinical Oncology 2008 Educational Book*, ed. R. Govindan, American Society of Clinical Oncology, Alexandria, 2008, pp. 448–453.
12 K. Schimmel, D. Richel, R. van den Brink and H. J. Guchelaar, *Cancer Treat. Rev.*, 2004, **30**, 181–191.
13 M. I. Gharib and A. K. Burnett, *Eur. J. Heart Failure*, 2002, **4**, 235–242.
14 L. C. M. Kremer, E. C. V. Dalen, M. Offringa and P. A. Voute, *Ann. Oncol.*, 2002, **13**, 503–512.
15 S. M. Swain, F. S. Whaley and M. S. Ewer, *Cancer*, 2003, **97**, 2869–2879.
16 D. Iarussi, P. Indolfi, F. Casale, V. Martino, M. T. Di Tullio and R. Calabrò, *Pediatr. Drugs*, 2005, **7**, 67–76.
17 D. L. Keefe, *Semin. Oncol.*, 2001, **28**, 2–7.
18 D. Cardinale, A. Colombo, G. Lamantia, N. Colombo, M. Civelli, G. D. Giacomi, M. Rubino, F. Veglia, C. Fiorentini and C. M. Cipolla, *J. Am. Coll. Cardiol.*, 2010, **55**, 213–220.
19 J. L. Speyer, M. D. Green, A. Zeleniuch-Jacquotte, J. C. Wernz, M. Rey, J. Sanger, E. Kramer, V. Ferrans, H. Hochster and M. Meyers, *J. Clin. Oncol.*, 1992, **10**, 117–127.
20 A. Moreno-Aspitia and E. A. Perez, *Clin. Ther.*, 2009, **31**, 1619–1640.
21 T. Pecere, M. V. Gazzola, C. Mucignat, C. Parolin, F. D. Vecchia, A. Cavaggioni, G. Basso, A. Diaspro, B. Salvato, M. Carli and G. Palù, *Cancer Res.*, 2000, **60**, 2800–2804.
22 G. Cozza, M. Mazzorana, E. Papinutto, J. Bain, M. Elliott, G. di Maira, A. Gianoncelli, M. A. Pagano, S. Sarno, M. Ruzzene, R. Battistutta, F. Meggio, S. Moro, G. Zagotto and L. A. Pinna, *Biochem. J.*, 2009, **421**, 387–395.
23 P. Das, P. S. Guin, P. C. Mandal, M. Paul, S. Paul and S. Das, *J. Phy. Org. Chem.*, 2011, **24**, 774–785.
24 P. S. Guin, S. Das and P. C. Mandal, *J. Phys. Org. Chem.*, 2010, **23**, 477–482.
25 S. Das, A. Saha and P. C. Mandal, *Talanta*, 1996, **43**, 95–102.
26 M. M. L. Fialo and A. G. Suillerot, *Biochim. Biophys. Acta, Gen. Subj.*, 1985, **840**, 91–98.
27 H. Beraldo, A. Garnier-Suillerot, L. Tosi and F. Lavelle, *Biochemistry*, 1985, **24**, 284–289.
28 C. Santini, M. Pellei, V. Gandin, M. Porchia, F. Tisato and C. Marzano, *Chem. Rev.*, 2014, **114**, 815–862.
29 A. Kheirolomoom, L. M. Mahakian, C. Y. Lai, H. A. Lindfors, J. W. Seo, E. E. Paoli, K. D. Watson, E. M. Haynam, E. S. Ingham, L. Xing, R. H. Cheng, A. D. Borowsky, R. D. Cardiff and K. W. Ferrara, *Mol. Pharmaceutics*, 2010, **7**, 1948–1958.
30 M. D. Vaira, P. Orioli, F. Piccioli, B. Bruni and L. Messori, *Inorg. Chem.*, 2003, **42**, 3157–3159.
31 D. Cova, M. Sassano, E. Monti and F. Piccinini, *Arch. Toxicol.*, 1990, **64**, 597–598.
32 P. S. Guin, S. Das and P. C. Mandal, *J. Inorg. Biochem.*, 2009, **103**, 1702–1710.
33 *Solvent extraction in Textbook of Quantitative Chemical analysis*, ed. G. H. Jeffery, J. Bassett, J. Mendham and R. C. Denney, 5th edn, ELBS, Longman, Great Britain, 1989, pp. 178–184.
34 A. Altomare, C. Giacovazzo, A. Guagliardi, A. G. G. Moliterni, R. Rizzi and P. E. Werner, *J. Appl. Crystallogr.*, 2000, **33**, 1180–1186.
35 V. Favre-Nicolin and R. Cerny, *J. Appl. Crystallogr.*, 2002, **35**, 734. http://objcryst.sourceforge.net.
36 J. J. P. Stewart, *MOPAC 5.0*, A general purpose Molecular Orbital Package (QCEP 455).
37 A. C. Larson and R. B. Von Dreele, General Structure Analysis System (GSAS), Los Alamos National Laboratory Report LAUR (2000) 86–748.
38 B. H. Toby, *J. Appl. Crystallogr.*, 2001, **34**, 210–213.
39 A. D. Becke, *J. Chem. Phys.*, 1993, **98**, 5648–5652.
40 C. Lee, W. Yang and R. G. Parr, *Phys. Rev. B*, 1988, **37**, 785–789.
41 M. J. Frisch, G. W. Trucks, H. B. Schlegel, G. E. Scuseria, M. A. Robb, J. R. Cheeseman, G. Scalmani, V. Barone, B. Mennucci, G. A. Petersson, H. Nakatsuji, M. Caricato, X. Li, H. P. Hratchian, A. F. Izmaylov, J. Bloino, G. Zheng,

J. L. Sonnenberg, M. Hada, M. Ehara, K. Toyota, R. Fukuda, J. Hasegawa, M. Ishida, T. Nakajima, Y. Honda, O. Kitao, H. Nakai, T. Vreven, J. A. Montgomery Jr, J. E. Peralta, F. Ogliaro, M. Bearpark, J. J. Heyd, E. Brothers, K. N. Kudin, V. N. Staroverov, R. Kobayashi, J. Normand, K. Raghavachari, A. Rendell, J. C. Burant, S. S. Iyengar, J. Tomasi, M. Cossi, N. Rega, J. M. Millam, M. Klene, J. E. Knox, J. B. Cross, V. Bakken, C. Adamo, J. Jaramillo, R. Gomperts, R. E. Stratmann, O. Yazyev, A. J. Austin, R. Cammi, C. Pomelli, J. W. Ochterski, R. L. Martin, K. Morokuma, V. G. Zakrzewski, G. A. Voth, P. Salvador, J. J. Dannenberg, S. Dapprich, A. D. Daniels, O. Farkas, J. B. Foresman, J. V. Ortiz, J. Cioslowski and D. J. Fox, *Gaussian 09 Revision A.02*, Gaussian, Inc., Wallingford CT, 2009.

42 T. H. Dunning Jr and P. J. Hay, in *Modern Theoretical Chemistry*, ed. H. F. Schaefer, New York, 1976, vol. III, pp. 1–28.

43 P. J. Hay and W. R. Wadt, *J. Chem. Phys.*, 1985, **82**, 299–310.

44 N. M. O'Boyle, *GaussSum 2.1*, 2007, available at http://www.gausssum.sf.net.

45 N. M. O'Boyle, A. L. Tenderhol and K. M. Langner, *J. Comput. Chem.*, 2008, **29**, 839–845.

46 E. D. Glendening, A. E. Reed, J. E. Carpenter and F. Weinhold, *NBO version 3.1*, Theoretical Chemistry Institute, University of Wisconsin, Madison, WI, 2001.

47 A. E. Reed and F. Weinhold, *J. Chem. Phys.*, 1985, **83**, 1736–1740.

48 A. E. Reed, L. A. Curtiss and F. Weinhold, *Chem. Rev.*, 1988, **88**, 899–926.

49 F. Weinhold, in *Natural Bond Orbital Methods in Encyclopedia of Computational Chemistry*, ed. P. V. R. Schleyer, Wiley, UK, 1998, pp. 1792–1811.

50 D. A. Zhurko and G. A. Zhurko, *ChemCraft 1.5*, Plimus, San Diego, CA, p. 92130, http://www.chemcraftprog.com.

51 S. Roy, R. Banerjee and M. Sarkar, *J. Inorg. Biochem.*, 2006, **100**, 1320–1331.

52 S. Chakraborti, B. Bhattacharyya and D. Dasgupta, *J. Phys. Chem. B*, 2002, **106**, 6947–6953.

53 H. R. Mahler, in *Methods in Enzymology 11*, ed. S. P. Colowick and N. O. Kaplan, Academic Press, New York, 1955, pp. 668–672.

54 S. Das, A. Bhattacharya, P. C. Mandal, M. C. Rath and T. Mukherjee, *Radiat. Phys. Chem.*, 2002, **65**, 93–100.

55 J. E. B. Randles, *Trans. Faraday Soc.*, 1948, **44**, 322–327.

56 A. J. Bard and L. R. Faulkner, *Electrochemical Methods Fundamental and Applications*, John Wiley & Sons, New York, 2nd edn, 2001.

57 R. S. Nicholson, *Anal. Chem.*, 1966, **38**, 1406.

58 S. Mukherjee, P. Das and S. Das, *J. Phys. Org. Chem.*, 2012, **25**, 385–393.

59 F. Frezard and G. Suillerot, *Biochim. Biophys. Acta, Gen. Subj.*, 1990, **1036**, 121–127.

60 S. Mukherjee, P. Gopal, S. Paul and S. Das, *J. Anal. Oncol.*, 2014, 3.

61 H. A. Benesi and J. H. Hildebrand, *J. Am. Chem. Soc.*, 1949, **71**, 2703–2707.

62 G. Scatchard, *Ann. N. Y. Acad. Sci.*, 1949, **51**, 660–672.

63 S. M. Attia, *Arch. Toxicol.*, 2012, **86**, 725–731.

64 S. Belin, F. Kaya, G. Duisit, S. Giacometti, J. Ciccolini and M. Fontés, *PLoS One*, 2009, **4**(2), e4409, DOI: 10.1371/journal.pone.0004409.

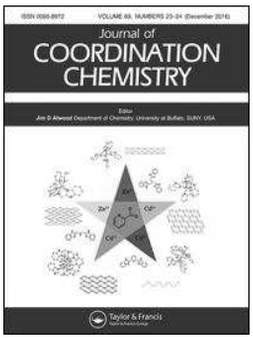

Journal of Coordination Chemistry

ISSN: 0095-8972 (Print) 1029-0389 (Online) Journal homepage: www.tandfonline.com/journals/gcoo20

Model studies on the interactions of a Cu(II)-quinone complex with surfactant micelles and DNA explore its induction of apoptosis in human MDA-MB-231 breast adenocarcinoma cells

Sanjay Roy, Gayathri Loganathan, Dhanasekaran Dharumadurai, Mohammad A. Akbarsha & Guin Partha Sarathi

To cite this article: Sanjay Roy, Gayathri Loganathan, Dhanasekaran Dharumadurai, Mohammad A. Akbarsha & Guin Partha Sarathi (2017) Model studies on the interactions of a Cu(II)-quinone complex with surfactant micelles and DNA explore its induction of apoptosis in human MDA-MB-231 breast adenocarcinoma cells, Journal of Coordination Chemistry, 70:12, 2128-2147, DOI: 10.1080/00958972.2017.1330466

To link to this article: https://doi.org/10.1080/00958972.2017.1330466

JOURNAL OF COORDINATION CHEMISTRY, 2017
VOL. 70, NO. 12, 2128–2147
https://doi.org/10.1080/00958972.2017.1330466

Taylor & Francis
Taylor & Francis Group

Model studies on the interactions of a Cu(II)-quinone complex with surfactant micelles and DNA explore its induction of apoptosis in human MDA-MB-231 breast adenocarcinoma cells

Sanjay Roy[a], Gayathri Loganathan[b], Dhanasekaran Dharumadurai[b], Mohammad A. Akbarsha[c,d] and Guin Partha Sarathi[a]

[a]Department of Chemistry, Shibpur Dinobundhoo Institution (College), Howrah, India; [b]Department of Microbiology, School of Life Sciences, Bharathidasan University, Tiruchirappalli, India; [c]Mahathma Gandhi-Doerenkamp Center, Bharathidasan University, Tiruchirappalli, India; [d]Department of Food Science and Nutrition, College of Food Science and Agriculture, King Saud University, Riyadh, Kingdom of Saudi Arabia

ABSTRACT

The interactions of copper complex (CuQ_2) of 1-amino-4-hydroxy-9, 10-anthraquinone (QH) with calf thymus DNA, anionic surfactant sodium dodecyl sulfate (SDS), and cationic surfactant cetyltrimethylammonium bromide (CTAB) were investigated in an aqueous solution at physiological pH (7.4). Affinities of such molecule to DNA and surfactant micelles, a model for a biological membrane, are important in determining its biological action. Using different models, various binding parameters were evaluated in both of molecule–DNA interaction and molecule–surfactant interaction. The study showed that hydrophobic interaction plays a major role in the binding of CuQ_2 to surfactant micelles. In addition, the hydrophobic interaction has an important role in the distribution of CuQ_2 between micelle-water phases. Gibbs free energy for the binding and distribution of CuQ_2 between the bulk aqueous medium and surfactant micelles were calculated. In order to correlate the physicochemical properties deciphered from the aforementioned studies with the biological property of the molecule, CuQ_2 was treated with MDA-MB-231 breast adenocarcinoma cells where it was found that the molecule affects the viability of the cancer cells. Fluorescent staining of the treated cells with AO/EB and Hoechst indicated that the CuQ_2 induces apoptosis, suggesting its use in the treatment of breast cancer.

ARTICLE HISTORY
Received 28 February 2017
Accepted 26 April 2017

KEYWORDS
CuQ_2; SDS; CTAB; DNA; apoptosis

CONTACT Guin Partha Sarathi parthasg@gmail.com
Supplemental data for this article can be accessed at https://doi.org/10.1080/00958972.2017.1330466.

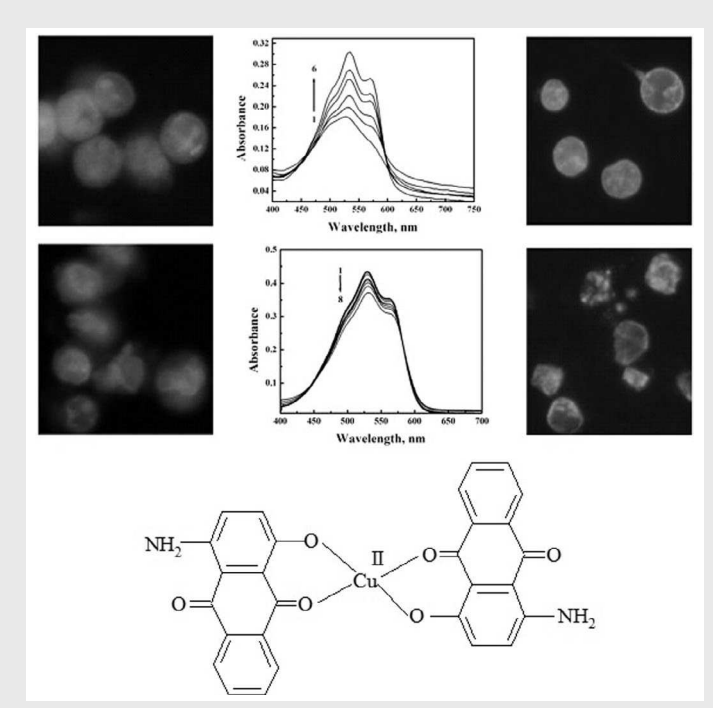

1. Introduction

Anthracyclines are most widely used effective antineoplastic drugs and are active against a wide variety of solid tumors and hematological malignancies including leukemia, lymphoma, breast cancer, lung cancer, multiple myeloma, and sarcoma. Unfortunately, their clinical use is hindered by tumor resistance and a cumulative dose-dependent cardiotoxicity, which can cause irreversible heart failure and high mortality [1–4]. Cardiotoxicity is due to the ability of anthracyclines to catalyze the flow of electrons from nicotinamide adenine dinucleotide (NAD) to molecular oxygen forming superoxide radicals through NADH dehydrogenase. The quinone moiety present in these drugs after one electron reduction forms a semiquinone which reacts with molecular oxygen to produce the superoxide radicals [5–9]. Studies have shown that metal complexes reduce the chances of formation of superoxide radicals in comparison to free drug molecules which is the reason that metal complexes are less toxic than the free drugs [5–9]. To reduce the toxic side effects of these drugs, several passive drug delivery systems such as nanoparticles [10], synthetic polymers [11, 12], liposomes [13, 14], and polymeric micelles [14–18] are employed to preserve or enhance efficacy against tumor cells while limiting exposure to critical target sites such as myocardium and bone marrow [19]. At the same time, the use of liposomes and polymeric micelles as drug carriers makes the studies on the interaction of drugs with micellar systems to be important, implying the elucidation of the characteristics of these interactions. Surfactants that form associate structure in aqueous as well as in nonaqueous solution above a certain concentration are called micelles and this phenomenon is known as critical micelles concentration (cmc) [20–22]. The addition of additives into an aggregate of amphiphiles will affect its physicochemical characteristics such as the degree of ionization, reaction rates as well as phase separation

[23–25]. A previous study [26] on the inclusion of adriamycin into polymeric micelles showed that electrostatic and hydrophobic interactions play a key role in ensuring its enhanced accumulation in the tumor tissue and a higher *in vivo* antitumor activity.

A second limitation of the use of these drugs is their high cost and it is particularly true for the cancer patients belonging to the third world countries. This encouraged many investigators to find cheaper substitutes for expensive anthracyclines. Earlier studies [9, 27-39] showed that less expensive and simple analogs of anthracyclines mimic the chemistry of established anthracycline drugs which inspired us to work further with a copper complex of 1-amino-4-hydroxy-9,10-anthraquinone (CuQ_2) in order to find if it could be developed as a less expensive alternative to anthracyclines.

Though several mechanisms of drug action were proposed, the anti-proliferative activity of anthracyclines is mostly related to topoisomerase II inhibition, which occurs as a result of intercalation of anthracycline between adjacent DNA-base pairs [1]. Many other studies also showed that the interaction of molecules with DNA is related to their anticancer actions [40, 41]. It is interesting to note that though there are several studies on anthracyclines concentrated on DNA and surfactant micelles, there is still no report on the interaction of metal complex of anthracyclines with surfactants. Thus, a model study on the interactions of the copper complex (CuQ_2) of 1-amino-4-hydroxy-9,10-anthraquinone (QH) with cationic and anionic surfactants would be an important contribution to the area of anthracycline research. The aim of the present paper has been to correlate the results obtained from interactions of CuQ_2 with calf thymus DNA (ct DNA), anionic surfactant sodium dodecyl sulfate (SDS), and cationic surfactant cetyltrimethylammonium bromide (CTAB) with its ability to induce apoptosis in MDA-MB-231 breast adenocarcinoma cells, with the expectation that a promising result may point to the use of the present molecule as a substitute for the expensive anthracycline drugs. In the present study, apoptosis was assayed adopting acridine orange (AO)/ethidium bromide (EB) and Hoechst 33258 staining methods as reported earlier [42].

2. Experimental

2.1. Materials and instrumentation

The copper(II) complex (CuQ_2) of 1-amino-4-hydroxy-9,10-anthraquinone (96%, purchased from Alfa Aesar, Germany) was prepared and characterized adopting our methods described earlier [9]. Since CuQ_2 is almost insoluble in water, a stock solution of 10 mM CuQ_2 was prepared in anhydrous dimethylsulfoxide (SRL, India). For the experiments in aqueous media, solutions were prepared by diluting the above stock in triple distilled water. Since CuQ_2 in solution is sensitive to light, all CuQ_2 solutions were prepared just before the experiment and kept in the dark. Extra-pure sodium salt of ct DNA (product code: 68451) was purchased from Sisco Research Laboratory Pvt. Ltd., India. After dissolving it in buffer, purity was checked from the absorbance ratio A_{260}/A_{280}. For all the solutions, the ratio (A_{260}/A_{280}) was in the range $1.8 < A_{260}/A_{280} < 1.9$ and provided a good indication of purity [43]. The concentration of ct DNA (in nucleotide) was determined by taking $\varepsilon_{260} = 6600\ M^{-1}\ cm^{-1}$ for ct DNA. The single-stranded DNA was prepared by boiling double-stranded ct DNA on a water bath at 100 °C for 5 min followed by rapid cooling in an ice bath as described earlier [44]. CTAB (Extra-pure AR grade, product code: 010323-100G), obtained from Spectrochem, India, and SDS (Extra-pure AR grade, product code: 61841905001730), obtained from E-Merck, India, were used without purification. N-[2-Hydroxyethyl]piperazine-N-[2-ethane sulfonic acid] buffer (Hepes

buffer, extra-pure for biochemistry, product code: 7365-45-9 obtained from Sisco Research Laboratories Pvt. Ltd., India) and phosphate buffer solution (prepared from disodium hydrogen phosphate, AR, CAS Number 10028-24-7, Sigma Aldrich, USA) were used to maintain the pH (7.4) of the solution in studying the interaction of the compound with ct DNA and surfactants, respectively. NaCl (BioXtra, ≥99.5% (AT), CAS Number 7647-14-5, Sigma Aldrich, USA), and NaOH (BioXtra, ≥98% (acidimetric), pellets (anhydrous), CAS Number 1310-73-2, Sigma Aldrich, USA) were used in the study. Dimethylsulfoxide (DMSO) (99.0%, Spectrochem, India) was first dried over fused $CaCl_2$ for 3–4 days, decanted, and then distilled under reduced pressure [45]. All other reagents used were of AR grade. Aqueous solutions were prepared in triple distilled water. UV–Vis spectra of CuQ_2 were recorded on a UV-1700 Pharmaspec, Shimadzu, Japan.

2.2. Cell culture

The MDA-MB-231 human breast adenocarcinoma cells were obtained from the National Center for Cell Science (NCCS), Pune, India. Cells were cultured in DMEM medium (Sigma–Aldrich, St. Louis, MO, USA), supplemented with 10% fetal bovine serum (Gibco) and 100 U/mL penicillin and 100 µg/mL streptomycin as antibiotics (Gibco), in 96 well culture plates at 37 °C in a humidified atmosphere of 5% CO_2 in a CO_2 incubator (Thermo Scientific, USA). All experiments were performed using cells from passage 15 or less.

2.3. Cytotoxicity assay (MTT assay)

CuQ_2 in the concentration range 20–200 µM, dissolved in DMSO, was added to the wells 24 h after seeding of 5×10^3 cells, MDA-MB-231 and HBL-100, separately, per well in 200 µL of fresh culture medium. DMSO solution was used as solvent control. A miniaturized viability assay using 3-(4,5-di-methylthiazol-2-yl)-2,5-diphenyl-2H-tetrazolium bromide (MTT) was carried out according to the method described by Mosmann [46]. After 24 and 48 h, respectively, 20 µL of MTT solution [5 mg/mL in phosphate-buffered saline (PBS)] was added to each well and the plates were wrapped with aluminum foil and incubated for 4 h at 37 °C. The purple formazan product was dissolved in 100 µL of DMSO added to each well. The absorbance was monitored at 570 nm (measurement) and 630 nm (reference) using a 96-well plate reader (Bio-Rad, Hercules, CA, USA). Data were collected for three replicates each and used for calculating the mean. Percentage inhibition was calculated from this data using the formula:

$$\text{Percentage inhibition} = \frac{[\text{Mean OD of untreated cells (control)} - \text{Mean OD of treated cells (treat)}] \times 100}{\text{Mean absorbance of untreated cells (control)}}$$

The IC_{50} values for the respective durations were obtained from the standard graph that was plotted.

2.4. Acridine orange and ethidium bromide staining

Acridine orange and ethidium bromide staining was performed according to Spector *et al.* [47]. Each well containing 5×10^5 MDA-MB-231 cells was treated with CuQ_2 at its IC_{50} for 24 h

when DMSO solution was used as solvent control. Afterward, the cells were stained with 25 µL of AO and EB solution (3.8 µM of AO and 2.5 µM of EB in PBS) and examined in a fluorescent microscope (Carl Zeiss, Jena, Germany) using an UV filter (450–490 nm). Three hundred cells per sample were counted in triplicate for each dose point. The cells were scored as viable, apoptotic, or necrotic as judged by the staining, nuclear morphology, and membrane integrity. Percentages of apoptotic and necrotic cells were then calculated. Morphological changes were also observed and photographed.

2.5. Hoechst 33528 staining

The MDA-MB-231 human breast carcinoma cells were cultured in a 6-well plate and treated with 24h IC_{50} concentration of CuQ_2. After 24-h incubation, the treated and untreated cells were harvested and stained with Hoechst 33258 (1 mg/mL, aqueous) [48] for 5 min at room temperature. A drop of cell suspension was placed on a glass slide, and a cover slip was laid over to reduce diffraction of light. At random 300 cells, in duplicate, were observed at ×400 in a fluorescent microscope (Carl Zeiss, Jena, Germany), and the percentage of cells reflecting pathological changes was calculated.

3. Results and discussion

3.1. Interaction of CuQ_2 with SDS

Interaction of CuQ_2 with anionic surfactant SDS was studied by UV–Vis spectroscopy in premicellar and micellar range of concentrations. In the absence of surfactant, absorption spectrum of CuQ_2 shows an absorption peak at 530 nm corresponding π*–π* and n–π* as characterized in our recent study [9]. The binding constant for the interaction of CuQ_2 with SDS surfactant micelles was determined by monitoring the absorption peak at 530 nm of a series of solutions containing a constant concentration of CuQ_2 and increasing concentrations of SDS. The experimental measurements were made after 1 to 2 min from the mixing of SDS with CuQ_2. Upon dissolution of CuQ_2 in aqueous buffer (pH 7.4), there would be the possibility of dissociation of CuQ_2 according to equation (2) to result in one Cu^{2+} and two 1-amino-4-hydroxy-9,10-anthraquinone ions [49].

$$CuQ_2 = Cu^{2+} + 2Q^{-}$$

However, owing to the very high stability constant (7.27×10^{16}) of CuQ_2 [9], the possibility that CuQ_2 would dissociate in solution giving Cu^{2+} and $2Q^{-}$ is almost negligible. It would be ~0.0409 µM for Cu^{2+} and ~0.0818 µM for free ligand for an initial concentration of CuQ_2 = 20 µM used in UV–Vis spectroscopy study. Therefore, almost the entire CuQ_2, i.e., 99.79% would be present in solution as CuQ_2 itself during the course of titration with SDS.

The UV–Vis spectra of CuQ_2 in the absence and presence of different concentrations of SDS are shown in figure 1a. The critical micelle concentration (CMC) of SDS in the presence of CuQ_2 was determined by monitoring the change in absorption spectra of CuQ_2. It was observed as 1.0×10^{-4} M and used throughout the calculations. This value is lower than the CMC value of SDS in pure water (8.08×10^{-3} M) and that in 50 mM phosphate buffer (1.99×10^{-3} M) [50], which is due to the influence of different ions and molecules present in the media [51]. The variation of absorbance at 530 nm as a function of surfactant

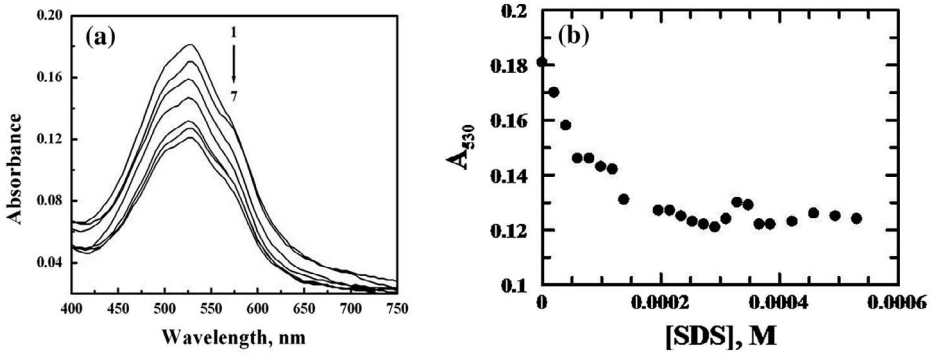

Figure 1. (a) Absorption spectra of CuQ_2 (20 μM) in the absence (curve 1) and in the presence of increasing concentrations of SDS: 19.56 μM (curve 2), 39.84 μM (curve 3), 59.64 μM (curve 4), 138.07 μM (curve 5), 196.84 μM (curve 6), 310.08 μM (curve 7). [Phosphate buffer] = 100 mM, pH 7.4, T = 298.15 K. (b) Absorbance at 530 nm of CuQ_2 as a function of SDS concentration.

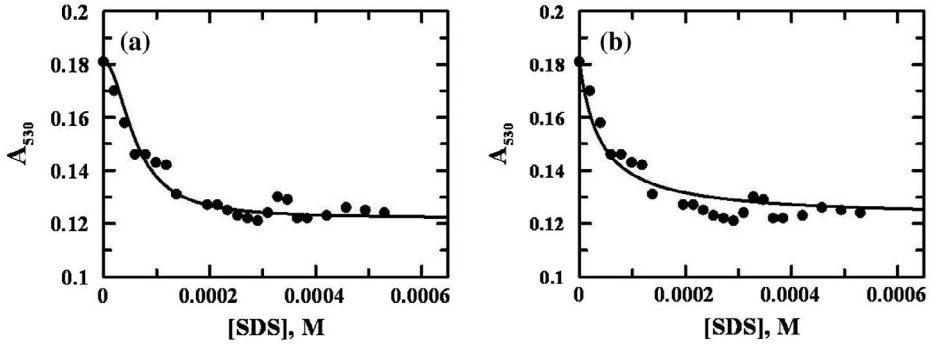

Figure 2. (a) Nonlinear fitting of the absorbance at 530 nm using equation (1) considering 1:2 interaction between CuQ_2 and SDS. (b) Nonlinear fitting of the absorbance at 530 nm using equation (2) considering 1:1 interaction between CuQ_2 and SDS.

concentration is shown in figure 1b which shows that the absorbance at 530 nm decreases with the increase in SDS concentration and reaches a saturation level after a certain concentration of SDS. This may be interpreted as due to incorporation of CuQ_2 molecules into SDS micelles. The interaction of CuQ_2 with SDS was further established using cyclic voltammetry, which showed that the reduction peak current of CuQ_2 at −695 mV decreases with an increase in the SDS concentration (figure S1) as observed in spectrometric studies. Thus, this also justifies the incorporation of CuQ_2 molecules into SDS micelles. The binding isotherm in spectrometric study was analyzed by nonlinear fit by assuming 1:2 and 1:1 interactions between CuQ_2 and SDS using equations (1) and (2), respectively (figure 2), and the binding constants were obtained as $K = (2.79 \pm 0.05)\times10^8\ M^{-1}$ for 1:2 interaction and $2.56(\pm0.04)\times10^4\ M^{-1}$ for 1:1, respectively [52, 53]. Considering the nature of the fitting of the experimental results according to equations (1) and (2) [52–54], shown in figure 2, one may conclude that the 1:2 interaction between CuQ_2 and SDS is probably more favorable than 1:1 interaction,

$$A = \frac{A_0 + A_\infty K[L^2]}{1 + K[L^2]} \tag{1}$$

$$A = \frac{A_0 + A_\infty K[L]}{1 + K[L]} \tag{2}$$

where L is the surfactant (here SDS), A and A_0 are the measured absorbances at 530 nm of CuQ_2 in the presence and absence of surfactant, respectivey, while A_∞ is the absorbance of CuQ_2 bound to surfactant.

The Gibbs free energy for the binding of CuQ_2 to the SDS surfactant micelles was evaluated by applying equation (3) [54],

$$\Delta G^0 = -RTlnK \tag{3}$$

where R is the molar gas constant and T is the absolute temperature (298.15 K). The Gibbs free energy values were found as −48.20 KJ mol^{-1} for 1:2 interaction and −25.16 KJ mol^{-1} for 1:1 interaction of CuQ_2 to the surfactant. Thus, the free energy for 1:2 interaction is almost double that for 1:1 interaction, suggesting that 1:2 interaction is more favorable than 1:1 interaction between CuQ_2 and surfactant.

A previous study [53] showed that the binding constants for 1:2 and 1:1 interactions between cationic anthracycline drug, mitoxantrone and anionic surfactant SDS are $6.84(\pm0.76) \times 10^7$ M^{-1} and $1.14(\pm0.05) \times 10^3$ M^{-1}, respectively. The binding constant for 1:1 interactions between cationic anthracycline drug, doxorubicin hydrochloride (adriamycin) and anionic surfactant, sodium lauryl sulfate, by two different methods were determined as 295 and 274 M^{-1} [55]. Enache and co-workers established that the interaction of cationic mitoxantrone or doxorubicin hydrochloride and anionic sodium dodecyl sulfate or sodium lauryl sulfate micelles consists of both electrostatic and hydrophobic contributions [53, 55].

Comparing the results of the present study with earlier ones [53, 55], it is clear that the binding constants for both the 1:2 and 1:1 interactions between CuQ_2 and SDS are significantly higher than those found in mitoxantrone and doxorubicin hydrochloride. It is interesting to note that though the molecule of interest in this study (CuQ_2) is uncharged, its interaction with anionic SDS micelles is stronger than that found between a cationic drug (mitoxantrone or doxorubicin hydrochloride) and anionic surfactant sodium dodecyl sulfate or sodium lauryl sulfate [53, 55]. However, the presence of Cu^{2+} at the center of CuQ_2 may result in an electrostatic contribution in addition to hydrophobic interaction between CuQ_2 and SDS due to the presence of the larger hydrophobic tail of SDS molecules .

Along with the measurement of binding constant and stoichiometry, the compound–surfactant interaction was further characterized by determining the partition coefficient (K_X), which is a thermodynamic parameter representing the affinity of a given compound to penetrate into the micellar phase from the aqueous phase. This is an important parameter elucidating the mechanism of solubilization of a drug molecule and definitely helps in understanding the biological phenomena like interaction between drugs and biological membranes. By applying the pseudo-phase model, the partition coefficient was determined using equation (4) [48, 56, 57],

$$\frac{1}{\Delta A} = \frac{1}{\Delta A_\infty} + \frac{1}{K_X A_\infty([L] + C_T - \mathrm{CMC}} \tag{4}$$

where $\Delta A = A - A_0$, $\Delta A_\infty = A_b - A_0$ and $n_w = 55.5$ M is the molarity of water. The value of K_X was obtained from the slope of the plot of $1/\Delta A$ versus $1/([SDS]+C_T-CMC)$ (figure S2) and it is $2.15(\pm 0.04) \times 10^6$. It is important to mention here that this linear relation holds good in a very high surfactant concentration region below which the curve tends to bend upward with decreasing surfactant concentration. This deviation from linearity was due to the approximation made in the evaluation of equation (4) [57].

The standard free energy change for the transfer of CuQ_2 from the bulk aqueous phase to micellar phase was obtained as –36.14 KJ mol^{-1} by putting the value of K_X in equation (5) [58].

$$\Delta G_x^0 = -RT \ln K_X \tag{5}$$

Comparison of the partition coefficient of CuQ_2 in the present study with the distribution of mitoxantrone in an earlier study [53] between water and SDS micelles clearly shows that the former has greater value of the partition coefficient than the latter. These results indicate that electrostatic as well as hydrophobic interactions have a significant role in the distribution of CuQ_2 between micelle/water phases as mentioned above.

3.2. Interaction of CuQ_2 with CTAB

The binding constant for the interaction of CuQ_2 with CTAB surfactant micelles and micelle – water partition coefficient were determined using UV–Vis spectroscopy by monitoring the absorbance at 530 nm of a series of solutions containing a constant concentration of CuQ_2 and increasing concentrations of CTAB. Experimental measurements were made after 1 to 2 min from the mixing of CTAB with CuQ_2 to ensure the attainment of equilibrium. The UV–Vis spectra of CuQ_2 in the absence and in the presence of different concentrations of CTAB are shown in figure 3a. This clearly shows that the absorbance of CuQ_2 at 530 nm increases gradually with an increase in the CTAB concentration. The interaction of CuQ_2 with CTAB was further established using cyclic voltammetry, which showed that the reduction peak current of CuQ_2 at –695 mV increases with an increase in the CTAB concentration (figure S3) as observed in spectrometric studies. This also justifies the incorporation of CuQ_2 molecules

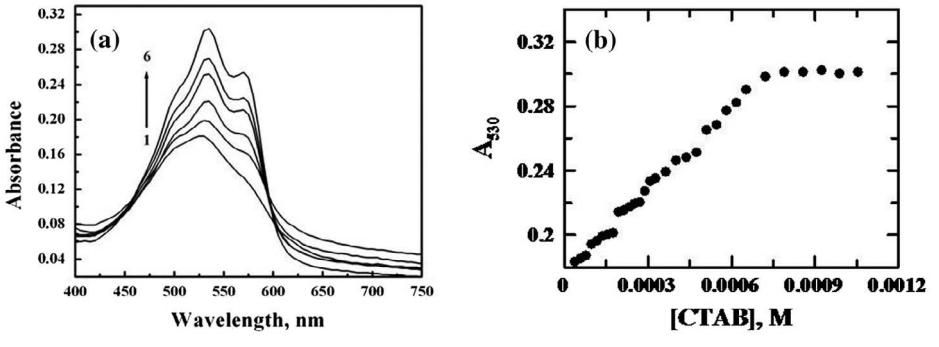

Figure 3. (a) Absorption spectra of CuQ_2 (20 μM) in the absence (curve 1) and in the presence of increasing concentrations of CTAB: 157.48 μM (curve 2), 272.37 μM (curve 3), 403.07 μM (curve 4), 476.19 μM (curve 5), 791.90 μM (curve 6). [Phosphate buffer] = 100 mM, pH 7.4, T = 298.15 K. (b) Absorbance at 530 nm of CuQ_2 as a function of CTAB concentration.

into CTAB micelles. In the spectrometric studies, the determination of CMC of CTAB in the presence of CuQ_2 was based on the change in absorption spectra of CuQ_2, which indicates the beginning of micelle formation [50] and it was deduced as 1.6×10^{-4} M. This value of CMC was used throughout the studies. The observed CMC value is lower than the CMC of CTAB in pure water (9.10×10^{-4} M) and in 0.1 M phosphate buffer (8.00×10^{-4} M) [58, 59]. The decrease of the CMC value is due to the presence of different ions and molecules in the present study as mentioned earlier [51]. In the presence of CTAB concentrations higher than CMC, the visible spectra of CuQ_2 shift to higher wavelengths as more CuQ_2 molecules are taken into the surfactant micelles. This red shift indicates that CuQ_2 molecules are located in micellar medium with lower polarity than the bulk water environment [54]. This indicates that hydrophobic interaction plays a great role in interaction of CuQ_2 with the cationic surfactant CTAB. The variation of the absorbance as a function of surfactant concentration is shown in figure 3b which indicates that with the increase in CTAB concentration the absorbance increases and reaches a saturation level after a certain concentration of CTAB. It is interesting to note that in a similar study on the interaction of SDS with CuQ_2 as mentioned above, SDS induces a decrease in the absorbance of CuQ_2 which is probably due to different modes of interaction of CuQ_2 with CTAB and SDS. The electrostatic contribution is important for CuQ_2–SDS interaction, while hydrophobic contribution is important for CuQ_2–CTAB interaction.

The binding isotherm for the interaction of CuQ_2 with CTAB was analyzed by nonlinear regression by assuming 1:2 and 1:1 interactions between the CuQ_2 and the CTAB using equations (1) and (2), respectively (in this case, $[L] = [\text{CTAB}]$) (figure S4), and the binding constants were obtained as $K = 6.11(\pm 0.06) \times 10^6\ M^{-1}$ for 1:2 interaction and $2.26(\pm 0.07) \times 10^3\ M^{-1}$ for 1:1, respectively. Considering the nature of the fitting of experimental results according to equations (1) and (2) shown in figure S4, one may conclude that the 1:2 interaction between CuQ_2 and the CTAB is probably more favorable than 1:1 interaction.

The Gibbs free energy values for the binding of CuQ_2 to the CTAB were then evaluated by applying equation (3) and found as –38.73 KJ mol^{-1} for 1:2 interaction and –19.14 KJ mol^{-1} for 1:1 interaction, respectively. The results clearly suggest that 1:2 interaction plays a major role in the binding of CuQ_2 with CTAB.

The interaction between uncharged CuQ_2 and cationic CTAB micelles should be stronger than that between a cationic drug and cationic CTAB micelles [54] because of the lower electrostatic repulsive forces in addition to hydrophobic interaction [54]. Comparison of the present results with the earlier one showed the binding constant for the 1:2 interaction of CuQ_2 with CTAB [$K = 6.11(\pm 0.06) \times 10^6\ M^{-1}$] to be higher than that for the interaction of cationic anthracycline drug mitoxantrone with CTAB [$K = 2933 \pm 625\ M^{-1}$] [54, 58], while it is lower than that observed in case of the interaction of cationic mitoxantrone with anionic surfactant, SDS [$K = 6.84(\pm 0.76) \times 10^7\ M^{-1}$] [53]. Enache and co-workers showed that the interaction of cationic mitoxantrone and anionic SDS micelle are of both electrostatic and hydrophobic in nature [53], whereas the interaction between cationic mitoxantrone with CTAB micelles is mainly hydrophobic in nature [54]. It is important to note that the Coulombic force of repulsion in the present study would be definitely smaller in comparison to that observed in case of cationic drug (mitoxantrone) and cationic surfactant (CTAB) [54]. Thus, one may conclude that in the present study the hydrophobic interactions have a great contribution to the binding of uncharged CuQ_2 to cationic CTAB micelles. Comparing the

present study with earlier ones [51, 54], it can be said that the uncharged aromatic ring of CuQ_2 interacts with cationic head group of CTAB through π-cation interaction when the CuQ_2 enters into the micelle.

Applying the pseudo-phase model [51, 56, 57], the partition coefficient for the distribution of CuQ_2 in between aqueous and micellar phases was determined with the help of equation (5), where [*L*] = [CTAB]. The value of K_X was evaluated from the slope of the plot of $1/\Delta A$ versus $1/([CTAB]+C_T-CMC)$] (figure S5) and it is $1.66(\pm0.05) \times 10^5$. The standard free energy change for the transfer of CuQ_2 from the bulk aqueous phase to micellar phase was obtained as -29.79 KJ mol^{-1} by putting the value of K_X in equation (5). The partition coefficient of 1-CuQ_2 between water and CTAB micelles in the present study is almost similar to that found for the distribution of mitoxantrone between water and CTAB micelles [$K_X = 1.72(\pm0.3) \times 10^5$)] [54]. The similarity in the results indicates that the hydrophobic interactions have a major role in the distribution of CuQ_2 between micelle and water phases due to the presence of the larger hydrophobic tail of CTAB molecules.

3.3. Interaction of CuQ_2 with ct DNA

The UV–Vis spectrum of the compound CuQ_2 in aqueous buffer at pH 7.4 containing 120 mM NaCl shows a peak at 530 nm (Curve 1, figure 4). Separate aliquots were prepared containing a constant concentration of CuQ_2 ($[CuQ_2]_0 = 20$ μM) and different concentrations of ct DNA. Absorption spectrum of each aliquot was recorded and the change in absorbance at 530 nm was used to monitor binding of the compound to ct DNA. The binding constant was evaluated using different methods of analysis. Figure 4 shows the absorption spectra of CuQ_2 in the absence and presence of different amounts of ct DNA. This exhibits that with the addition of ct DNA to a solution of the compound, the intensity of the peak at 530 nm decreases. This hypochromic effect may be attributed to an interaction between the electronic states of the compound chromophore and those of the DNA bases [60–72]. The hypochromism observed in this study indicates a close proximity of the compound to DNA bases [60–63]. In addition to a hypochromic shift, a slight bathochromic shift of about 2 nm was also observed. These spectral features are indicative of intercalation of the compound into the DNA helix [62].

Based on variations in the absorption spectra of CuQ_2 upon binding to ct DNA, the apparent binding constant K was calculated according to equation (6) [64],

$$\frac{A^0}{A - A^0} = \frac{\varepsilon}{\varepsilon_b - \varepsilon} + \frac{\varepsilon}{\varepsilon_b - \varepsilon}\frac{1}{K[\mathrm{DNA}]} \tag{6}$$

where A^0 and A are the absorbances of the compound in the absence and presence of DNA at 530 nm; ε and ε_b are the corresponding molar extinction coefficients of CuQ_2 and DNA. CuQ_2, respectively. Plot of $A^0/(A–A^0)$ versus 1/[DNA] (figure S6) is linear, with apparent binding constant $K = 1.19(\pm0.18) \times 10^3\ M^{-1}$.

The results of the spectrometric titration were also analyzed by non-linear fitting method considering the following compound–DNA equilibrium [equation (7)] [28–34, 65–68]:

$$CuQ_2 + \mathrm{DNA} \rightleftharpoons \mathrm{DNA} - CuQ_2 \tag{7}$$

The dissociation constant for this reaction can be given as [28–34, 65–68],

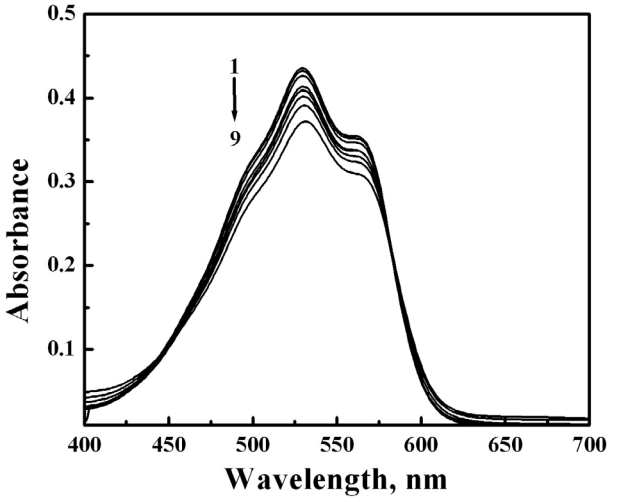

Figure 4. Absorption spectra of CuQ_2 (20 μM) in the absence (curve 1) and in the presence (curves 2–8) of different ct DNA concentrations: 30.51 μM (curve 2); 60.83 μM (curve 3); 120.95 μM (curve 4); 200.00 μM (curve 5); 239.06 μM (curve 6); 316.28 μM (curve 7); 467.18 μM (curve 8); 685.07 μM (curve 9). pH = 7.4, [NaCl] = 120 mM, 25 °C.

$$K_d = \frac{[CuQ_2][DNA]}{[DNA.CuQ_2]} \tag{8}$$

$$K_d = \frac{\{[CuQ_2]_0 - [DNA.CuQ_2]\}\{[DNA_0] - [DNA.CuQ_2]\}}{[DNA.CuQ_2]} \tag{9}$$

where the dissociation constant (K_d) = 1/K, K being the apparent binding constant of CuQ_2 to DNA. Here, $[CuQ_2]_0$ = initial concentration of CuQ_2 (which was kept constant during the titration experiment) and $[DNA_0]$ = concentration of DNA added to an aliquot. The concentration of CuQ_2 was 20 μM and ct DNA concentration was kept 60- to 65-fold higher than that of the compound. This is the basic assumption of this study where the DNA concentration is much higher than the concentration of CuQ_2. Now, if $C_0 = [CuQ_2]_0 = 20$ μM and $C_D = [DNA_0]$ = the concentration of DNA added to an aliquot then [28–34, 65–68]:

$$K_d = \frac{\{C_0 - [DNA.CuQ_2]\}\{C_D - [DNA.CuQ_2]\}}{[DNA.CuQ_2]} \tag{10}$$

Now, the change in absorbance at 530 nm of CuQ_2 in each addition of DNA during titration is $\Delta A = A^0 - A$, where A^0 and A are absorbances at 530 nm of 20 μM CuQ_2 in the absence and presence of DNA, respectively. Let, ΔA_m is the same parameter when CuQ_2 is totally bound to ct DNA. Therefore, ($\Delta A/\Delta A_m$) denotes the fraction of CuQ_2 bound to DNA. Hence, one gets ($\Delta A/\Delta A_m$)C_0 = [DNA-CuQ_2]. Then equation (10) becomes [28–34, 65–68]:

$$K_d = \frac{\left[C_0 - \left(\frac{\Delta A}{\Delta A_m}\right)C_0\right]\left[C_D - \left(\frac{\Delta A}{\Delta A_m}\right)C_0\right]}{\left(\frac{\Delta A}{\Delta A_m}\right)C_0} \tag{11}$$

$$C_0\left(\frac{\Delta A}{\Delta A_m}\right)^2 - (C_0 + C_D + K_d)\left(\frac{\Delta A}{\Delta A_m}\right) + C_D = 0 \quad (12)$$

All the experimental points for the binding were fitted according to equation (12) by least-square fit analysis and ultimately K_d was determined. As can be understood from equations (11) and (12), one needs to know the value of ΔA_m. For the determination of ΔA_m, a double reciprocal plot (figure S7a) of $1/\Delta A$ against $1/(C_D - C_0)$ was used according to equation (13) [28–34, 65–68]. Using this plot (figure S7a), values of ΔA_m and K_d were calculated:

$$\frac{1}{\Delta A} = \frac{1}{\Delta A_m} + \frac{K_d}{\Delta A_m(C_D - C_0)} \quad (13)$$

This approach is based on the assumption that absorbance is linearly proportional to concentration of CuQ_2. Figure 5a shows binding isotherms of CuQ_2 with ct DNA. The binding constant was calculated using equation (12) as described above. The apparent binding constant obtained from non-linear fit analysis was $1.38(\pm 0.08) \times 10^3\ M^{-1}$, while the same parameter obtained from double reciprocal plot (figure S7a) was $1.25(\pm 0.11) \times 10^3\ M^{-1}$. The apparent binding constant obtained from the plot of $A_0/(A-A_0)$ versus 1/[DNA] (figure S6) was $1.19(\pm 0.18) \times 10^3\ M^{-1}$. The values indicate that apparent binding constants obtained from three different methods of analysis are similar. Binding stoichiometry or binding site size for the interaction of CuQ_2 with ct DNA was determined from the point of intersection of two straight lines obtained from the least square fit plot of normalized increase of $\Delta A/\Delta A_m$ against ratio of concentration of ct DNA (in bases) to CuQ_2. Figure 5b shows such a plot of normalized increase of $\Delta A/\Delta A_m$ as a function of mole-ratio of DNA to CuQ_2. For CuQ_2, the value of 'n' binding to ct DNA was found to be 27.92 ± 0.82 bases i.e. 13.96 ± 0.41 base pairs. Knowing n, the intrinsic binding constant K', i.e. $(K \times n)$ was obtained as $(1.38(10^3 \times 27.92)$ i.e. $3.85(\pm 0.11) \times 10^4\ M^{-1}$.

The apparent binding constant K was also calculated considering equation (14) [69],

$$\frac{1}{f} = 1 + \frac{1}{K[DNA]} \quad (14)$$

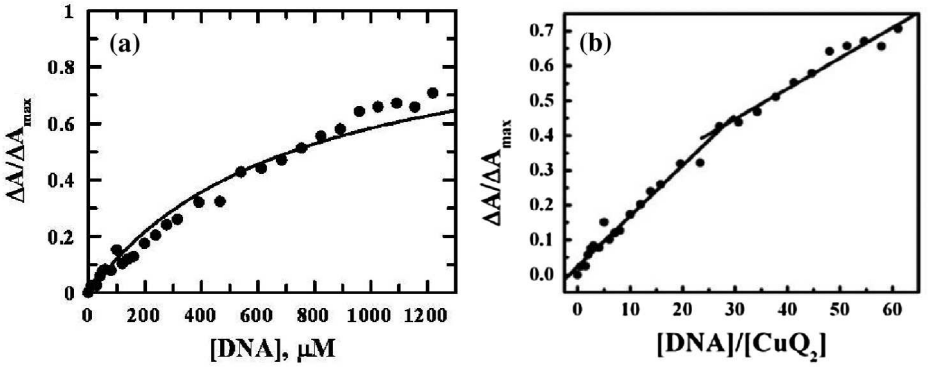

Figure 5. (a) Binding isotherm of CuQ_2 and ct DNA and corresponding non-linear fit; $[CuQ_2]_0$ = 20 μM, [Hepes buffer] = 50 mM, pH = 7.4, [NaCl] = 120 mM, 298.15 K. (b) Plot of normalized increase of absorbance as a function of mole-ratio of ct DNA to CuQ_2.

where f = fraction of total CuQ_2 bound = C_b/C_0 = [DNA-CuQ_2]/[CuQ_2]$_0$ = {($\Delta A/\Delta A_m$)C_0}/C_0 = ($\Delta A/\Delta A_m$) and [DNA] refers to the total DNA concentration (in base). The above condition is valid when the concentration of free DNA is in large excess over the concentration of bound compound [69]. If this condition is met, K can be determined from a plot of 1/f versus 1/[DNA] as the inverse of the slope. In our study, since DNA was present in large excess in comparison to CuQ_2 such a double-reciprocal plot (figure S7b) should be useful. The binding constant K was calculated and found to be 1.36(±0.13)×10^3 M^{-1}. Thus, the K value obtained from this plot also justifies the values obtained from other fitting methods. It was observed that intrinsic and apparent binding constants obtained in this study fall in the range of binding constants reported for mitoxantrone and other anthracycline drugs [70]. The binding constant and stoichiometry values of the current study also corroborate very nicely with the results obtained for Cu(II) and Ni(II) complexes of sodium 1,4-dihydroxy-9,10-anthraquinoe-2-sulphonate [27, 49, 71].

3.4. Mode of interaction of CuQ_2 with DNA

The mode of interaction of CuQ_2 with ct DNA was established by carrying out binding studies of CuQ_2 with single-stranded ct DNA under similar conditions of pH, ionic strength, and temperature. An aliquot containing CuQ_2 and single-stranded ct DNA under the aforementioned experimental conditions was prepared and absorption spectrum was recorded. Figure 6a shows the absorption spectra of CuQ_2 in the absence and presence of single-stranded DNA which shows that the addition of such DNA does not bring a significant change in intensity of the peak at 530 nm. This clearly indicates that CuQ_2 does not undergo any groove-binding with DNA. Thus, the hypochromic effect observed in the interaction of CuQ_2 with double-stranded ct DNA is definitely due to intercalation of the compound into DNA bases. As mentioned above, the intercalation of this class of molecules into DNA-base pairs plays a key role in their drug action and the interaction of such molecule with surfactant can be visualized as an approximation for their interactions with biological membranes. The binding affinity of the current molecule with DNA and anionic and cationic surfactant micelles being comparable to anthracycline drugs may raise the hope that CuQ_2 might be a potent antitumor agent like the established anthracyclines. In order to check if these physicochemical and biophysical phenomena result in an induction of apoptosis on cancer cells, the molecule was applied to MDA-MB-231 breast adenocarcinoma cell and the outcomes of these entire studies were correlated.

The mode of interaction of CuQ_2 with ct DNA was further established by performing a competitive binding study using the established DNA-intercalator EB and monitoring the change in fluorescence under the similar experimental conditions of pH, ionic strength, and temperature. Previous study showed that EB intercalates into the DNA backbone via the minor-groove [44]. A solution of EB exhibits a strong absorption band with λ_{max} at 470 nm which upon interaction with DNA shifts to 510 nm. When DNA–EB complex was excited at 510 nm, the fluorescence emission maximum was found at 590 nm. A solution containing 200 μM ct DNA and a saturating concentration of EB (4000 μM) was incubated for 1 h and the fluorescence was finally measured (figure 6b). To this experimental solution, CuQ_2 was added and the fluorescence of the resultant mixture was measured with an incubation time of 1 h (figure 6b). It is evident from this figure that the addition of CuQ_2 results in a decrease in the fluorescence intensity. Since EB is an intercalator and fluorescence is due to the

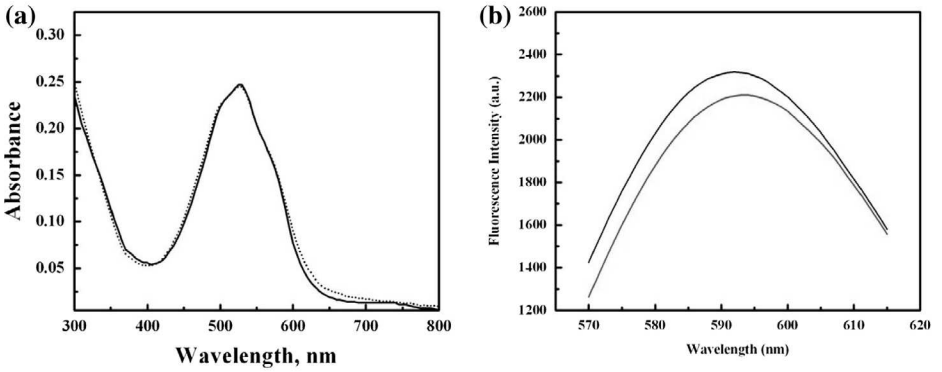

Figure 6. (a) Absorption spectra of CuQ_2 in the absence (solid line) and presence (dotted line) of single-stranded ct DNA in phosphate buffer at pH 7.4. [CuQ_2] = 20 μM, [Phosphate Buffer] = 100 mM, [NaCl] = 120 mM, [ss DNA] = 80 μM, 298.15 K. (b) Fluorescence spectra of 200 μM DNA with saturating EB (4000 μM) incubated for 1 h (black line); 200 μM DNA with saturating EB (4000 μM) incubated for 1 h followed by addition of 30 μM CuQ_2 (red line). pH = 7.4, [NaCl] = 120 mM, 298.15 K.

intercalation of it into DNA-backbone, therefore, a decrease in fluorescence intensity observed upon addition of CuQ_2 clearly suggests that it also intercalates into the double strands of DNA by replacing EB.

3.5. Viscosity measurements

The measurements of viscosity of ct DNA in the absence and presence of an experimental molecule are regarded as the least ambiguous and the most decisive tests of a binding model in solution in the absence of crystallographic structural data [72–74]. A conventional model of intercalation requires that the DNA-helix lengthens as base pairs are separated to put up the bound molecule which ultimately leads to an increase in the DNA viscosity. On the other hand, a partial non-classical intercalation of a molecule could bend (or kink) the DNA helix, thereby reducing its length and its viscosity. Further, a molecule which binds exclusively in the DNA grooves by partial and/or non-classical intercalation, characteristically leads to negligibly small or no change in viscosity of DNA [73, 74]. The values of relative specific viscosity $(\eta/\eta_0)^{1/3}$ (where η_0 and η correspond to specific viscosity contributions of DNA in the absence and presence of CuQ_2) were plotted against $1/R$ (where R = [DNA]/[CuQ_2]) (figure S8) [73]. Earlier studies showed that a groove-binder such as Hoechst 33258 does not increase the axial length of DNA [61] and, thus, does not bring a change in relative viscosity of DNA. In comparison, cisplatin which has been established to kink DNA by means of covalent binding, reducing the axial length of the DNA double helix [75], results in a decrease in the relative viscosity of the solution. It has been found that a partial intercalator also decreases the axial length thereby reducing in relative viscosity. The classical organic intercalator such as EB increases the axial length of DNA and it becomes more rigid [61, 72] which results in an increase in the relative viscosity. In the present study, it was found that with increase in the concentration of CuQ_2, the viscosity of DNA solution increases. This clearly shows that CuQ_2, certainly, is a DNA-intercalator. Since the interaction of CuQ_2 with DNA lets DNA longer, one will expect that the relative viscosity of DNA increases with a slope between 0 and 0.96

[76], if the intercalation of the experimental molecule was either only one interaction mode or much stronger than other interaction(s) [72, 76]. In the present study, the relative viscosity of DNA increases with a slope of 0.90 (figure S8). Thus, comparing the current value with earlier results [76], it can be said that the mode of interaction between DNA and CuQ_2 is definitely intercalation.

3.6. Effect of CuQ_2 on the viability of breast cancer cells

CuQ_2 was applied to MDA-MB-231 breast adenocarcinoma cells, and its inhibitory effect at different concentrations (20–200 μM) and time intervals (24 and 48 h) was investigated by MTT assay (figure 7). The assay determines the integrity of mitochondria and reflects the viability of cells. It was observed that CuQ_2 affected the viability of MDA-MB-231 breast adenocarcinoma cells in a dose-dependent manner. Figure 7 and table 1 show the inhibitory rates and corresponding concentrations at which CuQ_2 is cytotoxic to MDA-MB-231 cells and clearly indicate that CuQ_2 is able to cause 50% inhibition at 140 μM when incubated for 24 h and at 110 μM when incubated for 48 h on the cancer cells. Though the IC_{50} would appear to be fairly high, it is still promising since MDA-MB-231 represents a sub-type of breast tumor known as triple negative (ER^- PR^- $Her2^-$) for which, unlike the other subtypes, targeted agents specifically aimed at triple-negative breast tumors are not yet available, intensifying the need and interest in advancing novel therapeutic strategies beyond chemotherapy for this subset of high-risk patients [77]. Further, our very recent study [78] showed that 1-amino-4-hydroxy-9,10-anthraquinone (QH) causes 50% growth inhibition of the same cancer cells at 200 mM concentration when incubated for 24 h and at 140 mM concentration

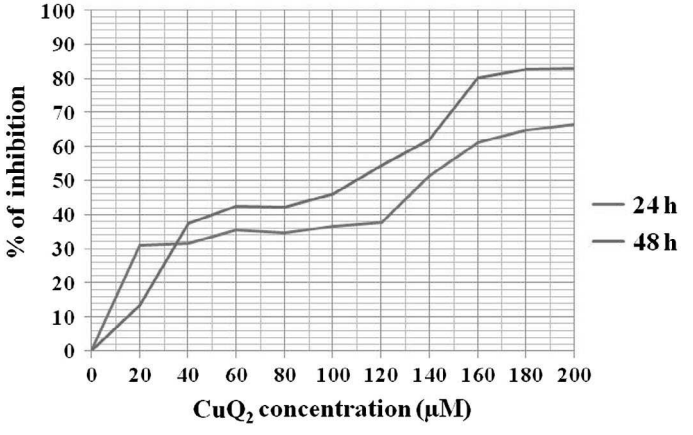

Figure 7. MTT assay for CuQ_2 for 24 h and 48 h on MDA-MB-231 cells.

Table 1. Inhibitory concentration of CuQ_2 against MDA-MB-231 breast adenocarcinoma cells.

	Concentration (μM)	
Inhibitory rates (%)	24 h	48 h
50	140 ± 0.02	110 ± 0.03

when incubated for 48 h. Thus, comparing the results of CuQ_2 with that of QH, it may be said that CuQ_2 is a better potent anticancer agent than QH which means that the formation of CuQ_2 brings better antitumor activity in comparison to the free QH. The MTT assay in a very recent study [79] with carminic acid (CA), an analog of anthracycline anticancer agent, and its copper(II) complex (Cu-CA) showed their IC_{50} values for 72 h against MOLT-4 breast cancer cells as 23.16 μM and 13.97 μM, respectively. In that study [79] cell killing by the copper(II)-carminic acid complex has been attributed to inhibition of human DNA topoisomerase I and II enzymes in the nucleus of MOLT-4 cells. In another very recent study [80], Das *et al.* evaluated IC_{50} values of 1,2,4-trihydroxy-9,10-anthraquinone (THA) and its copper complex (Cu-THA) against MCF-7, MDA-MB-231, MDA-MB-468 and HDF breast cancer cells which are 95.51, 101.62, 90.97, and 220.44 μM, respectively, for THA and 75.09, 55.69, 45.11, and 154.04 μM, respectively, for Cu-THA complex. Thus, earlier studies [79, 80] clearly established that the formation of copper(II) complex brings better results of IC_{50} values against various breast cancer cells which is followed well in the present study.

3.7. AO/EB staining

Apoptotic cell death was characterized by different cellular changes such as cell shrinkage, nuclear condensation, DNA-fragmentation, membrane blebbing, and formation of apoptotic bodies. These apoptotic characteristics produced by CuQ_2 were analyzed using AO/EB staining against MDA-MB-231 cell. In this staining method, the fluorescence pattern of the stain depends on the viability and membrane integrity of the cells. In general, dead cells are permeable to EB and fluoresce orange-red, while living cells are permeable to AO only and thus fluoresce green. Cytological changes observed in the treated cells are classified into four types based on fluorescence emission and morphological features of chromatin condensation in the AO/EB stained nuclei: (1) Viable cells having highly organized nuclei, fluoresce green. (2) Early apoptotic cells which show nuclear condensation emit orange-green fluorescence. (3) Late apoptotic cells, the nuclei fluoresce in orange-to-red due to the highly condensed or fragmented chromatin. (4) Necrotic cells appear in orange-to-red fluorescence with no indication of chromatin fragmentation. All these morphological changes were observed after the treatment of cancer cells with CuQ_2. Figure 8a indicates the apoptotic and necrotic morphologies induced at IC_{50} concentration of CuQ_2 for 24 h. The data presented in figure 8b revealed that CuQ_2 is efficient in inducing apoptotic death.

3.8. Hoechst staining

Morphological changes in the nucleus and chromatin produced in MDA-MB-231 cells by treatment with CuQ_2 were revealed by the Hoechst 33528 staining method. The cells treated with IC_{50} concentration of CuQ_2 showed some dramatic changes in the morphology of nuclei compared to the nuclei of vehicle control cells. In the latter the nuclei were round with compact chromatin while after treatment with CuQ_2 for 24 h, changes such as chromatin marginalization, condensation, and fragmentation were observed. Figure 9 indicates the apoptotic nuclear morphology induced by CuQ_2 at its IC_{50} concentration for 24-h incubation and the present molecule induced 52% of abnormal nuclei. Considering the entire aspects of the apoptotic effect of CuQ_2 on MDA-MB-231 breast adenocarcinoma cells and its mode

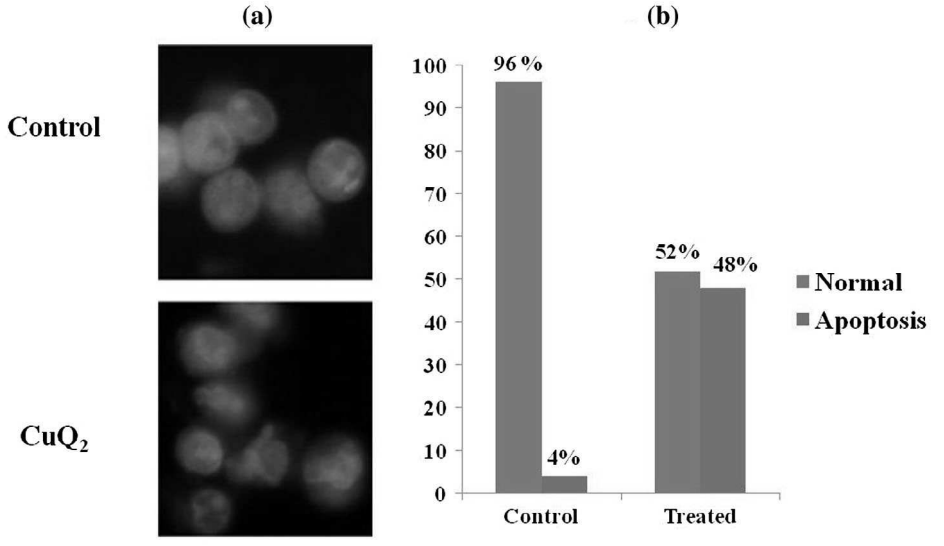

Figure 8. The effect of CuQ_2 on MDA-MB-231 cells with AO and EB staining. (a) Representative morphological changes observed in MDA-MB-231 cells after 24-h incubation with CuQ_2. (b) Relative percentage of morphological changes was determined and classified into three categories: viable, apoptosis, and necrosis as compared with the control cells after 24-h incubation.

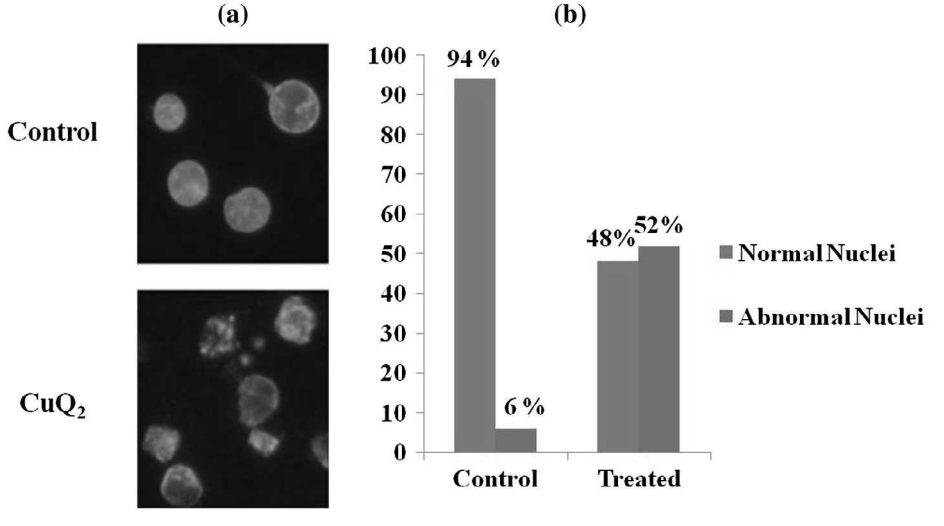

Figure 9. The effect of CuQ_2 on MDA-MB-231 cells are released in Hoechst staining. (a) Representative morphological changes observed in MDA-MB-231 cells after 24-h incubation with CuQ_2. (b) Relative percentage of morphological changes was determined and classified into two categories: Normal and abnormal nuclei as compared with the control cells after 24 h incubation.

of action during the course of such reaction, it is recommended that the less expensive CuQ_2 may be used as a viable alternative to the highly priced anthracycline drugs in the near future.

4. Conclusion

The copper complex of (CuQ_2)1-amino-4-hydroxy-9,10-anthraquinone (QH) interacts with both the anionic and cationic surfactants, SDS and CTAB, respectively, in an aqueous solution at physiological pH (7.4). Electrostatic as well as hydrophobic interaction play a role in the binding process of CuQ_2 with SDS, while hydrophobic interaction plays a major role in the binding process of CuQ_2 with CTAB. The mode of interaction of CuQ_2 with surfactant micelles is in harmony as anthracycline drugs interact with CTAB and SDS or sodium lauryl sulfate micelles [53–55] which clearly indicates that CuQ_2 mimics the action of anthracycline drugs. CuQ_2 intercalates into DNA base pairs under the same experimental conditions. The binding parameters were evaluated using different fitting models. The affinity of such molecule to intercalate into DNA and to interact with surfactant micelles being important in determining its biological action, the results of these studies were correlated with the biological efficiency of the molecule. In order to do so, CuQ_2 was applied to human MDA-MB-231 breast adenocarcinoma cells and the indications of apoptosis and the morphological changes in the cells were evaluated by AO/EB and Hoechst staining methods. Considering the entire aspect of the present study and comparing the results with those of anthracycline anticancer drugs, one may say that the copper complex of 1-amino-4-hydroxy-9,10-anthraquinone mimics the action of the established anthracycline anticancer drugs.

Disclosure statement

No potential conflict of interest was reported by the authors.

Funding

PG is grateful to University Grants Commission, New Delhi, INDIA for funding the Major Research Project (F. No. 41-225/2012 (SR) dated 18th July 2012).

References

[1] G.N. Hortobágyi. *Drugs*, **54**, 1 (1997).
[2] G. Minotti, P. Menna, E. Salvatorelli, G. Cairo, L. Gianni. *Pharmacol. Rev.*, **56**, 185 (2004).
[3] M.M. Abu-Khalaf, V. Juneja, G.G. Chung, M.P. DiGiovanna, R. Sipples, M. McGurk, D. Zelterman, B. Haffty, M. Reiss, F.J. Wackers, F.A. Lee, B.A. Burtness. *Breast Cancer Res. Treat.*, **104**, 341 (2007).
[4] M. Volkova, R. Russell. *Curr. Cardiol. Rev.*, **7**, 214 (2011).
[5] M.M.L. Fiallo, A. Gurnier-Suillerot. *Biochemistry*, **25**, 924 (1986).
[6] H. Beraldo, A. Gurnier-Suillerot, L. Tosi, F. Lavelle. *Biochemistry*, **24**, 284 (1985).
[7] M.M.L. Fiallo, A. Gurnier-Suillerot. *Biochim. Biophys. Acta*, **840**, 91 (1985).
[8] X. Xu, H.L. Persson, D.R. Richardson. *Mol. Pharmacol.*, **68**, 261 (2005).
[9] S. Roy, P. Mondal, P.S. Sengupta, D. Dhak, R.C. Santra, S. Das, P.S. Guin. *Dalton Trans.*, **44**, 5428 (2015).
[10] P. Ma, R.J. Mumper. *Nano Today*, **8**, 313 (2013).
[11] D. Putnam. *J. Kopecek. Adv. Polym. Sci.*, **122**, 55 (1995).
[12] R. Duncan, S. Dimitrijevic, E.G. Evagorou. *Pharma. Sci.*, **6**, 237 (1996).
[13] S. Wang, T. Peng, C.F. Yang. *J. Biochem. Biophys. Methods*, **55**, 191 (2003).
[14] X. Chu, G.L. Shen, J.H. Jiang, R.O. Yu. *Anal Lett.*, **32**, 717 (1999).
[15] G. Kwon, M. Naito, M. Yokoyama, T. Okano, Y. Sakurai, K. Kataoka. *J. Control. Rel.*, **48**, 195 (1997).
[16] M. Yokoyama, T. Okano, Y. Sakurai, S. Fukushima, K. Okamoto, K. Kataoka. *J. Drug Target.*, **7**, 171 (1999).
[17] N.M. Dand, P.B. Patel, A.P. Ayre, V.J. Kadam. *Chronicl. Young Sci.*, **4**, 94 (2013).

[18] X.-Y. Ke, V.W.L. Ng, S.-J. Gao, Y.W. Tong, J.L. Hedrick, Y.Y. Yang. *Biomaterials*, **35**, 1096 (2014).
[19] J.W. Park. *Breast Cancer Res.*, **4**, 193 (2002).
[20] M.J. Rosen. *Surfactants and Interfacial Phenomena*, 3rd Edn, John Wiley & Sons, New York, NY (2004).
[21] D. Kumar, M. Abdul. *J. Phys. Org. Chem.*, **29**, 394 (2016).
[22] M.A. Rub, F. Khan, M.S. Sheikh, N. Azum, A.M. Asiri. *J. Chem. Thermodyn.*, **96**, 196 (2016).
[23] S. Schreier, S.V.P. Malheiros, E. de Paula. *Biochim. Biophys. Acta*, **1508**, 210 (2000).
[24] D. Kumar, M. Abdul Rub, M. Akram, K-ud-Din. *Spectrochim. Acta Part A*, **132**, 288 (2014).
[25] A.Z. Naqvi, M.A. Rub, K. Din. *Colloid J.*, **77**, 525 (2015).
[26] S. Fukushima, M. Machida, T. Akutsu, K. Shimizu, S. Tanaka, K. Okamoto, H. Mashiba, M. Yokoyama, T. Okano, Y. Sakurai, K. Kataoka. *Colloids and Surf. B*, **16**, 227 (1999).
[27] P.S. Guin, S. Das, P.C. Mandal. *J. Inorg. Biochem.*, **103**, 1702 (2009).
[28] L. Yang, Z. Fu, X. Niu, G. Zhang, F. Cui, C. Zhou. *Chem. Biol. Interact.*, **233**, 65 (2015).
[29] C. Qiao, S. Bi, Y. Sun, D. Song, H. Zhang, W. Zhou. *Spectrochim. Acta Part A*, **70**, 136 (2008).
[30] A. Das, S. Roy, P. Mondal, A. Datta, K. Mahali, G. Loganathan, D. Dharumadurai, P.S. Sengupta, M.A. Akbarsha, P.S. Guin. *RSC Adv.*, **6**, 28200 (2016).
[31] S. Mukherjee, P. Das, S. Das. *J. Phys. Org. Chem.*, **25**, 385 (2012).
[32] P. Das, C.K. Jain, S.K. Dey, R. Saha, A.D. Chowdhury, S. Roychoudhury, S. Kumar, H.K. Majumder, S. Das. *RSC Adv.*, **4**, 59344 (2014).
[33] S. Roy, P.S. Guin. *J. Electrochem. Soc.*, **162**, H124 (2015).
[34] G.-Z. Jin, G.-Y. Song, X.-G. Zheng, Y. Kim, D.-E. Sok, B.-Z. Ahn. *Arch. Pharma. Res.*, **21**, 198 (1998).
[35] J. Blasiak, E. Gloc, M.A. Warszawski. *Acta Biochim. Pol.*, **49**, 145 (2002).
[36] S. Rossi, C. Tabolacci, A. Lentini, B. Provenzano, F. Carlomosti, S. Frezzotti, S. Beninati. *Anticancer Res.*, **30**, 445 (2010).
[37] J. Li-li, J. Guang-zhu. *Chem. Res. Chinese Univ.*, **28**, 971 (2012).
[38] C. Batchelor-McAuley, I.B. Dimov, L. Aldous, R.G. Compton. *Proc. Nat. Acad. Sci. USA*, **108**, 19891 (2011).
[39] P.S. Guin, S. Das, P.C. Mandal. *Int. J. Electrochem.*, 22 (2011), Article ID 816202.
[40] G.-B. Jiang, J.-H. Yao, J. Wang, W. Li, B.-J. Han, Y.-Y. Xie, G.-J. Lin, H.-L. Huang, Y.J. Liu. *New J. Chem.*, **38**, 2554 (2014).
[41] Y.-Y. Xie, H.-L. Huang, J.-H. Yao, G.-J. Lin, G.-B. Jiang, Y.-J. Liu. *Eur. J. Med. Chem.*, **63**, 603 (2013).
[42] S.-H. Lai, W. Li, X.-Z. Wang, C. Zhang, C.-C. Zeng, B. Tang, D. Wan, Y.-J. Liu. *RSC Adv.*, **6**, 63143 (2016).
[43] O. Warburg, W. Christian. *Biochem. Z.*, **310**, 384 (1942).
[44] M.M.S. Silva, I.T. Cavalcanti, M.F. Barroso, M.G.F. Sales, R.F. Dutra. *J. Chem. Sci.*, **122**, 911 (2010).
[45] P.B. Undre, P.W. Khirade, V.S. Rajenimbalkar, S.N. Helambe, S.C. Mehrotra. *J. Korean Chem. Soc.*, **56**, 416 (2012).
[46] T. Mosmann. *J. Immunol. Methods*, **65**, 55 (1983).
[47] D.L. Spector, R.D. Goldman, L.A. Leinwand. Cold Spring Harbor Laboratory Press, Cold Spring Harbor, New York, **1**, 341–349 (1998).
[48] S.A. Latt, G. Stetten, L.A. Juergens, H.F. Willard, C.D. Scher. *J. Histochem. Cytochem.*, **23**, 493 (1975).
[49] P.S. Guin, P. Mandal, S. Das, P.C. Mandal. *ChemPlusChem*, **77**, 361 (2012).
[50] E. Fuguet, C. Ràfols, M. Rosés, E. Bosch. *Anal. Chim. Acta*, **548**, 95 (2005).
[51] M. Sarkar, S. Poddar. *J. Colloid Interface Sci.*, **221**, 181 (2002).
[52] X. Shen, M. Belletête, G. Durocher. *Chem. Phys. Lett.*, **298**, 201 (1998).
[53] M. Enache, I. Anghelache, E. Volanschi. *Int. J. Pharm.*, **390**, 100 (2010).
[54] M. Enache, E. Volanschi. *J. Pharm. Sci.*, **100**, 558 (2011).
[55] I. Serbanescu, D. Bulcu, E. Volanschi. *Analele UniversităŃii din Bucuresti – Chimie, Anul XIV (serie nouă)*, Vol. **I–II**, p. 369 (2005).
[56] R. Sabaté, M. Gallardo, J. Estelrich. *J. Colloid Interface Sci.*, **233**, 205 (2001).
[57] R. Sabaté, M. Gallardo, A. de la Maza. *Langmuir*, **17**, 6433 (2001).
[58] M.A. Awan, S.S. Shah. *Colloids Surf. A: Physicochem. Eng. Asp.*, **122**, 97 (1997).
[59] R. Sarkar, M. Ghosh, A.K. Shaw, S.K. Pal. *J. Photochem. Photobiol. B: Biol.*, **79**, 67 (2005).
[60] R. Fakuda, S. Takenaka, M. Takagi. *J. Chem. Soc., Chem. Commun.*, 1028, (1990).
[61] E.C. Long, J.K. Barton. *Acc. Chem. Res.*, **23**, 271 (1990).
[62] C. Cantor, P.R. Schimmel. *Biophysical Chemistry*, Vol 2, Freeman WH, San Francisco (1980).

[63] I. Takenaka, T. Ihara, M. Takagi. *J. Chem. Soc., Chem. Commun.*, 1485, (1990).
[64] X.J. Dang, M.Y. Nie, H.L. Li. *J. Electroanal. Chem.*, **448**, 61 (1998).
[65] T. Deb, D. Choudhury, P.S. Guin, M.B. Saha, G. Chakrabarti, S. Das. *Chem. Biol. Interact.*, **189**, 206 (2011).
[66] S. Roy, R. Banerjee, M. Sarkar. *J. Inorg. Biochem.*, **100**, 1320 (2006).
[67] S. Chakraborti, B. Bhattacharyya, D. Dasgupta. *J. Phys. Chem. B*, **106**, 6947 (2008).
[68] M.A. Mir, S. Majee, S. Das, D. Dasgupta. *Bioorg. Med. Chem.*, **11**, 2791 (2003).
[69] F. Frezard, A. Garnier-Suillerot. *Biochim. Biophys. Acta*, **1036**, 121 (1990).
[70] N. Li, Y. Ma, C. Yang, L. Guo, X. Yang. *Biophys. Chem.*, **116**, 199 (2005).
[71] P.S. Guin, P. Das, S. Das, P.C. Mandal. *Int. J. Electrochem.*, 10 (2012), Article ID 183745.
[72] N. Shahabadi, S. Mohammadi. *Bioinorg. Chem. Appl.*, **2012**, 8 (2012), Article ID 571913.
[73] S. Ramakrishnan, M. Palaniandavar. *Dalton Trans.*, **29**, 3866 (2008).
[74] J.M. Kelly, A.B. Tossi, D.J. McConnell, C. OhUigin. *Nucl. Acids Res.*, **13**, 6017 (1985).
[75] L. Kapicak, E.J. Gabbay. *J. Am. Chem. Soc.*, **97**, 403 (1975).
[76] F. Li, G. Zhao, H. Wu, H. Lin, X. Wu, S. Zhu, H. Lin. *J. Inorg. Biochem.*, **100**, 36 (2006).
[77] C. Anders, L.A. Carey. *Oncology (Williston Park)*, **22**, 1233 (2008).
[78] P. Mondal, S. Roy, G. Loganathan, B. Mandal, D. Dharumadurai, M.A. Akbarsha, P.S. Sengupta, S. Chattopadhyay, P.S. Guin. *Biochem. Biophys. Rep.*, **4**, 312 (2015).
[79] P. Das, C.K. Jain, S. Roychoudhury, H.K. Majumder, S. Das. *ChemistrySelect*, **1**, 6623 (2016).
[80] P. Das, D. Bhattacharya, P. Karmakar, S. Das. *RSC Adv.*, **5**, 73099 (2015).

República Federativa do Brasil
Ministério do Desenvolvimento, Indústria e do Comércio Exterior
Instituto Nacional da Propriedade Industrial.

(21) **PI 1002523-5 A2**

BRPI1002523A2

(22) Data de Depósito: 14/07/2010
(43) Data da Publicação: 15/05/2012
(RPI 2158)

(51) Int.Cl.:
A61K 31/30
C07F 1/08
A61P 35/00

(54) Título: PROCESSO DE SÍNTESE DE COMPLEXOS DE COBRE COM ATIVIDADE ANTITUMORAL

(73) Titular(es): Universidade Federal de Minas Gerais

(72) Inventor(es): Elene Cristina Pereira Maia, Priscila Pereira Silva, Wendell Guerra

(57) Resumo: PROCESSO DE SÍNTESE DE COMPLEXOS DE COBRE COM ATIVIDADE ANTITUMORAL. A presente invenção descreve a síntese e a caracterização de complexos ternários de cobre possuindo como ligantes a 1,10-fenantrolina ou seus derivados e antibióticos da família das tetraciclinas, modificadas quimicamente ou não, ou ligantes do grupo das hidrazidas substituidas do ácido furóico ou do ácido benzóico, bem como composições farmacêuticas contendo os mesmos, como agentes antineoplásicos. O aspecto inovador desta invenção inclui tanto os complexos descritos, que são inéditos, o método de preparação dos mesmos, como também suas atividades antitumorais.

"PROCESSO DE SÍNTESE DE COMPLEXOS DE COBRE COM ATIVIDADE ANTITUMORAL"

Campo da invenção

A presente invenção descreve a síntese e a caracterização de complexos ternários de cobre possuindo como ligantes a 1,10-fenantrolina ou seus derivados e antibióticos da família das tetraciclinas, modificadas quimicamente ou não, ou ligantes do grupo das hidrazidas substituídas do ácido furóico ou do ácido benzóico, bem como composições farmacêuticas contendo os mesmos, como agentes antineoplásicos.

O aspecto inovador desta invenção inclui tanto os complexos descritos, que são inéditos, o método de preparação dos mesmos, como também suas atividades antitumorais.

Estado da técnica

A pesquisa de complexos metálicos com propriedades antitumorais iniciou-se com a descoberta da ação antitumoral da cisplatina, cis-diaminodicloroplatina(II), por Rosenberg e Van Camp no final dos anos sessenta (**B. Rosenberg, L. Van Camp, J.E. Trosco, V.H. Mansour, *Nature*, 222, 1969, 385**) e tem sido estimulada com a descoberta da atividade citotóxica de complexos com outros metais como o cobre, rutênio, gálio, vanádio, paládio, titânio, etc (**C.X. Zhang, S.J. Lippard, *Curr. Opin. Chem. Biol.*, 7,2003,481**). A introdução da cisplatina na clínica médica em 1971 causou, sem dúvida, um grande impacto, possibilitando a cura completa de diversos tumores, particularmente, o testicular e o ovariano (**B. Rosenberg, L. Van Camp, *Cancer Research*, 30, 1970, 1799**). Infelizmente, apesar do sucesso terapêutico da cisplatina, ela apresenta algumas desvantagens como baixa solubilidade em água, efeitos colaterais indesejáveis, além do aparecimento de resistência celular. Por isso, segue-se a procura por compostos que apresentem melhor solubilidade, possuam menos efeitos colaterais e atividade em tumores resistentes à cisplatina.

O ADN é o principal alvo de drogas antitumorais. Complexos metálicos podem ligar-se diretamente ao ADN, como é o caso da cisplatina (**A.M.J.**

Fichtinger-Schepman, J.L. Van der Veer, J.H.J. den Hartog, P.H.M. Lohman, J. Reedijk, *Biochemistry*, 24, 1985, 707), ou indiretamente, através de reações de oxi-redução, gerando espécies ativas que podem quebrar a molécula do ADN, como é o caso da bleomicina, um glicopeptídeo natural e potente antitumoral (**J. Reedijk, *Proc. Natl. Acad. Sci. USA*, 100, 2003, 3611**).

Alguns complexos de metais de transição podem promover a formação de radicais livres via reação de Fenton e reação de Haber-Weiss. São formadas espécies radicalares que degradam o anel ribose do ADN.

Por outro lado, o composto 1,10-fenantrolina e seus derivados são de interesse na síntese de novos metalofármacos com atividade antitumoral, uma vez que possuem estruturas planas e, portanto, são capazes de intercalar-se na fita de ADN e impedir a replicação celular. Outra vantagem desses compostos é a ausência de atividade antibacteriana contra a flora intestinal, o que reduz os efeitos colaterais de um possível metalofármaco com esses compostos (**S. Roy, K.D. Hagen, P.U. Maheswari, M. Lutz, A.L. Spek, J. Reedijk, G.P. van Wezel, *Chem. Med. Chem.*, 3, 9, 2008,1427**).

Um exemplo bem estudado é o do complexo de Cu(II) da 1,10-fenantrolina. A espécie reativa $[Cu(Phen)_2]^+$ faz um ataque oxidativo em um carbono da ribose. Peróxido de hidrogênio pode ser gerado pela redução do oxigênio pela espécie $[Cu(Phen)_2]^+$ (**T. Hirohama, Y. Kuranuki, E. Ebina, T. Sugizaki, H. Arii, M. Chikira, P.T. Selvi, M. Palaniandavar, *J. Inorg. Biochem.*, 99, 2005, 1205**).

Algumas patentes contendo compostos metálicos com derivados da 1,10-fenantrolina que possuem atividades antitumorais encontram-se disponíveis na literatura. Como exemplos podem ser citadas duas patentes americanas: **4,699,978** (**Site-specific chiral ruthenium (II) and cobalt (III) antitumor agents**) e **5,225,556** (**Chemical probes for left-handed DNA and for A-DNA; chiral metal complexes as Z-specific antitumor agents and as double strand cleavers**) que compreendem sínteses, caracterizações e estudos citotóxicos de complexos com derivados da 1,10-fenantrolina. Os mesmos mostraram-se eficazes em quebrar a molécula do ADN e conseqüentemente impedir a proliferação de células tumorais. Também podem

ser citados dois pedidos de patentes chinesas registradas no escritório europeu de patentes: **CN101190925** (**Copper complex, preparation method and application)** e **CN101225092** (**Manganese complex as well as preparation method and uses**) que descrevem as sínteses, caracterizações e aplicações de complexos de cobre e manganês com 1,10-fenantrolina como agentes antitumorais.

Por outro lado, as tetraciclinas são vastamente conhecidas pelas suas propriedades antibióticas, possuindo várias vantagens sobre os agentes atualmente conhecidos, como amplo espectro de ação, baixa toxicidade, administração oral e baixo custo. No entanto, essa família de compostos possui outras propriedades farmacológicas além da atividade antimicrobiana. Algumas patentes contendo tetraciclinas e análogos como compostos capazes de inibir o crescimento do câncer já se encontram disponíveis na literatura. Como exemplos podem ser citados dois documentos de pedido de patente americano: **WO/1998/031224** (**Method of inhibiting cancer growth**) que compreende o emprego de um análogo da tetraciclina para induzir efeitos citotóxicos contra o câncer em mamíferos, sendo particularmente eficaz para inibir a formação, crescimento e metástase de tumores sólidos, tais como tumores derivados das células de câncer de cólon, de mama, de próstata ou de pulmão e **WO/1987/003489** (**Combinations of tumor necrosis factors and antibiotics and methods for treating tumors**) que se refere a métodos para o tratamento de tumores e doenças neoplásicas com a combinação de fármacos antitumorais e tetraciclina, afim de que a mesma iniba a síntese de proteínas na célula-alvo.

A perspectiva do uso farmacêutico de tetraciclina ou derivados complexados com metais, também, é outra vertente de estudos. É descrita no pedido de patente americana **WO/2003/066064** (**Methods of disease treatment using metal-complexed tetracycline antibiotics)** a aplicação de compostos de tetraciclinas e quinonas complexadas a metais, ferro, cobre e cálcio, para tratamento de doenças bacterianas.

Também foi relatado que a doxiciclina e outras tetraciclinas quimicamente modificadas são capazes de inibir metaloproteinases de matriz,

que estão envolvidas em diferentes estágios da progressão do cancro. Foi sugerido que essa inibição esteja relacionada à coordenação a átomos de zinco ou de cálcio da proteína **(R.A. Garcia, D.P. Pantazatos, C.R. Gessner, K.V. Go, V.L. Woods Jr., F.J. Villarreal, *Mol. Pharmacol.* 67, 4, 2005, 1128)**.

Além disso, estudos recentes mostram que complexos de platina (II) com doxiciclina e tetraciclina inibem o crescimento de células de leucemia mielóide crônica e essa atividade antitumoral possivelmente esteja relacionada à interação do complexo com o ADN por mecanismo intercalativo (**P.P. Silva, F.C.S. de Paula, W. Guerra, J.N. Silveira, F.V. Botelho, L.Q. Vieira, T. Bortolotto, F.L. Fischer, G. Bussi, H. Terenzi, E.C. Pereira- Maia, *J. Braz. Chem. Soc.*, 21, 2010, 1237**).

Outra estratégia que pode ser usada para o desenvolvimento de drogas anticancerígenas é a de aliar as propriedades antitumorais do composto $[Cu(Phen)_2]^{2+}$ às de derivados de hidrazida, uma vez que esses últimos também apresentam propriedades neoplásicas. Sobre a atividade antitumoral dos derivados de hidrazida, podemos citar o pedido de patente brasileira **PI0512526-0 (Composto, composição farmacêutica, método para tratar um paciente com câncer e método para preparar um di-sal de bis(tio-hidrazida amida)**) que sugere a utilização de uma composição farmacêutica que compreende um sal derivado de hidrazida,sal de bis(tio-hidrazida amida), para tratamento de pacientes com câncer.

Descrição detalhada da invenção

O processo de síntese e caracterização de novos metalofármacos como agentes anticancerígenos é proposto nesta invenção, onde o metal focalizado é o cobre, já que ele é um metal endógeno e, possivelmente, seja menos tóxico que a platina. Os ligantes empregados podem ser a tetraciclina (tc), a doxiciclina (dox), a minociclina (min), a tigeciclina (tig), todos pertencentes à família das tetraciclinas, as hidrazidas do ácido benzóico (hydb) ou do ácido furóico (hydf), como também a 1,10-fenantrolina (phen) ou seus derivados, a 2,9-dimetil-1,10-fenantrolina (neocuprina) (2,9-dmphen) ou a 4,7-difenil-1,10-fenantrolina (batofenantrolina) (4,7-dfphen).

A presente invenção propõe a síntese de compostos inéditos que podem ser usados em formulações farmacêuticas para tratar casos de neoplasias. As estruturas de três dentre os compostos $[Cu(R)(R_1)(R_2)(ClO_4)](ClO_4)$, onde R= tc, dox, min, tig, hydf, hydb; R_1= phen, 2,9-dmphen, 4,7-dfphen e R_2= H_2O, acetonitrila, são apresentadas na **Figura 1.** Os compostos foram sintetizados e caracterizados através de análises elementar e condutimétrica, ressonância paramagnética eletrônica (EPR), espectrometrias no ultravioleta-visível (UV-Vis) e infravermelho (IV), espectrometria de massas e cristalografia de raios X de monocristal, para o complexo **III**.

Todos os compostos apresentam atividade citotóxica significativa em linhagens de células tumorais e podem vir a ser usados no tratamento do câncer.

As composições da presente invenção caracterizam-se pelo uso dos complexos de cobre combinados com excipientes farmaceuticamente aceitáveis. As composições padrões podem ser líquidas e sólidas. Sendo que as preparações líquidas podem se apresentar na forma de solução, suspensão ou emulsão. As sólidas na forma de cápsulas, comprimidos, drágeas ou pastilhas.

Essas composições podem ser administradas via intramuscular, intravenosa, oral ou como dispositivos que possam ser implantados ou injetados.

A tecnologia pode ser melhor compreendida a partir da análise dos exemplos a seguir, não limitantes:

A) Sínteses dos complexos

Exemplo 1 - Síntese dos complexos **I** e **II**:

O complexo **I** foi preparado pela reação do $Cu(ClO_4)_2 \cdot 6H_2O$ (0.1853g, 0.5 mmol) com doxiciclina (0.2405g, 0.5 mmol), em água (10 mL). A mistura permaneceu em agitação por 40 minutos, em seguida, adicionaram-se 5 mL de uma solução metanólica de 1,10- fenantrolina (0.0996g, 0.5 mmol). A mistura resultante permaneceu em agitação por mais três horas. O precipitado formado foi separado por filtração, lavado com água e secado sob vácuo. Obteve-se um sólido verde de composição $[Cu(C_{22}H_{24}N_2O_8)(C_{12}H_8N_2)(H_2O)(ClO_4)](ClO_4)$.

O complexo **II** foi preparado de forma semelhante, com adição de tetraciclina ao invés de doxiciclina.

Exemplo 2 - Síntese do complexo **III**:

O complexo **III** foi preparado pela reação do $Cu(ClO_4)_2 \cdot 6H_2O$ (0.1853g, 0.5 mmol) com a hidrazida do ácido 2-furóico (0.2405g, 0.5 mmol), em acetonitrila (5 mL), seguida da adição de uma solução de 1,10- fenantrolina (0.0996g, 0.5 mmol), em acetonitrila (3 mL). Obtiveram-se cristais azuis de composição $[Cu(C_5H_6N_2O_2)(C_{12}H_8N_2)(C_2H_3N)(ClO_4)](ClO_4)$.

Também é possível obter um complexo semelhante, utilizando como solvente a água ao invés da acetonitrila, cuja composição final é $[Cu(C_5H_6N_2O_2)(C_{12}H_8N_2)(H_2O)(ClO_4)](ClO_4)$.

B) Caracterização dos complexos de cobre com tetraciclinas (complexos I e II) e com a hidrazida do ácido 2-furóico (complexo III)

Os complexos foram obtidos segundo o seguinte esquema:

$$Cu^{2+}_{(sol1)} + L^1_{(sol1)} \rightarrow CuL^1 + L^2_{(sol2)} \rightarrow \mathbf{C_I},\ \mathbf{C_{II}} \text{ ou } \mathbf{C_{III}}$$

Sendo o complexo **I** ($\mathbf{C_I}$)= $[CuL^1L^2(ClO_4)(H_2O)]ClO_4$, quando sol1=água e sol2= metanol, L^1=dox e L^2=phen; o complexo **II** ($\mathbf{C_{II}}$)= $[CuL^1L^2(ClO_4)(H_2O)]ClO_4$, quando sol1=água e sol2=metanol, L^1=tc e L^2=phen e o complexo **III** ($\mathbf{C_{III}}$)= $[CuL^1L^2(ClO_4)(CH_3CN)]ClO_4$, quando sol1=água e sol2=acetonitrila, L^1=hydf e L^2=phen.

Os compostos foram caracterizados por análise elementar, condutimetria, EPR, espectrometrias na região do IV e UV-Vis, espectrometria de massas (complexos **I** e **II**) e cristalografia de raios X de monocristal (complexo **III**). Os dados de análise elementar e condutividade molar são relatados na **Tabela 1** e os dados de EPR são relatados na **Tabela 2**.

Tabela 1: Dados das análises elementares e condutimétricas para os complexos **I**, **II** e **III**. Os valores entre parênteses são calculados para $[Cu(C_{12}H_8N_2)(C_{22}H_{24}N_2O_8)(H_2O)(ClO_4)](ClO_4)$, complexos **I** e **II** e $[Cu(C_5H_6N_2O_2)(C_{12}H_8N_2)(C_2H_3N)(ClO_4)](ClO_4)$, complexo **III**.

Complexos	*%C*	*%H*	*%N*	*%Cu*	Λ_M (μS/cm)
Complexo **I**	45,00	3,82	6,11	6,98	173,9
MM= 905,11 g.mol^{-1}	(45,12)	(3,79)	(6,19)	(7,02)	-
Complexo **II**	45,63	4,01	6,49	7,12	187,9
MM= 905,11 g.mol^{-1}	(45,12)	(3,79)	(6,19)	(7,02)	-
Complexo **III**	37,87	2,49	11,14	10,36	202,9
MM= 609,55 g.mol^{-1}	(37,42)	(2,81)	(11,49)	(10,83)	-

Os dados de análise elementar estão coerentes com as fórmulas propostas. A condutividade molar foi medida em soluções de nitrometano (10^{-3} molL^{-1}), a 25°C. Os valores obtidos para esses três complexos indicam que, em solução, eles são eletrólitos do tipo 2:1. Isto significa que, em solução, os dois íons percloratos atuam como contra-íons.

Tabela 2: Parâmetros de EPR para os complexos **I**, **II** e **III**.

Compostos	**Parâmetros de EPR**				
	$g_\perp$	$g_{//}$	$A_{//}$ (G)	$A_{//}$ (10^{-4} cm^{-1})	$g_{//}$ / $\lvert A_{//} \rvert$ (cm)
Complexo **I**	2,63	2,271	172,3	182,7	124,3
Complexo **II**	2,063	2,271	172,3	182,7	124,3
Complexo **III**	2,062	2,256	173,6	182,8	123,4

Os valores obtidos estão de acordo com a estrutura proposta e os espectros de EPR dos complexos **I** e **III** podem ser observados na **Figura 2**. O espectro EPR do composto **II** é idêntico ao do composto **I**.

As análises dos espectros de absorção na região do UV-Vis, para os complexos **I** e **II**, sugeriram o envolvimento do anel A da tc e da dox na coordenação ao metal. A banda de absorção em 269 deslocou-se para 293 nm no complexo **I**, como apresentado na **Figura 3a**, e de 270 para 296 nm no

complexo **II** (**Figura 3b**), enquanto que a banda centrada em 362 nm referente ao cromóforo BCD da tc ou dox não sofreu alteração em ambos os complexos. Já para o complexo **III** a banda da phen centrada em 264 nm sofre um deslocamento batocrômico para 272 nm no complexo indicando a complexação do ligante ao metal (**Figura 3c**).

As atribuições das absorções nos espectros de infravermelho dos complexos **I** e **II** foram feitas com base em um estudo detalhado de tetraciclinas e análogos feito por Dziegielewski et al. (**J. Dziegielewski, J. Hanuza, B. Jezowska-Trzebiatowska, *Bull Acad. Pol. Sci., Ser. Sci. Chim.* 24, 1976, 307**). Como os espectros no infravermelho dos complexos **I** e **II** são muito semelhantes, apenas o espectro do complexo de cobre da doxiciclina e fenantrolina **(Figura 4)** será discutido.

O espectro no infravermelho de doxiciclina mostra absorções características em 3426 e 3200 cm^{-1}, correspondentes a νOH e νNH, respectivamente. Essas absorções são sobrepostas no complexo, produzindo uma banda larga centrada em cerca de 3370 cm^{-1}. A banda da amida, ν(C=O), que aparece no espectro da doxiciclina em 1670 cm^{-1}, não pode ser distinguida no espectro do complexo, indicando que o oxigênio do grupo amida está envolvido na esfera de coordenação. Duas bandas muito fortes, em 1618 e 1578 cm^{-1}, que são atribuídas a estiramentos das carbonilas dos anéis A e C, ν(C=O), aparecem no mesmo número de onda, descartando a participação destes oxigênios na esfera de coordenação. O comportamento do íon perclorato fracamente coordenado ou como contra-íon pode ser distinguido pelas freqüências de νCl-O. O abaixamento de simetria de Td para C_{3v}, que ocorre quando um dos oxigênios do perclorato liga-se a outro átomo, induz o desdobramento de ν_3, em duas bandas. Três bandas intensas em 1121, 1108 e 1087 cm^{-1} aparecem no espectro do complexo, o que pode ser explicado pela presença de um íon perclorato unidentado e outro livre.

A análise do espectro na região do IV para o complexo **III,** que pode ser visualizado na **Figura 5**, confirmou a coordenação da hydf de forma bidentada ao metal. A hydf livre apresenta uma absorção em 1657 cm^{-1}, referente a νC=O que se desloca para 1645 cm^{-1} no complexo. Também pode ser verificada uma

mudança nas absorções referentes a νNH de 3257 e 3147 cm^{-1} no ligante livre para 3149 e 3079 cm^{-1} no complexo. A coordenação do metal à phen pode ser confirmada pela presença da banda em 1599 cm^{-1} referente ao estiramento νC=NH.

Os espectros ESI-MS no modo positivo mostram, para os complexos **I** e **II**, um pico principal em *m/z* 686, característico de íon contendo $^{63}Cu/^{65}Cu$ (2,2%), atribuído à espécie monocarregada $[Cu(dox)(phen)\text{-}H^+]^+$ ou $[Cu(tc)(phen)\text{-}H^+]^+$ (massa calculada = 686,14), que pode ser visualizado na **Figura 6**. Nos espectros dos dois complexos, um pico de menor intensidade em *m/z* 785,9, corresponde à espécie $[Cu(dox)(phen)(ClO_4)]^+$ ou $[Cu(tc)(phen)(ClO_4)]^+$ (massa calculada = 786,1).

A estrutura do complexo **III**, determinada por cristalografia de raios X de monocristal, revelou uma geometria octaédrica distorcida ao redor do átomo de cobre, apresentada na **Figura 7**. O complexo cristaliza-se no grupo espacial triclínico P-1 com a = 9.8120(2) Å, b = 11.2001(3) Å, c = 11.3551(2) Å, α =104.564(2)°, β =100.049(2)°, γ = 90.218(2)°. As posições equatoriais são ocupadas pela hydf, que está ligada ao cobre de forma bidentada via um nitrogênio e um oxigênio carbonílico e à 1,10-fenantrolina que se liga ao metal via dois nitrogênios heterocíclicos. Os sítios axiais são ocupados por um oxigênio do perclorato e pelo nitrogênio da acetonitrila. O segundo ânion perclorato atua como contra-íon do complexo e o mesmo é estabilizado por ligações de hidrogênio.

C) Avaliação da atividade antitumoral dos complexos de cobre

Exemplo 3: Inibição do crescimento celular da linhagem K562

A linhagem celular K562 foi adquirida do Banco de células do Rio de Janeiro (CR083 número da coleção RJCB). Esta linhagem celular foi criada a partir de derrame pleural de uma mulher de 53 anos de idade com leucemia mielóide crônica em crise blástica terminal. As células foram cultivadas em meio RPMI 1640 (Sigma Chemical Co.) suplementado com 10% de soro fetal bovino (CULTILAB, São Paulo, Brasil), a 37°C, em uma atmosfera a 5% de CO_2. A viabilidade celular foi verificada pelo azul de Trypan. O número de células foi determinado pela análise em contador automático Coulter.

Para avaliação de citotoxicidade, 1 x 10^5 células mL^{-1} foram incubadas por 72 h na ausência e na presença de concentrações crescentes dos complexos testados. A sensibilidade das células frente aos complexos foi avaliada pela concentração que inibe o crescimento celular em 50%, CI_{50}. Os valores obtidos são apresentados na **Tabela 3**.

Tabela 3: Inibição do crescimento celular da linhagem K562 pelos complexos **I, II** e **III**.

Composto	**CI_{50} (µmol L^{-1} ± s.d.)**
dox	17,70 ± 0.9
tc	52,37 ± 3.1
hyd	455,62 ± 20,9
Phen	3,17 ± 0.25
$[Cu(Phen)_2](ClO_4)_2$	3,44 ± 0.30
Complexo **I**	1,93 ± 0.18
Complexo **II**	2,59 ± 0.26
Complexo **III**	2,15 ± 0.23

Os complexos **I**, **II** e **III** inibiram o crescimento de células K562 com os valores CI_{50} de 1,93, 2,59 µmol L^{-1} e 2,15 µmol L^{-1}, respectivamente. O complexo **I** é o mais ativo entre eles e, em todos os casos, as atividades dos complexos foram superiores às dos ligantes livres.

Exemplo 4: Acumulação intracelular dos complexos testados

Células K562 (1x10^5 células mL^{-1}) foram incubadas por 72 h na ausência e na presença de concentrações crescentes dos complexos. Após a incubação, uma alíquota foi tomada, lavada três vezes com solução gelada de tampão isotônico e o sedimento ressuspendido em uma solução a 33% de HNO_3. A concentração de cobre foi determinada por espectrometria de absorção atômica em forno de grafite. Os dados apresentados na **Figura 8** permitem

concluir que existe uma boa correlação entre a atividade citotóxica e acumulação intracelular, ou seja, a inibição do crescimento celular aumenta com o aumento da concentração intracelular do complexo.

Exemplo 5: Avaliação das interações dos novos complexos com o ADN

Com o objetivo de verificar se os complexos ligam-se ao ADN dentro das células, elas foram incubadas por 2 horas com concentrações crescentes dos complexos **I** e **II** (**Figura 9a**), o ADN foi extraído, segundo protocolo descrito na literatura (**N.A. Rey, A. Neves, P.P. Silva, F.C.S. Paula, J.N. Silveira, F.V. Botelho, L.Q. Vieira, C.T. Pich, H. Terenzi, E.C. Pereira-Maia, *J. Inorg. Biochem. 103*, 2009, 1323**) e os adutos formados foram quantificados. A concentração de ADN por nucleotídeos foi determinada por espectrofotometria (ε = 6600 $molL^{-1}cm^{-1}$ em 260 nm). A razão da absorvância em 260 e 280 nm ficou entre 1,6-1,9. O cobre foi dosado por espectrometria de absorção atômica em forno de grafite. O número de adutos formados cresce com o aumento da concentração de complexo. Estudo semelhante foi realizado para o complexo **III** (**Figura 9b**) com tempo de incubação de 72 horas.

As interações dos complexos com o ADN também foram estudadas por espectrometria UV-Vis (**Figura 10**). Espectros de soluções dos complexos na ausência e na presença de concentrações crescentes de ADN de timo de vitelo foram registrados. A adição de ADN induz um efeito hipocrômico, indicando que os compostos testados formam complexos ternários com o ADN. Para comparar a estabilidade dos complexos, a constante de afinidade, K, foi calculada a partir dos dados espectrofotométricos, de acordo com a equação abaixo:

$$[ADN] / (\varepsilon_a - \varepsilon_f) = [ADN] / (\varepsilon_0 - \varepsilon_f) + 1/K(\varepsilon_0 - \varepsilon_f)$$

onde [ADN] é a concentração de ADN em pares de bases, ε_a é a relação entre a absorvância / [Pt], ε_f é o coeficiente de extinção do complexo livre e ε_0 é o coeficiente de extinção do complexo na forma totalmente ligada. A razão entre a inclinação e a interseção do gráfico [ADN] / (ε_a - ε_f) versus [ADN] fornece o valor da constante de afinidade do complexo pelo ADN. As constantes de afinidade calculadas foram 2.02 x 10^4; 2.95 x 10^4 e 2,19 x 10^4 para os

complexos **I**, **II** e **III**, respectivamente. O complexo **II** possui afinidade pelo ADN ligeiramente maior que os demais.

Descrição das figuras

A **Figura 1** apresenta as estruturas químicas propostas para os complexos **I**, **II** e **III**.

A **Figura 2** mostra os espectros de ressonância paramagnética eletrônica dos complexos **I** e **III**.

A **Figura 3** mostra os espectros de absorção na região do UV-Vis de soluções metanólicas 1,6 x 10^{-4} $molL^{-1}$ de: (a) phen, dox e complexo **I**; (b) phen, tc, complexo **II** e (c) phen, hydf e complexo **III**.

A **Figura 4** apresenta os espectros na região do IV para: (a) dox e complexo **I** e (b) tc e complexo **II**.

A **Figura 5** apresenta o espectro na região do IV para o complexo **III**.

A **Figura 6** apresenta o espectro de massas de eletrospray: (a) espectro do complexo **II** dissolvido em solução metanol:água (1:1) e (b) distribuição isotópica calculada a partir do programa Qual Browser version 2.0.7copyright®.

A **Figura 7** mostra a representação ORTEP do complexo **III**.

A **Figura 8** apresenta as porcentagens de sobrevivência das células após incubação de 72 horas com concentrações equitóxicas dos compostos **I** e **II** em função da concentração intracelular de cobre.

A **Figura 9** mostra a quantidade de adutos Cu-ADN em função da concentração de complexo: (a) complexos **I** e **II**, incubação por 2 h e (b) complexo **III**, incubação por 72 h.

A **Figura 10** mostra o resultado da titulação do complexo **II** com ADN. [[Cu(dox)(phen)(H_2O)(ClO_4)](ClO_4)] = 2 x 10^{-5} $molL^{-1}$, [DNA] 0 a 3 x 10^{-4} $molL^{-1}$.

REIVINDICAÇÕES

1- Complexos de cobre, caracterizados por apresentar a seguinte fórmula estrutural:

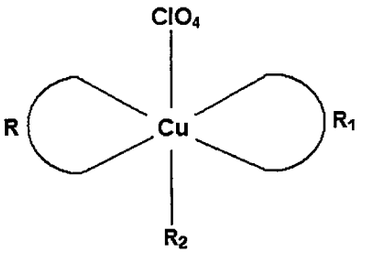

onde R= tetraciclina, doxiciclina, minociclina, tigeciclina, hidrazidas do ácido benzóico, hidrazidas do ácido furóico;

R_1= 1,10-fenantrolina, 2,9-dimetil-1,10-fenantrolina, 4,7-difenil-1,10-fenantrolina; e

R_2 = água, acetonitrila.

2- Complexos de cobre, de acordo com a reivindicação 1, caracterizada por apresentar concentração necessária para inibir 50% do crescimento celular (CI_{50}), em linhagem K562, inferior a 3 µmol L^{-1}

3- Composição farmacêutica, caracterizada por compreender um complexo de cobre II conforme seguinte fórmula estrutural:

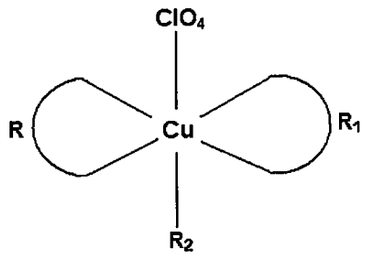

onde R= tetraciclina, doxiciclina, minociclina, tigeciclina, hidrazidas do ácido benzóico, hidrazidas do ácido furóico;

R_1= 1,10-fenantrolina, 2,9-dimetil-1,10-fenantrolina, 4,7-difenil-1,10-fenantrolina;

R_2 = água, acetonitrila; e

ao menos, um excipiente farmaceuticamente aceitável.

4- Processo de síntese de complexos de cobre, caracterizado por compreender as etapas:

a) adição de uma solução de cobre (II) a uma solução de um antibiótico selecionado da família das tetraciclinas ou a uma solução de uma hidrazida do ácido furóico ou do ácido benzóico;

b) adição de uma solução de uma fenantrolina à mistura obtida na **etapa a**;

c) filtração, lavagem com água e secagem do sólido obtido.

5- Processo de síntese de complexos de cobre, de acordo com a reivindicação 4, caracterizado pela solução de cobre ser preferencialmente a de perclorato de cobre (II).

6- Processo de síntese de complexos de cobre, de acordo com a reivindicação 4**, c**aracterizado pelo **a**ntibiótico da família das tetraciclinas ser selecionado do grupo compreendendo doxiciclina, tetraciclina, minociclina e tigeciclina.

7- Processo de síntese de complexos de cobre, de acordo com a reivindicação 4, caracterizado pela fenantrolina ser selecionada do grupo compreendendo a 1,10-fenantrolina; 2,9-dimetil-1,10-fenantrolina e 4,7-difenil-1,10-fenantrolina.

8- Processo de síntese de complexos de cobre com atividade antitumoral**,** de acordo com a reivindicação 4, caracterizado pela solubilização de fenantrolina compreender um solvente orgânico, preferencialmente metanol ou acetonitrila.

9- Complexos de cobre, caracterizada por ser na preparação de um medicamento antitumoral.

FIGURAS

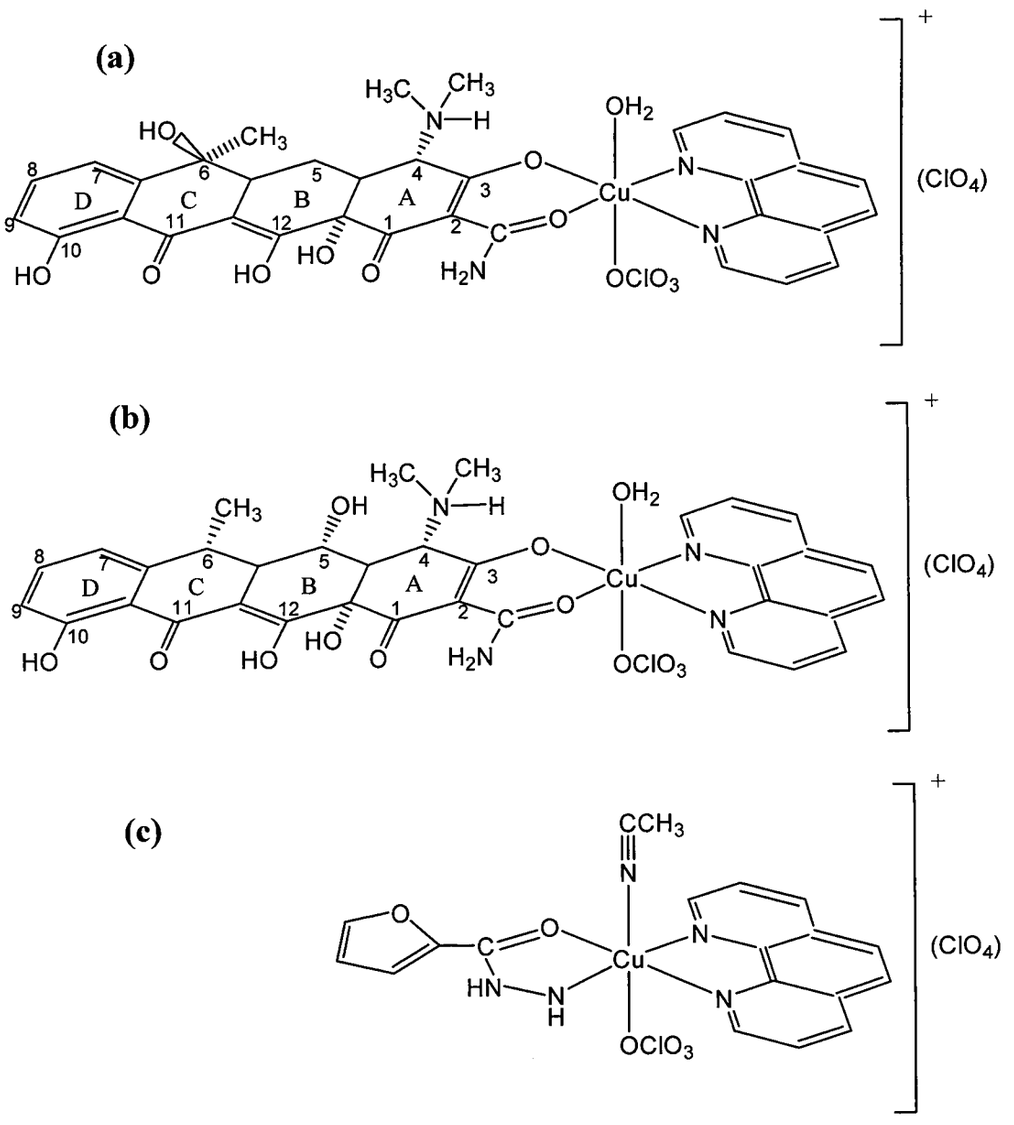

Figura 1

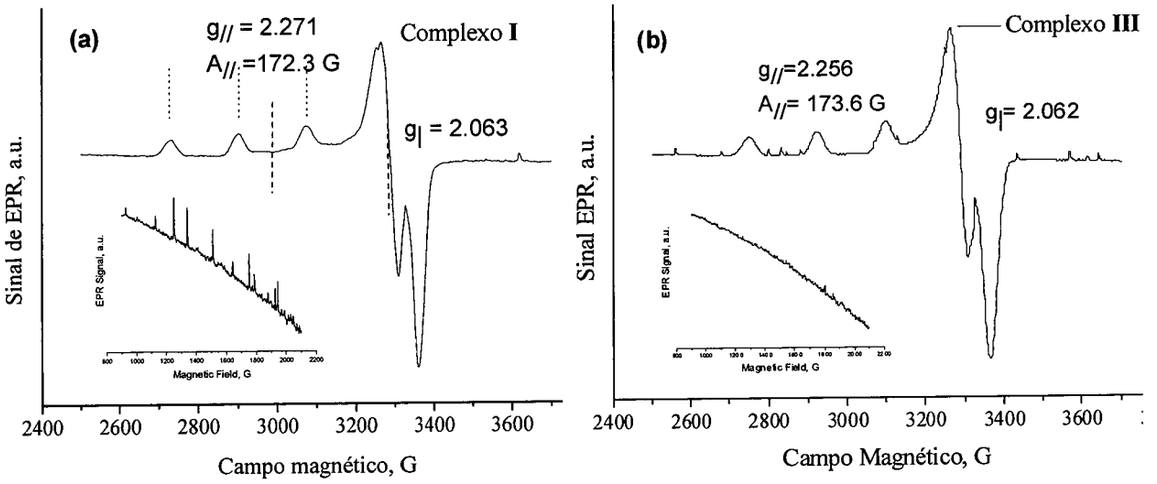

Figura 2

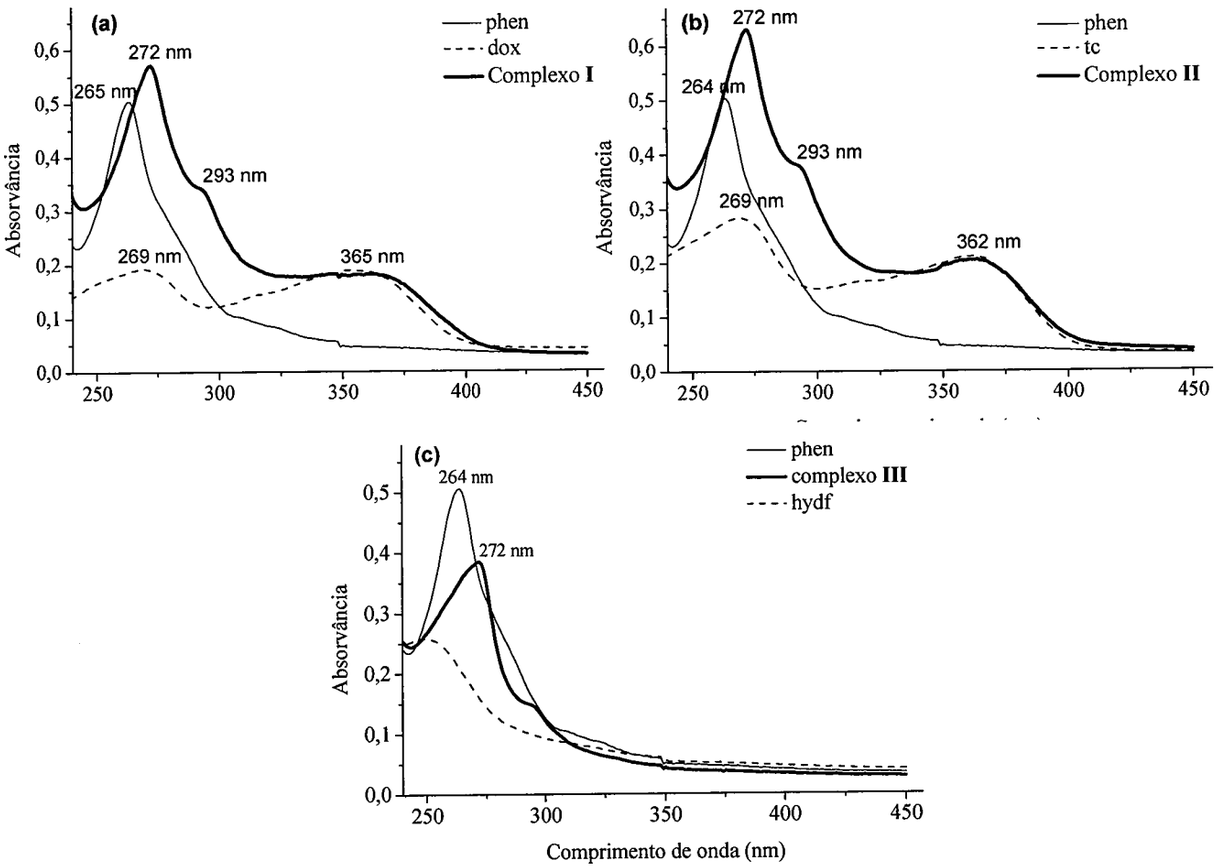

Figura 3

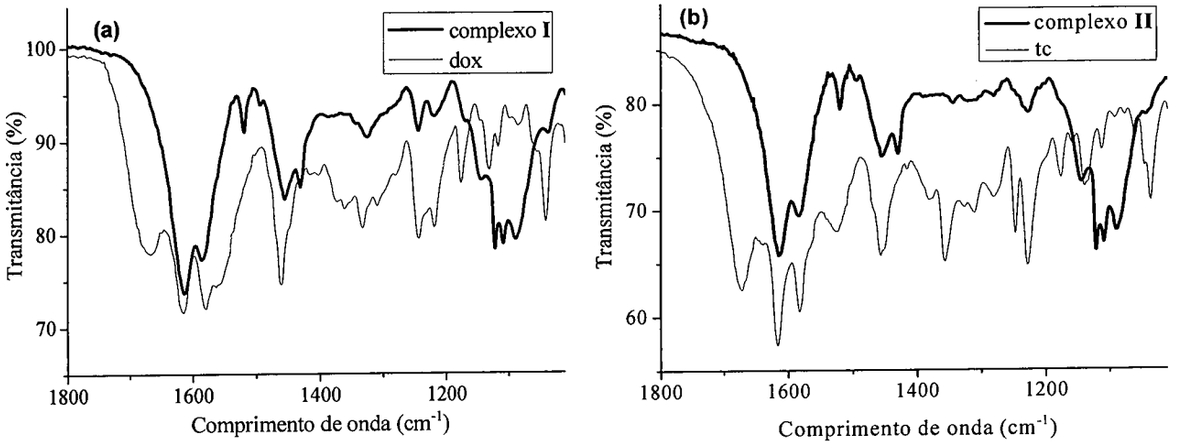

Figura 4

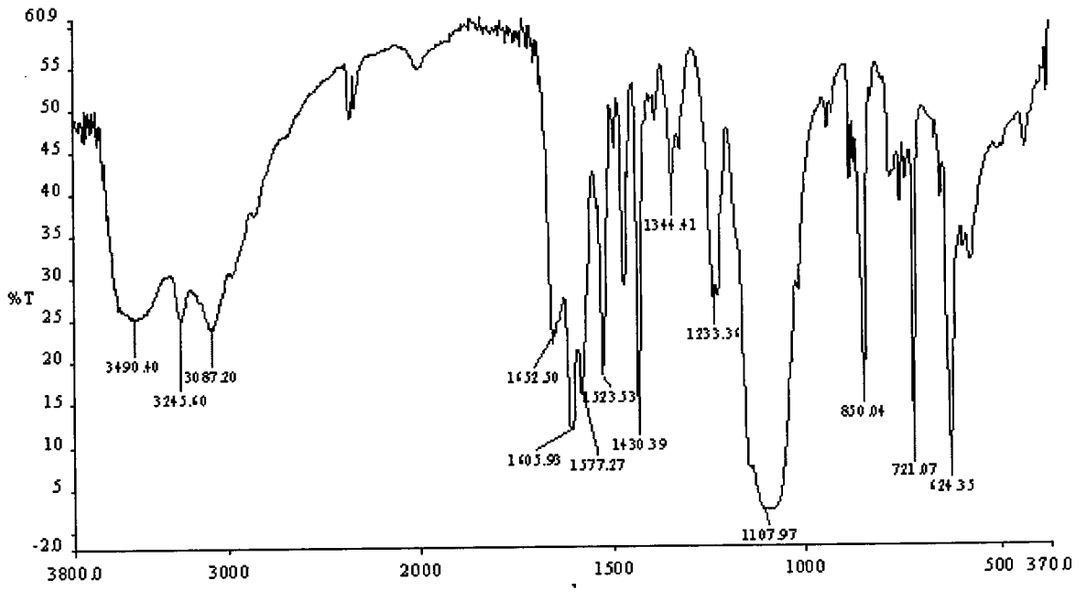

Figura 5

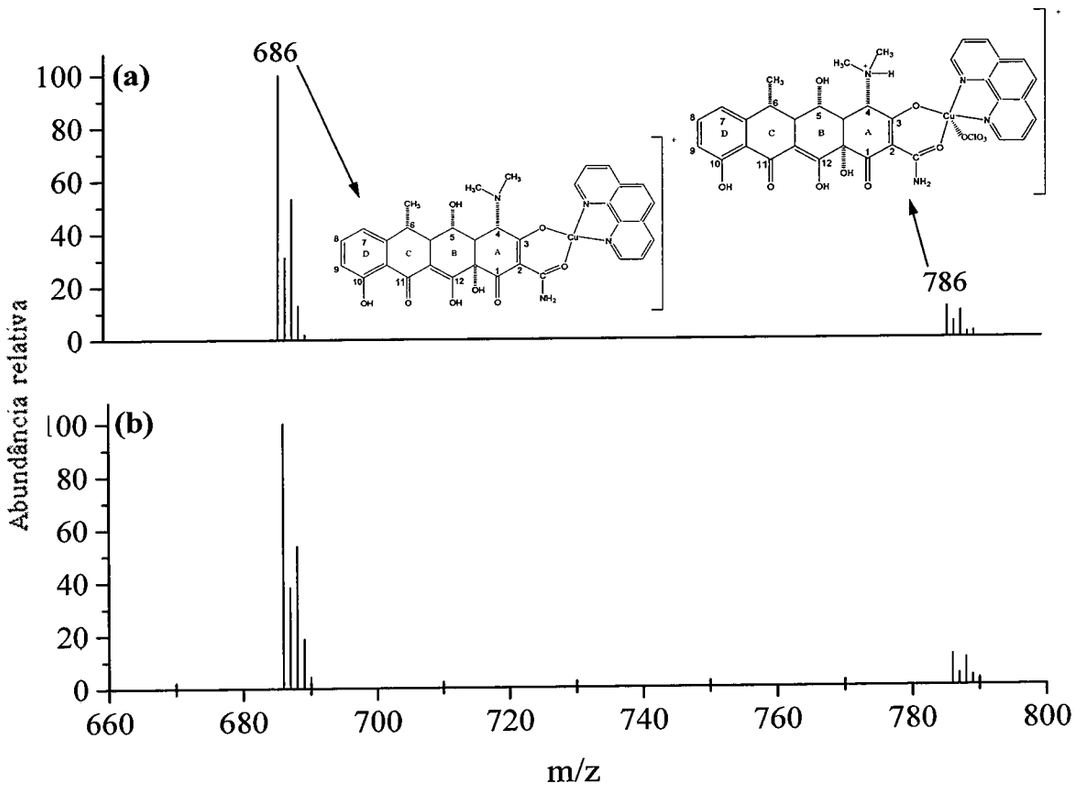

Figura 6

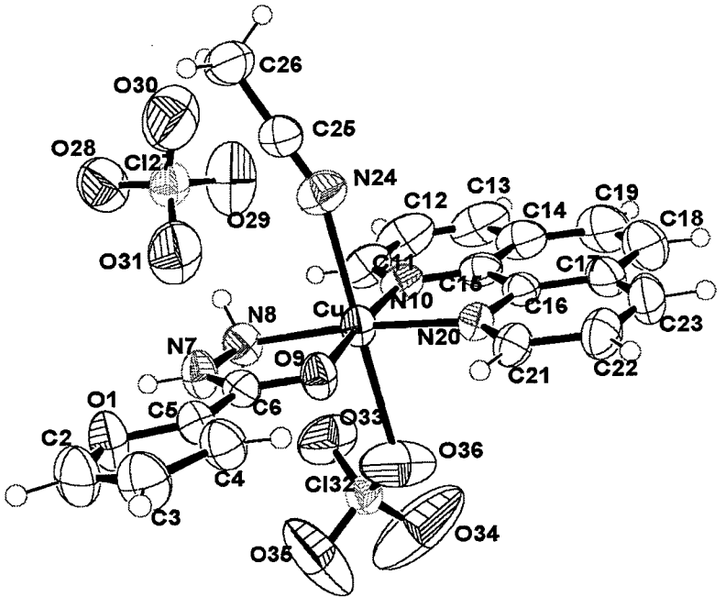

Figura 7

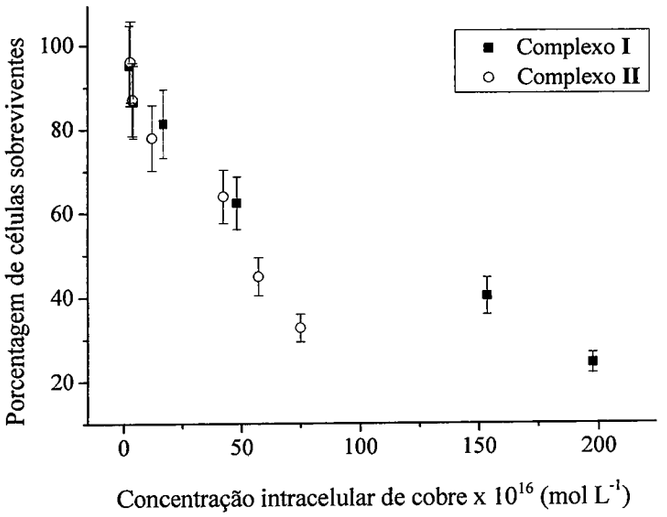

Figura 8

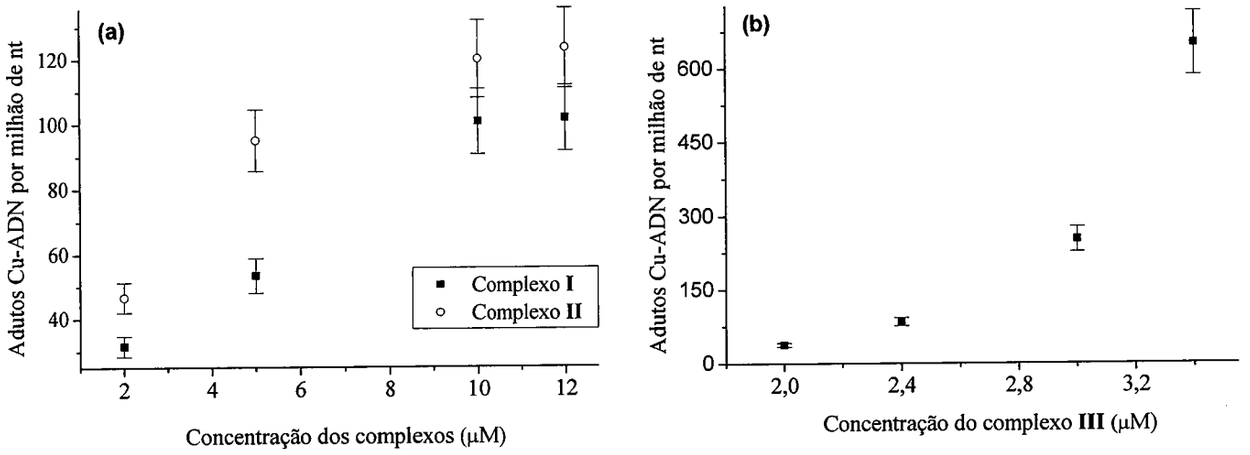

Figura 9

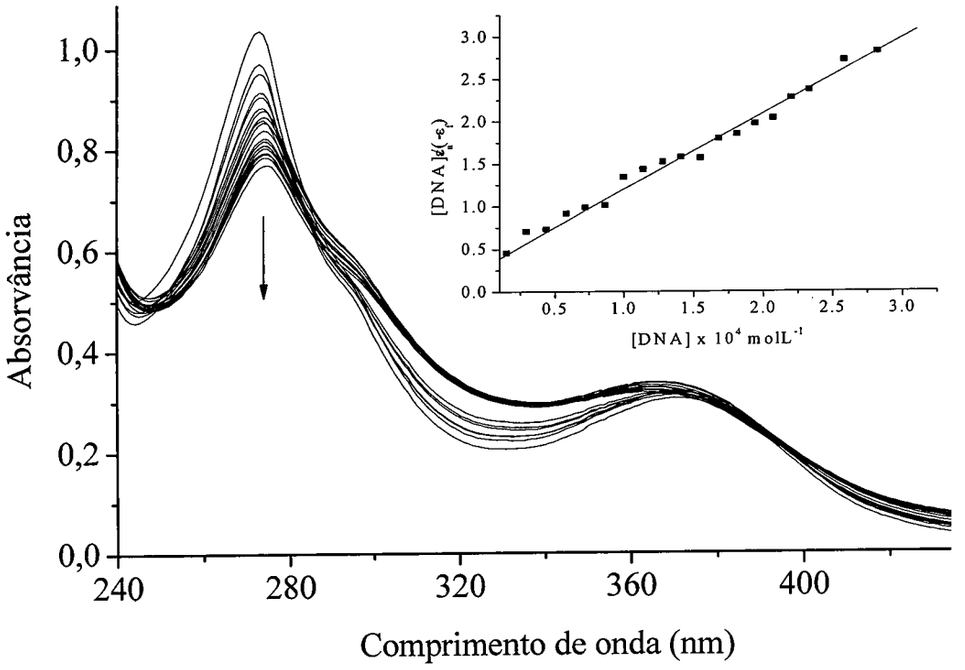
Absorvância
1,0
0,8
0,6
0,4
0,2
0,0
240
280
320
360
400
Comprimento de onda (nm)
[DNA]/(ε_a-ε_f)
3.0
2.5
2.0
1.5
1.0
0.5
0.0
0.5
1.0
1.5
2.0
2.5
3.0
[DNA] x 10^4 molL^-1

Figura 10

RESUMO

"PROCESSO DE SÍNTESE DE COMPLEXOS DE COBRE COM ATIVIDADE ANTITUMORAL"

A presente invenção descreve a síntese e a caracterização de complexos ternários de cobre possuindo como ligantes a 1,10-fenantrolina ou seus derivados e antibióticos da família das tetraciclinas, modificadas quimicamente ou não, ou ligantes do grupo das hidrazidas substituídas do ácido furóico ou do ácido benzóico, bem como composições farmacêuticas contendo os mesmos, como agentes antineoplásicos.

O aspecto inovador desta invenção inclui tanto os complexos descritos, que são inéditos, o método de preparação dos mesmos, como também suas atividades antitumorais.

Inorganica Chimica Acta 446 (2016) 87–92

Contents lists available at ScienceDirect

Inorganica Chimica Acta

journal homepage: www.elsevier.com/locate/ica

Synthesis, cytotoxic and antitubercular activities of copper(II) complexes with heterocyclic bases and 3-hydroxypicolinic acid

Janaina do Couto Almeida [a], Ivana M. Marzano [b], Marcos Pivatto [a], Norberto P. Lopes [c], Ana M. Da Costa Ferreira [d], F.R. Pavan [e], I.C. Silva [e], Elene C. Pereira-Maia [b], G. Von Poelhsitz [a], Wendell Guerra [a,*]

[a] Instituto de Química, Universidade Federal de Uberlândia, Uberlândia, MG, Brazil
[b] Departamento de Química, Universidade Federal de Minas Gerais, Belo Horizonte, MG, Brazil
[c] Núcleo de Pesquisa em Produtos Naturais e Sintéticos (NPPNS), Faculdade de Ciências Farmacêuticas de Ribeirão Preto, Universidade de São Paulo, 14.040-903 Ribeirão Preto, SP, Brazil
[d] Instituto de Química, Universidade de São Paulo, São Paulo, SP, Brazil
[e] Faculdade de Ciências Farmacêuticas, Departamento de Ciências Biológicas, Universidade Estadual Paulista, Campus Araraquara, 14.801-902 Araraquara, SP, Brazil

ARTICLE INFO

Article history:
Received 8 January 2016
Received in revised form 29 February 2016
Accepted 3 March 2016
Available online 9 March 2016

Keywords:
Copper complexes
N-donor heterocyclic ligands
Antimycobacterial activity
3-Hydroxypicolinic acid
Cytotoxicity activity

ABSTRACT

Two new copper(II) complexes with the deprotonated ligand 3-hydroxypicolinic acid (3-HPA) and heterocyclic bases (1,10-phenanthroline – phen or 2,2′-bipyridine – bpy) were synthesized. [Cu(3-HPA)(phen)ClO_4] **I** and [Cu(3-HPA)(bpy)ClO_4] **II** were characterized by elemental analyses, conductivity measurements, FT-IR, UV–Vis, EPR and High-resolution Electrospray Ionization Mass Spectrometry (HRESIMS). The results indicate that the geometry around the copper ion is distorted square-pyramidal, and that the copper ion is coordinated to 3-HPA *via* oxygen and nitrogen atoms, and to heterocyclic bases *via* their two nitrogen atoms. A perchlorate ion weakly bonded occupies the apical position, completing the metal coordination sphere. In this work, the compound [Cu(3-HPA)$_2$] **III** was also synthesized using a new method, different from that described in the literature. The cytotoxic activity of these compounds against tumor and normal cell lines was investigated. Complex **I** exhibited a strong antitumor activity, being the most active in the series of studied complexes. The compounds were also evaluated for activity against *Mycobacterium tuberculosis*, and the complex **I** displays good antimycobacterial activity, while compounds **II** and **III** were only moderately active.

1. Introduction

Metal complexes are useful as drugs in the treatment of a series of diseases, mainly in cancer chemotherapy. Since the discovery of the antitumoral activity of cisplatin, *cis*-[$PtCl_2(NH_3)_2$], in 1965, a great number of coordination compounds have been synthesized and tested in order to develop clinically more effective and safe drugs [1]. Although all approved drugs are based in platinum, having a *cis*-[PtX_2(amine)$_2$] chemotype (where X = leaving group, amine = neutral or carrier group) [2], some ruthenium compounds, as KP1019 and NAMI-A, have also entered clinical tests [3]. Other examples of metal complexes as candidates to therapeutic agents include gold [4] and cobalt [5], showing different mechanisms of action. Copper is very promising in the development of new pharmacological agents, because is an essential trace element important for the function of several enzymes involved in energy metabolism, respiration and DNA synthesis in the cell, having its homeostasis strictly regulated [6,7]. Therefore, copper complexes have been investigated for many therapeutic purposes, such as antitumoral, antimalarial, antifungal, and antibacterial agents, in the treatment of Alzheimer's disease, diabetes, rheumatoid arthritis, skin wounds, cardiovascular diseases, and leishmaniasis and more recently as potential drugs to combat Parkinson's disease [8]. Two copper complexes developed by Ruiz and co-workers, are already approved for clinical trials as antitumor drugs [9], and many copper complexes with *N*-donor heterocyclic ligands, such as 1,10-phenantroline and 2,2′-bipyridine were described to cleave DNA and inhibit tumoral cell growth [10–13]. We have previously reported the DNA cleavage ability of copper(II)-phenanthroline complexes with tetracycline and doxycycline [14]. These compounds inhibit the growth of a chronic myelogenous leukemia cell line and cleave DNA in mild conditions, in the absence of additional

* Corresponding author at: Instituto de Química, Universidade Federal de Uberlândia, João Naves de Ávila Avenue, 2121, Campus Santa Mônica, 38.400-902 Uberlândia, MG, Brazil. Tel.: +55 34 3239 4143.
E-mail address: wg@iqufu.ufu.br (W. Guerra).

http://dx.doi.org/10.1016/j.ica.2016.03.005
0020-1693/

agents [14]. In other studies, our research group also showed that copper complexes containing β-diketones or hydrazides and 2,2′-bipyridine or 1,10-phenanthroline are promising antitumoral agents [15–17]. Indeed, the synthesis of new copper(II) complexes with potential pharmacological activity is highly desired.

Here, our strategy to obtain new active compounds was to use the 3-hydroxypicolinic acid (3-HPA) as ligand to synthesize complexes of the type [Cu(3-HPA)(N–N)ClO_4], in which N–N = 1,10-phenantroline or 2,2′-bipyridine. The compound [Cu(3-$HPA)_2$] was also synthesized using a different method from that described in the literature. The complexes were characterized by elemental analyses, conductivity measurements, FT-IR, UV–Vis, EPR and High-resolution Electrospray Ionization Mass Spectrometry (HRESIMS). Regarding the 3-hydroxypicolinic acid, Barbosa et al. [18] reported a ruthenium(II) complex with 3-HPA that showed a good activity against *Mycobacterium tuberculosis* H37Rv ATCC 27294. These findings encourage us to prepare a new series of copper complexes and to evaluate its potentiality as antitumoral and antimycobacterial agents.

2. Experimental

2.1. Starting materials

The reagents (ligands and metallic salts) are commercially available (Aldrich).

2.2. Preparation of the complexes

The complexes with heterocyclic bases were synthesized following the same general procedure. For example, [Cu(3-HPA)(phen)ClO_4] was prepared by the reaction of $Cu(ClO_4)_2{\cdot}6H_2O$ (60.4 mg, 0.25 mmol) with 0.25 mmol of 3-hydroxypicolinic acid (3-HPA) in methanol (5 mL). The mixture was stirred for 20 min followed by the slow addition of 1,10-phenanthroline (0.25 mmol) previously dissolved in methanol. After 48 h, the solid formed was separated by filtration, washed with water and dried under reduced pressure.

2.2.1. [Cu(3-HPA)(phen)ClO_4] **I**

M.M.: 481.30 g mol^{-1}. Yield: 62%. Color: Blue. *Anal.* Calc. for ($CuC_{18}H_{12}N_3O_7Cl$): C, 44.92; H, 2.51; N, 8.73. Found: C, 44.98; H, 2.37; N, 8.69%. HRESIMS (methanol), *m/z*: 381.0184 $[M-ClO_4]^+$. IR (KBr) ν (cm^{-1}): 3447, 3105, 3068, 2374, 2338, 1653, 1646, 1637, 1629, 1608, 1560, 1522, 1508, 1457, 1429, 1397, 1388, 1340, 1320, 1275, 1239, 1219, 1150, 1110, 1087, 900, 872, 847, 832, 820, 809, 777, 767, 736, 720, 692, 623, 588, 453. UV–Vis (methanol), λ_{max} (nm) = 342 (4.8×10^2 mol^{-1} L cm^{-1}), 294 (1.9×10^3 mol^{-1} L cm^{-1}), 272 (4.60×10^3 mol^{-1} L cm^{-1}), 265 (5.00×10^3 mol^{-1} L cm^{-1}), 227 (7.80×10^3 mol^{-1} L cm^{-1}), 670 (3.00×10^1 mol^{-1} L cm^{-1}), 700 (solid). EPR parameters, in solid: $g_\perp$ 2.051, $g_{//}$ 2.164; in frozen acetonitrile solution: $g_\perp$ 2.079, $g_{//}$ 2.271, $A_{//}$ 167G, or $177{\cdot}10^{-4}$ cm^{-1}, $g_{//}/A_{//}$, 128 cm. Molar conductivity, ΛM (ethanol) = 39.12 μS cm^{-1}.

2.2.2. [Cu(3-HPA)(bpy)ClO_4] **II**

M.M.: 457.2814 g mol^{-1}. Yield: 50%. Color: Blue. *Anal.* Calc. for ($CuC_{16}H_{12}N_3O_7Cl$): C, 42.02; H, 2.65; N, 9.19. Found: C, 41.77; H, 2.37; N, 9.01%. HRESIMS (ethanol), *m/z*: 357.0176 $[M-ClO_4]^+$. IR (KBr) ν (cm^{-1}): 3450, 2375, 2344, 1653, 1647, 1637, 1629, 1624, 1616, 1608, 1473, 1465, 1458, 1448, 1319, 1276, 1240, 1217, 1152, 1122, 1089, 899, 832, 819, 809, 769, 729, 691, 621, 590, 452. UV–Vis (ethanol), λ_{max} (nm) = 309 (1.30×10^4 mol^{-1} L cm^{-1}), 297 (1.50×10^4 mol^{-1} L cm^{-1}), 224 (2.63×10^4 mol^{-1} L cm^{-1}), 661 (3.10×10^1 mol^{-1} L cm^{-1}), 633 (solid). ΛM (ethanol) = 35.93 μS cm^{-1}.

2.2.3. [Cu(3-$HPA)_2$] **III**

This complex was synthesized by Girginova et al. using a different method [19]. In this work, [Cu(3-$HPA)_2$] was prepared by the reaction of $Cu(ClO_4)_2{\cdot}6H_2O$ (60.4 g, 0.25 mmol) with 0.50 mmol of 3-hydroxypicolinic acid (3-HPA) in methanol (5 mL). The mixture was stirred for 48 h and the crystalline solid formed was separated by filtration, washed with water and dried under reduced pressure.

M.M.: 339.7477 g mol^{-1}. Yield: 51%. Color: Dark blue. *Anal.* Calc. for ($CuC_{12}H_8N_2O_6$): C, 42.42; H, 2.37; N, 8.25. Found: C, 42.84; H, 2.51; N, 8.13%. IR (KBr) ν (cm^{-1}): 3453, 3100, 3069, 2376, 2344, 1653, 1647, 1608, 1576, 1570, 1559, 1508, 1456, 1394, 1388, 1321, 1309, 1275, 1240, 1217, 1153, 1128, 1058, 903, 833, 819, 810, 765, 691, 588, 452. UV–Vis (ethanol), λ_{max} (nm) = 302 (1.21×10^4 mol^{-1} L cm^{-1}), 653 (3.5×10^1 mol^{-1} L cm^{-1}), 598 (solid). ΛM (ethanol) = 0.69 μS cm^{-1}.

2.3. Physical measurements

Conductivity studies were carried out with a Digimed DM 31 conductivity meter using a cell of constant 0.95 cm^{-1}, and spectroscopic grade ethanol (ΛM = 0.93 μS cm^{-1}) as solvent.

Elemental analyses were performed using a Perkin-Elmer 2400 CHN Elemental Analyser.

IR spectra were registered in KBr pellets on a Shimadzu FTIR-Irprestige-21 spectrometer.

Diffuse reflectance spectra and UV–Vis were obtained on a Shimadzu UV-2501 PC spectrophotometer.

High-resolution Electrospray Ionization Mass Spectrometry (HRESIMS) were measured on an ultrOTOF (Bruker Daltonics) spectrometer, operating in the positive mode. Methanol–water (1:1, v/v) was used as solvent system and the samples were infused into the ESI source at a flow rate of 5 μL/min. The calculated values for the charged complex ions were made using ChemDraw Ultra 14.0.

For the EPR spectra registration, a Bruker instrument (Karlsruhe, Germany), model EMX, operating at X-band (9.50 GHz frequency, 20 mW power, 100 kHz modulation frequency) was used. Measurements were performed at 77 K, with samples in solid state or in frozen acetonitrile solution, using Wilmad quartz tubes. DPPH (α,α′-diphenyl-β-picrylhydrazyl) was used for frequency calibration (g = 2.0036).

2.4. Cells and culture

2.4.1. K562 cells

The K562 cell line was purchased from the Rio de Janeiro Cell Bank (number CR083 of the RJCB collection). This cell line was established from pleural effusion of a 53 year-old female with chronic myelogenous leukemia in terminal blast crisis. Cells were cultured in RPMI 1640 (Sigma Chemical Co.) medium supplemented with 10% fetal calf serum (CULTILAB, São Paulo, Brazil) at 37 °C in a humidified 5% CO_2 atmosphere. Cultures grow exponentially from 10^5 cells mL^{-1} to about 8×10^5 cells mL^{-1} in three days. Cell viability was checked by Trypan Blue exclusion. The cell number was determined by coulter counter analysis.

For cytotoxicity assessment, 1×10^5 cells mL^{-1} was cultured for 72 h in the absence and presence of a range of concentrations of tested compounds. The sensitivity to compound was evaluated by the concentration that inhibits cell growth by 50% (IC_{50}). Stock solutions were prepared in DMSO and diluted accordingly to obtain the concentrations used in the cytotoxic assays. The final concentration of DMSO in the experiments was below 0.5% and we have checked that the solvent has no effect on cell growth at this concentration.

2.4.2. MRC-5 and A549 cells

MRC-5 (normal fibroblast pulmonary cells) and A549 (human lung adenocarcinoma epithelial) cells line were obtained from the American Type Culture Collection (Manassas, VA, USA), and incubated in DMEM medium with supplemented with 10% FBS and 1% penicillin (100 U/ml)–streptomycin (100 μg/ml). Cells were maintained in a humidified environment at 37 °C with 5% CO_2 and sub-cultured twice per week.

A resazurin reduction assay was used to investigate cytotoxicity of several drugs toward MRC-5 and A549 cells. The assay is based on reduction of the indicator dye, resazurin, to the highly fluorescent resorufin by viable cells. Nonviable cells rapidly lose the metabolic capacity to reduce resazurin and thus do not produce a fluorescent signal.

Briefly, the cells were detached by treatment with 0.25% trypsin/EDTA (VitroCell, Brazil) and 2.5×10^4 cells were placed in each well of a 96-well cell culture plate (Costar, USA) in a total volume of 100 μl. Cells were allowed to adhere overnight and then were treated with different concentrations of drugs. After 24 h or 72 h incubation in the presence of the compounds, the medium was removed and 50 μl resazurin (Sigma–Aldrich, Germany) 0.01%w/v in DMEM, was added to each well and the plates were incubated at 37 °C for 3 h.

The fluorescence was measured on Biotek Synergy H1 plate reader (Biotek, Winooski, VT) using an excitation wavelength of 530 nm and an emission wavelength of 590 nm. Untreated cells constituted the negative control (viable cells), and cells treated with doxorubicin at 100 nmol (Sigma–Aldrich, St. Louis, MO, USA) constituted the positive control (death control, DC). All the tests were performed in three independents assays. A test was done on plates without cells to verify that the reaction cannot occur between the compounds and the reagent to avoid false-positive results (data not shown).

The IC_{50} values represent the samples concentrations required to inhibit 50% of cell proliferation and were calculated from a calibration curve by regression curves using Microsoft Excel.

2.5. Anti-Mycobacterium tuberculosis activity assay

The anti-MTB activity of the compounds was determined by the REMA (Resazurin Microtiter Assay) method [20]. Stock solutions of the tested compounds were prepared in DMSO and diluted in Middlebrook 7H9 broth (Difco) supplemented with oleic acid, albumin, dextrose and catalase (OADC), performed by Precision XS (Biotek®) to obtain the final drug concentration range of 0.09–25 μg/mL. Isoniazid was dissolved in distilled water and rifampicin in DMSO, and both were used as standard drugs. A suspension of MTB H_{37}Rv ATCC 27 294 was cultured in Middlebrook 7H9 broth supplemented with OADC and 0.05% Tween 80. The cultures were frozen at −80 °C in aliquots. After two days the CFU per mL (colony formation unit per mL) of an aliquot was determined. The concentrations were adjusted by 5×10^5 CFU per mL and 100 μL of the inoculum were added to each well of a 96-well microplate (Kasvi®) together with 100 μL of the compounds. Samples were set up in triplicate. The plates were incubated for 7 days at 37 °C. Resazurin (solubilized in water) was added (30 μL of 0.01%). The fluorescence of the wells was read after 24 h with a Cytation 3 (Biotek®). The MIC was defined as the lowest concentration resulting in 90% inhibition of growth of MTB.

3. Results and discussion

Copper(II) complexes with the deprotonated ligand 3-hydroxypicolinic acid (3-HPA) were synthesized and characterized by elemental analyses, conductivity measurements, FT-IR, UV–Vis, High-resolution Electrospray Ionization Mass Spectrometry (HRESIMS) and EPR. All the copper complexes are colourful, non hygroscopic, stable to air and light and soluble in organic solvents such as DMSO, ethanol and acetonitrile. The chemical structures of the complexes with 3-HPA are presented in Fig. 1.

The results of the elemental analyses are in good agreement with the proposed structures. The molar conductivity values of solutions (10^{-3} M; ethanol) for all complexes with heterocyclic bases fall in the range observed for 1:1 electrolytes [21]. The labilization of the axial ligands in solution (perchlorate anion) results in the generation of compounds of type $[Cu(3\text{-HPA})(N\text{–}N)]^+$. On the other hand, as expected, the molar conductivity value for **III** indicates that this compound is nonelectrolyte. The crystal structure of the complex **III** has been described in the literature [19] and it will not be discussed further here. Nevertheless, for this complex, the metal ion is coordinated to two N,O-chelating anionic ligands and exhibits a distorted square planar coordination geometry [19].

The high-resolution mass spectra of the synthesized complexes were performed and the obtained data are according to the proposed structures. In this work, the m/z values listed in the text (see Section 2) refer to the peak containing the most abundant isotope (^{63}Cu). For example, mass spectrum of the complex **II** (Fig. S1) exhibited the charged ion at m/z 357.0176 $[M-ClO_4]^+$ (calcd. 357.0175). The experimental isotopic patterns for [Cu(3-HPA)(bpy)]$^+$ and [Cu(3-HPA)(phen)]$^+$ ions match the theoretical isotopic patterns considering the proposed compositions.

The UV–Vis spectra of the complexes were recorded in ethanol (10^{-4} M) in the range of 200–900 nm. A bathochromic shift in relation to free ligands confirms the presence of the complexes in solution. The absorption spectra of the complex **II** and of the corresponding ligands are shown in Fig. 2. The splitting observed in the spectrum of the complex is also consistent with the coordination of the ligand to metal. Complexes **I** and **II** exhibit only one broad and asymmetric d–d band centered at ≈660 nm. For example, the complex **II** exhibits a d–d band (Fig. S2) centered at 661 nm ($\varepsilon = 31\ mol^{-1}\ L\ cm^{-1}$). These observations are consistent with a distortion from the square-pyramidal geometry, due to the Jahn–Teller effect [15]. In the solid state (diffuse reflectance), the complexes **I** and **II** exhibit the d–d band centered at 633 and 700 nm, respectively, indicating that the geometry of the complexes in solution differs from that in solid state [17].

The IR spectra of the new complexes are in accordance with the presence of 3-HPA coordinated to the copper(II) ions via the carboxylate group and nitrogen. The carboxylate group may coordinate to a metal atom in one of the unidentate, bidentate or bridging modes. For all complexes, bands corresponding to the $\nu as(COO^-)$ and $\nu s(COO^-)$ vibrational modes appeared close to 1654 (1703 cm^{-1} in the uncoordinated ligand) and 1320 cm^{-1} (1295 cm^{-1} in the uncoordinated ligand), respectively. The value of $\Delta(\nu as - \nu s) = 331\ cm^{-1}$ indicates the presence of monodentate carboxylate group. Peaks of medium intensity around 1580 cm^{-1} are assigned to ν(C=N) of the coordinated ligand, in good agreement with the N,O-chelation [19,22]. The same coordination mode was observed in previous works for some complexes containing 3-HPA as ligands [18,19,22–24]. The stretching vibrations of the uncoordinated hydroxyl group of ligand appear in the range 3448–3455 cm^{-1}. The weak bands at 3100 and 3000 cm^{-1} are attributed to the stretching vibrations of aromatic C–H bonds. Infrared spectroscopy is very useful to determine the mode of coordination of the ClO_4 ligand. The behavior of the weakly coordinating perchlorate ion can be distinguished by the Cl–O stretching frequencies [14]. The infrared spectra of **I** and **II** indicate the presence of one unidentate perchlorate ion. Bands in the region 578–559 and 443–437 cm^{-1} were assigned to νCu–N and νCu–O.

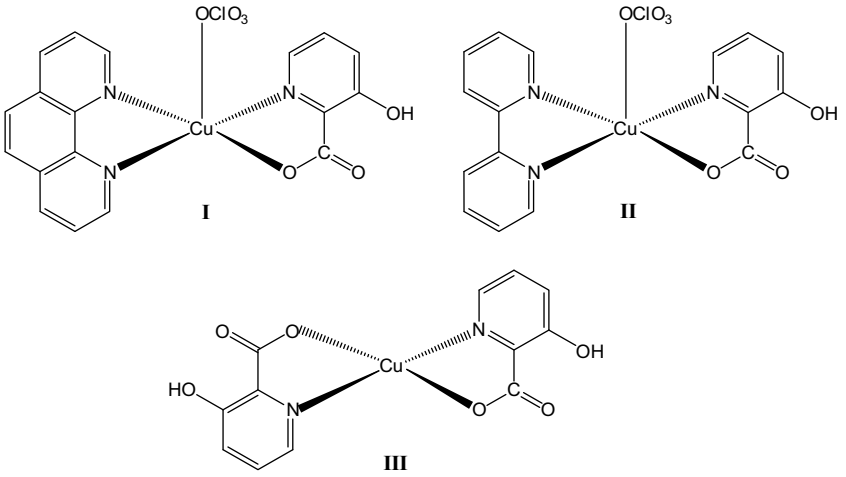

Fig. 1. Proposals structures for the complexes **I**–**III**.

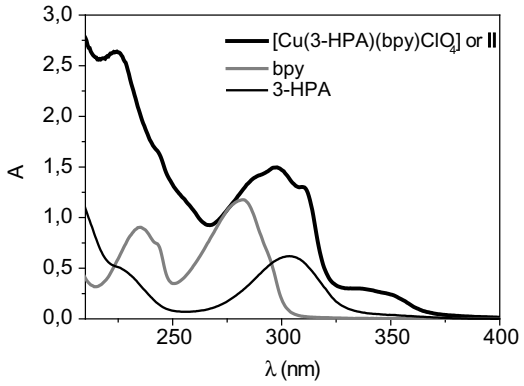

Fig. 2. Electronic spectra of [Cu(3-HPA)(bpy)ClO_4], 3-HPA, and bpy, in ethanol (1.0×10^{-4} M).

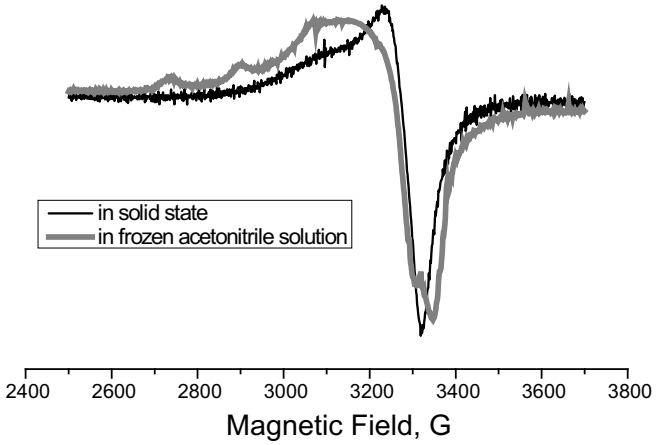

Fig. 3. EPR spectra of the complex **I** (solution and in solid-state).

EPR spectra for complex **I** (Fig. 3) in solid state and in frozen acetonitrile solution corroborate the change of geometry observed in electronic spectra. In the solid, a perchlorate anion is bound at the apical position, providing a penta-coordinate environment around the metal ion, while in solution a tetragonal geometry with little tetrahedral distortion is observed, as indicated by the spectroscopic parameters ratio obtained, $g_{//}/A_{//}$ (128 cm) [17,25] (see Table 1).

Table 1
EPR spectroscopic parameters.

Compound	$g_{\perp}$	$g_{//}$	$A_{//}$ (G)	$A_{//}$ (10^{-4} cm^{-1})	$g_{//}/A_{//}$ (cm)
[Cu(3-HPA)(Phen)ClO_4] **I**					
In frozen acetonitrile solution	2.079	2.271	167	177	128
In solid state	2.050	2.162			

3.1. Stability of complexes

Stability is a very important factor for the development of clinical metal complexes [13]. Thus, the stability of the complex **I** was evaluated by UV–Vis spectral analysis at different times in a mixture containing H_2O/DMSO (1:99 v/v). According to the Fig. 4, the values of absorbance and wavelength were not affected. These observations indicate that the complex is stable in solution for at least 8 h under the test conditions [26].

3.2. Cytotoxic studies

The cytotoxic activity of compounds is depicted in Table 2. IC_{50} values obtained for two platinum complexes used in chemotherapy, cisplatin and carboplatin, are also shown for the sake of comparison.

As it can be seen in Table 2, phenanthroline (phen) displays high activity and selectivity index (SI) against the K562 cell line.

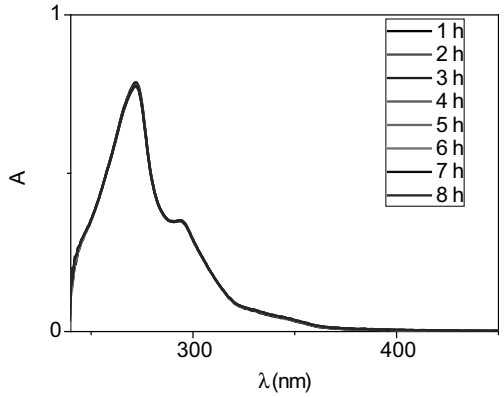

Fig. 4. Ultraviolet spectra of complex **I** as a function of time.

Table 2
[a]IC_{50} (μM) values for ligands, cisplatin, carboplatin and complexes.

Compound	K562 (72 h)	MRC-5 (72 h)	[b]SI	MRC-5 (24 h)	A549 (24 h)	[b]SI
3-HPA	130.0	2767.6	21.3	2228.4	2264.4	0.9
phen	3.2	166.4	52	305.0	77.6	3.9
bpy	30.0	>2560.9	>85.4	320.1	>2560.9	<0.12
I	2.3	0.4	0.17	4.8	8.3	0.6
II	21.8	32.8	1.50	43.7	52.5	0.8
III	20.8	70.6	3.40	53.0	82.4	0.6
Carboplatin	10.0	–		–	–	–
Cisplatin	1.1	–		–	–	–

K562: chronic myelogenous leukemia cell line.
MRC-5: lung cell line (normal).
A549: human lung adenocarcinoma epithelial cell line.
[a] IC_{50} – concentration required to inhibit 50% of cell growth.
[b] SI – selectivity index.

However, in the literature, for the phenanthroline and its derivatives, it is assumed that the sequestering of trace metals in situ is involved and that the resulting metallic complexes are the active species [27]. All organic compounds exhibited low activity against A549 and MRC-5.

The copper complexes inhibit the growth of K562 and A549 cells with IC_{50} values between 2.3 and 82.4 μM. The results showed that activity of the complexes follows the order **I > II = III**. Copper coordination improves the cytotoxic activity: all complexes are more potent than the corresponding free ligands. The substitution of one molecule of 3-HPA by one molecule of phen significantly increases the cytotoxic activity; though, it does not improve the selectivity index, which is low and suggests a generic toxicity. Regarding the complexes **I** and **II**, compared to similar compounds containing aromatic diimine ligands (N–N) already described, they show very similar results, as shown in Table 3. In the complexes with heterocyclic bases, the substitution of bpy by phen increases the activity. As a general behaviour of those aromatic diamine ligands, copper complexes with phenanthroline are more reactive than similar ones with bipyridine ligands [8c,14]. An accepted explanation for this order of reactivity is that the planar polycyclic phen ring interacts better with DNA [28]. However, the mode of action of these complexes can be quite different. Casiopeines [Cu(N–N)L]X, for example, have been described as interacting with mitochondria, inhibiting oxidative phosphorylation and, eventually, also cellular ATP depletion, in addition to DNA binding [30].

Table 3
Comparison of the cytotoxicity of different copper complexes with the chemotype [Cu(N–N)L]X (where N–N = 1,10-phen or 2,2′-bpy, and X = counterion, NO_3^-, or ClO_4^-).

Complex	IC_{50} (μmol/L)	Cytotoxicity	References
[Cu(3-hydroxypicolinic acid) (phen) ClO_4]	2.3 ± 0.2	K562 cells	This work
[Cu(3-hydroxypicolinic acid) (bpy) ClO_4]	21.8 ± 2.2	K562 cells	This work
[Cu(BTA)(phen)NO_3]	2.9 ± 0.3	K562 cells	[17]
[Cu(BTA)(bpy)NO_3]	13.7 ± 1.4	K562 cells	[17]
[Cu(BTACl)(phen)NO_3]	2.1 ± 0.2	K562 cells	[17]
[Cu(BTACl)(bpy)NO_3]	9.2 ± 1.0	K562 cells	[17]
[Cu(doxycycline)(1,10-phen) (H_2O) (ClO_4)]ClO_4	1.93 ± 0.2	K562 cells	[14]
[Cu(tetracycline)(1,10-phen)(H_2O) (ClO_4)]ClO_4	2.59 ± 0.3	K562 cells	[14]
[Cu(phen)(α-glycinate)]NO_3	13.9 ± 1.3 27.3 ± 2.2	HeLa MCF-7	[28]
[Cu(5,6-dimethylphen) (α-glycinate)]NO_3	5.3 ± 0.1 4.4 ± 0.3	HeLa MCF-7	[28]
Cu(4,7-dimethylphen)(glycinate)] NO_3	6	A549	[29]

Table 4
Anti-MTB activity (MIC) of the copper complexes and their free ligands.

Compound	MIC_{90} (μg/mL)	MIC_{90} (μM)
phen	4.1	22.7
bpy	>25	>160.0
3-HPA	>25	179.7
[Cu(3-HPA)(phen)ClO_4] **I**	11.9	24.72
[Cu(3-HPA)(bpy)ClO_4] **II**	>25	>54.7
[Cu(3-HPA)$_2$] **III**	24.2	71.23

3.3. Anti-M. tuberculosis activity

The antimycobacterial activity of compounds was evaluated in vitro against *M. tuberculosis* H37Rv strains by the REMA (Resazurin Microtiter Assay) method. As can be seen in Table 4, phen shows good activity against the *M. tuberculosis* H37Rv strain with MIC value equal to 22.7 μM. Regarding the phenanthroline (phen), this molecule and its derivatives have been identified as new agents with antimycobacterial activity [24,31,32]. Concerning the complexes, the results showed that the activity of the complex **I** was higher than that of free 3-HPA, displaying good antimycobacterial activity, while compounds **II** and **III** were only moderately active. Regarding the activity of compound **I**, this should be more lipophilic than complex **II**, consequently it has a higher ability to diffuse into the cell membrane and reach their biological target [33].

4. Concluding remarks

Two new copper(II) complexes containing 3-hydroxypicolinic acid and heterocyclic bases were prepared and characterized. For these complexes, the results indicate a distorted square-pyramidal geometry around the copper ion in the solid, where the copper ion is penta-coordinated to 3-HPA ligand via their oxygen and nitrogen atoms, and to the heterocyclic bases by its nitrogen atoms. The axial position is occupied by a perchlorate ion. However, in solution this anion acts only as counter-ion, and the geometry around copper becomes tetragonal, as attested by UV–Vis and EPR spectra (in the case of [Cu(3-HPA)(Phen)]ClO_4 species). The biological activities of the copper complexes make them good candidates for further studies, once small structural modifications may result in an increase of the selectivity index. Indeed, these complexes can be useful for the design of new antitumoral and antibacterial agents.

Acknowledgments

To CNPq (Conselho Nacional de Desenvolvimento Científico e Tecnológico, Brazil), FAPEMIG (Fundação de Amparo à Pesquisa de Minas Gerais, Brazil), and INCT-Catálise by financial support and fellowships. The authors are also thankful to the Grupo de Materiais Inorgânicos do Triângulo – GMIT research group supported by FAPEMIG (APQ-00330-14). This work is a collaboration research project of members of the Rede Mineira de Química (RQ-MG) supported by FAPEMIG (Project: CEX – RED-00010-14).

Appendix A. Supplementary material

Supplementary data associated with this article can be found, in the online version, at http://dx.doi.org/10.1016/j.ica.2016.03.005.

References

[1] F. Trudu, F. Amato, P. Vaňhara, T. Pivetta, E.M. Peña-Méndez, J. Havel, J. Appl. Biomed. 13 (2015) 79.
[2] N.P. Farrell, Chem. Soc. Rev. (2015), http://dx.doi.org/10.1039/c5cs00201j.

[3] R. Trondl, P. Heffeter, C.R. Kowol, M.A. Jakupec, W. Berger, B.K. Keppler, Chem. Sci. 5 (2014) 2925.
[4] T. Zou, C.T. Lum, C.-N. Lok, J.-J. Zhang, C.-M. Che, Chem. Soc. Rev. (2015), http://dx.doi.org/10.1039/c5cs00132c.
[5] M.C. Heffern, N. Yamamoto, R.J. Holbrook, A.L. Eckermann, T.J. Meade, Curr. Opin. Chem. Biol. 17 (2013) 189.
[6] C. Duncan, A.R. White, Metallomics 4 (2012) 127.
[7] (a) A.K. Boal, A.C. Rosenzweig, Chem. Rev. 109 (2009) 4760;
(b) M.J. Burkitt, Arch. Biochem. Biophys. 394 (2001) 117;
(c) E.R. Stadtman, R.L. Levine, Amino Acids 25 (2003) 207.
[8] (a) S. Medici, M. Peana, V.M. Nurchi, J.I. Lachowicz, G. Crisponi, M.A. Zoroddu, Coord. Chem. Rev. 284 (2015) 329;
(b) C. Santini, M. Pellei, V. Gandin, M. Porchia, F. Tisato, C. Marzano, Chem. Rev. 114 (2014) 815.
[9] R. Galindo-Murillo, J.C. García-Ramos, L. Ruiz-Azuara, T.E. Cheatham, F. Cortés-Guzmán, Nucleic Acids Res. 4 (2015) 5364.
[10] C. Marzano, M. Pellei, F. Tisato, C. Santini, Anticancer Agents Med. Chem. 9 (2009) 185.
[11] L. Ruiz-Azuara, M.E. Bravo-Gomez, Curr. Med. Chem. 17 (2010) 3606.
[12] S. Tardito, L. Marchio, Curr. Med. Chem. 16 (2009) 1325.
[13] F. Tisato, C. Marzano, M. Porchia, M. Pellei, C. Santini, Med. Res. Rev. 30 (2010) 708.
[14] P.P. Silva, W. Guerra, J.N. Silveira, A.M.D.C. Ferreira, T. Bortolotto, F.L. Fischer, H. Terenzi, A. Neves, E.C. Pereira-Maia, Inorg. Chem. 50 (2011) 6414.
[15] P.S. Lopes, D.A. Paixão, F.C.S. de Paula, A.M.D.C. Ferreira, J. Ellena, S. Guilardi, E. C. Pereira-Maia, W. Guerra, J. Mol. Struct. 1034 (2013) 84.
[16] P.P. Silva, W. Guerra, G.C. dos Santos, N.G. Fernandes, J.N. Silveira, A.M. da Costa Ferreira, T. Bortolotto, H. Terenzi, A.J. Bortoluzzi, A. Neves, E.C. Pereira-Maia, J. Inorg. Biochem. 132 (2014) 67.
[17] J.C. Almeida, D.A. Paixão, I.M. Marzano, J. Ellena, M. Pivatto, N.P. Lopes, A.M.D. C. Ferreira, E.C. Pereira-Maia, S. Guilardi, W. Guerra, Polyhedron 89 (2015) 1.
[18] M.I.F. Barbosa, R.S. Corrêa, L.V. Pozzi, E.O. Lopes, F.R. Pavan, C.Q.F. Leite, J. Ellena, S.P. Machado, G.V. Poelhsitz, A.A. Batista, Polyhedron 85 (2015) 376.
[19] P.I. Girginova, F.A.A. Paz, H.I.S. Nogueira, N.J.O. Silva, V.S. Amaral, J. Klinowski, T. Trindade, J. Mol. Struct. 737 (2005) 221.
[20] J.C. Palomino, A. Martin, M. Camacho, H. Guerra, J. Swings, F. Portaels, Antimicrob. Agents Chemother. 46 (2002) 2720.
[21] W. Geary, Coord. Chem. Rev. 7 (1971) 81.
[22] C. Sun, X. Zheng, L.P. Jin, J. Mol. Struct. 646 (2003) 201.
[23] M. Boris-Marko Kukovec, Croat. Chem. Acta 85 (2012) 479.
[24] F.R. Pavan, G.V. Poelhsitz, M.I.F. Barbosa, S.R.A. Leite, Alzir.A. Batista, J. Ellena, L. S. Sato, S.G. Franzblau, V. Moreno, D. Gambino, C.Q.F. Leite, Eur. J. Med. Chem. 46 (2011) 5099.
[25] J.C. García-Ramos, R. Galindo-Murillo, A. Tovar-Tovar, A.L. Alonso-Saenz, V. Gómes-Vidales, M. Flores-Álamo, L. Ortiz-Frade, F. Cortes-Guzmán, R. Moreno-Esparza, A. Campero, L. Ruiz-Azuara, Chem. Eur. J. 20 (2014) 13730.
[26] B. Li-Jun Li, Inorg. Chim. Acta 419 (2014) 135.
[27] (a) R.A. MacLeod, J. Biol. Chem. 197 (1952) 751;
(b) F.P. Dwyer, I.K. Reid, A. Shulman, G.M. Laycock, S. Dixon, Aust. J. Exp. Biol. Med. Sci. 47 (1969) 203;
(c) M. McCann, A.L.S. Santos, B.A. da Silva, M.T.V. Romanos, A.S. Pyrrho, M. Devereux, K. Kavanagh, I. Fichtner, A. Kellet, Toxicol. Res. 1 (2012) 47.
[28] M.E. Bravo-Gómez, J.C. García-Ramos, I. Gracia-Mora, L. Ruiz-Azuara, J. Inorg. Biochem. 103 (2009) 299.
[29] R. Kachadourian, H.M. Brechbuhl, L. Ruiz-Azuara, I. Gracia-Mora, B.J. Day, Toxicology 268 (2010) 176.
[30] A. Marín-Hernandez, I. Gracia-Mora, L. Ruiz-Ramírez, R. Moreno-Sanchez, Biochem. Pharmacol. 65 (2003) 1979.
[31] R. Danac, C.M.A. Matarneh, S. Shova, T. Daniloaia, M. Balan, I.I. Mangalagiu, Bioorg. Med. Chem. 23 (2015) 2318.
[32] R. Danac, I.I. Mangalagiu, Eur. J. Med. Chem. 74 (2014) 664.
[33] J.C. Almeida, I.M. Marzano, F.C. Silva de Paula, M. Pivatto, N.P. Lopes, P.C. de Souza, F.R. Pavan, A.L.B. Formiga, E.C. Pereira-Maia, W. Guerra, J. Mol. Struct. 1075 (2014) 370.

Journal of Inorganic Biochemistry 172 (2017) 138–146

Contents lists available at ScienceDirect

Journal of Inorganic Biochemistry

journal homepage: www.elsevier.com/locate/jinorgbio

Novel copper(II) complexes with hydrazides and heterocyclic bases: Synthesis, structure and biological studies

Drielly A. Paixão[a], Ivana M. Marzano[b], Edgar H.L. Jaimes[b], Marcos Pivatto[a], Débora L. Campos[c], Fernando R. Pavan[c], Victor M. Deflon[d], Pedro Ivo da S. Maia[e], Ana M. Da Costa Ferreira[f], Isadora A. Uehara[g], Marcelo J.B. Silva[g], Françoise V. Botelho[h], Elene C. Pereira-Maia[b], Silvana Guilardi[a], Wendell Guerra[a,*]

[a] Instituto de Química, Universidade Federal de Uberlândia, Uberlândia, MG, Brazil
[b] Departamento de Química, Universidade Federal de Minas Gerais, Belo Horizonte, MG, Brazil
[c] Faculdade de Ciências Farmacêuticas, UNESP - Universidade Estadual Paulista, Campus Araraquara, 14.800-903 Araraquara, SP, Brazil
[d] Instituto de Química de São Carlos, Universidade de São Paulo, São Carlos, SP, Brazil
[e] Instituto de Ciências Naturais, Exatas e Educação, Universidade Federal do Triângulo Mineiro, Uberaba, MG, Brazil
[f] Instituto de Química, Universidade de São Paulo, São Paulo, SP, Brazil
[g] Instituto de Ciências Biomédicas, Universidade Federal de Uberlândia, Uberlândia, MG, Brazil
[h] Instituto de Genética e Bioquímica, Universidade Federal de Uberlândia, Uberlândia, MG, Brazil

ARTICLE INFO

Keywords:
Copper(II) complexes
Hydrazide
DNA binding
Apoptosis
Antitumoral activity
Mycobacterium tuberculosis

ABSTRACT

Five new copper(II) complexes of the type $[Cu(N{-}O)(N{-}N)(ClO_4)_2]$, in which N−O = 4-fluorophenoxyacetic acid hydrazide (4-FH) or 4-nitrobenzoic hydrazide (4-NH) and N−N = 1,10-phenanthroline (phen), 4–4′-dimethoxy-2-2′-bipyridine (dmb) or 2,2-bipyridine (bipy) were synthesized and characterized using various spectroscopic methods. The X-ray structural analysis of one representative compound indicates that the geometry around the copper ion is distorted octahedron, in which the ion is coordinated to hydrazide *via* the terminal nitrogen and the carbonyl oxygen, and to heterocyclic bases *via* their two nitrogen atoms. Two perchlorate anions occupy the apical positions, completing the coordination sphere. The cytotoxic activity of compounds was investigated in three tumor cell lines (K562, MDA-MB-231 and MCF-7). Concerning K562 cell line, the complexes with 1,10-phenanthroline exhibit high cytotoxic activity and are more active than carboplatin, free ligands and $[Cu(phen)_2]^{2+}$. Considering the cytotoxicity results, further investigations for the compounds $[Cu(4\text{-}FH)(phen)(ClO_4)_2]$ **I** and $[Cu(4\text{-}NH)(phen)(ClO_4)_2]{\cdot}H_2O$ **III** were performed. Flow cytometric analysis revealed that these complexes induce apoptotic cell death in MDA-MB-231 cell line and bind to DNA with K values of 4.38×10^4 and 2.62×10^4, respectively. These compounds were also evaluated against wild type Mycobacterium tuberculosis (ATCC 27294) and exhibited antimycobacterial activity, displayed MIC values lower than those of the corresponding free ligands.

1. Introduction

Nowadays, there is a great interest in the use of copper complexes in cancer chemotherapy, mainly those containing *N,N*-heterocyclic ligands, such as 1,10-phenanthroline, 2,2′-bipyridine, 2,2′:6′,2″-terpyridine, and derivatives, that facilitate intercalation to DNA. After the report that $[Cu(phen)_2]^+$ complex cleaves DNA, a great number of copper complexes with *N,N*-donors ligands have been synthesized and utilized as artificial nucleases [1]. Moreover, many of these copper compounds have been described to inhibit tumoral cell growth [2–14]. Regarding the clinical utility of these complexes, two of them developed by L. Ruiz and co-workers, are already approved for clinical trials as antitumor drugs [15,16].

Our research group has a great interest in the synthesis and biological evaluation of ternary complexes of copper. As a first example, we reported the DNA cleavage ability of two copper(II)-phenanthroline complexes with tetracycline and doxycycline. Both complexes showed an expressive plasmid DNA cleavage activity, under mild reaction conditions, even in the absence of any additional reducing agent, besides inhibited the growth of a chronic myelogenous leukemia cell line [17]. Furthermore, it was reported that UV-light exposure increases the cytotoxic activities of these copper complexes,

* Corresponding author at: Instituto de Química, Universidade Federal de Uberlândia, João Naves de Ávila Avenue, 2121, Campus Santa Mônica, 38.400-902 Uberlândia, MG, Brazil.
E-mail address: wendell.guerra@ufu.br (W. Guerra).

http://dx.doi.org/10.1016/j.jinorgbio.2017.04.024
Received 21 December 2016; Received in revised form 27 March 2017; Accepted 23 April 2017
Available online 26 April 2017
0162-0134/

which makes them potential agents for photodynamic therapy [18]. In other studies, our research group has also shown that copper(II) complexes containing β-diketones and 2,2′-bipyridine or 1,10-phenanthroline are promising antitumoral agents [19,20]. For example, the compound [Cu(L)(phen)NO_3], in which L = 1-(4-chlorophenyl)-4,4,4-trifluoro-1,3-butanedione, inhibits the growth of K562 cells with an IC_{50} value equal to 2.1 μM [19].

Regarding hydrazides and derivatives, it is known that these compounds exhibit a wide variety of biological activities, including antimycobacterial, antifungal, antibacterial, antioxidant, anti-inflammatory, and antitumoral, among others [21]. This class of compounds has the ability to readily coordinate to many transition metals. Therefore, several hydrazide complexes have been synthesized and characterized [22,23]. Some of these compounds exhibit remarkable biological properties, mainly antimycobacterial and antitumoral [24–32]. For instance, the effect of copper(II) complexes containing hydrazides and *N,N*-heterocyclic ligands on the growth of tumor cells was evaluated by our research group. These complexes were able to enter the cells and inhibit cellular growth in a concentration-dependent manner, with an activity higher than that of the corresponding free ligands [31]. Concerning the pharmacological potential of metal-based drugs, this work was, as much as is from our knowledge, the first to describe anticancer properties of copper(II) complexes with hydrazides and 1,10 phenanthroline or derivatives. In addition, more recently, Bortolotto et al. showed that under UV-light exposure, these complexes enhance the DNA cleavage activity [32]. Indeed, these results show clearly that ternary complexes of copper(II) with hydrazides and heterocyclic bases, such as 1,10-phenanthroline, are very promising as anticancer agents. Aiming to continue this work, we describe herein the synthesis of a new series of complexes containing hydrazides and *N,N*-heterocyclic ligands (Fig. 1). The new complexes were characterized by elemental analyses, conductivity measurements, high-resolution electrospray ionization mass spectrometry (HRESIMS), FT-IR, UV–Vis and EPR. Thereafter, DNA interactions, pro-apoptotic properties, cytotoxicity and antitubercular activity of the synthesized compounds were evaluated.

2. Experimental

2.1. Starting materials

The reagents (ligands and metallic salts) are commercially available (Sigma-Aldrich).

2.2. Physical measurements

Conductivity studies were carried out with a Tecnal Tec-4MP conductivity meter using a cell of constant 1.03 cm^{-1}. Spectroscopic grade methanol (Sigma-Aldrich) (Λ_M = 2.13 μs/cm) was used as solvent.

Elemental analyses were performed using a Perkin-Elmer 2400 CHN Elemental Analyzer.

Infrared spectra were obtained on a PerkinElmer Spectrum Two spectrophotometer equipped with an attenuated total reflectance (ATR) sample holder and ZnSe crystal. The spectra were recorded in the range of 4000–600 cm^{-1}.

Diffuse reflectance spectra and UV–Vis were obtained on a Shimadzu UV-2501 PC spectrophotometer.

High-resolution electrospray ionization mass spectra (HRESIMS) were measured on an ultrOTOF (Bruker Daltonics) spectrometer, operating in the positive mode. Methanol was used as solvent system and the samples were infused into the ESI source at a flow rate of 5 μL/min. The calculated values for the charged complex ions were made using ChemDraw Ultra 15.0.

To register EPR spectra of the metal complexes, a Bruker instrument (Karlsruhe, Germany) model EMX was used, operating at X-band (9.50 GHz frequency, 20 mW power, 100 kHz modulation frequency), at 77 K. Samples in solid or as frozen methanol solution were used, in Wilmad quartz tubes, and frequency calibration was provided with DPPH (α,α'-diphenyl-β-picrylhydrazyl; g = 2.0036).

2.3. Crystal structure determination

The data collection was performed at room temperature (296 K) using Mo-Kα radiation (λ = 0.71073 Å) on a BRUKER APEX II Duo diffractometer. Standard procedures were applied for data reduction and absorption correction. The structure was solved with SHELXS97 using direct methods [33] and refined by full-matrix least-square methods against F^2 (SHELXL2014) [34]. All non-hydrogen atoms were refined with anisotropic displacement parameters with SHELXL2014 [34]. The hydrogen atoms were calculated at idealized positions using the riding model option of SHELXL2014 [34]. Crystallographic data, experimental details, data collection and refinement are reported in Table 1.

2.4. Preparation of the complexes

All complexes were prepared by the reaction of $Cu(ClO_4)_2 \cdot 6H_2O$

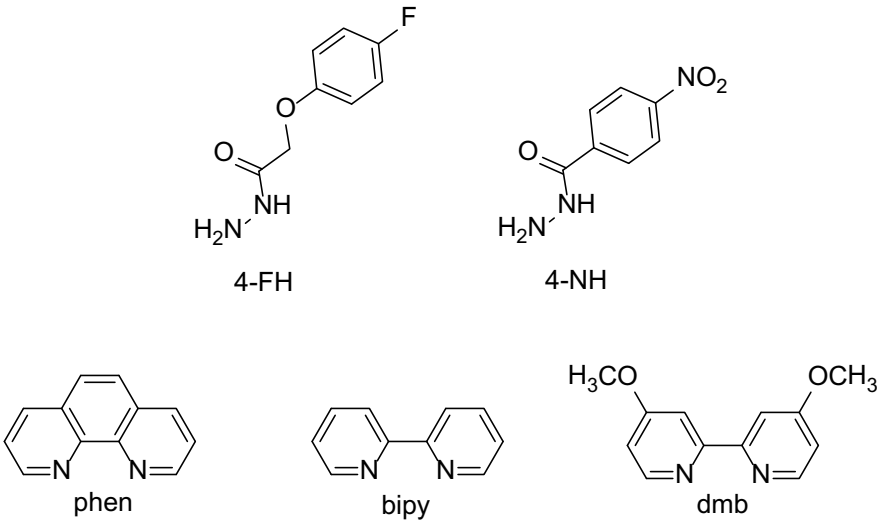

Fig. 1. Organic compounds used as ligands.

Table 1
Crystal data and structure refinement for complex **I**.

Empirical formula	$C_{20}\ H_{17}\ Cl_2\ Cu\ F\ N_4\ O_{10}$
Formula weight	626.82
Temperature	296(2) K
Wavelength	0.71073 Å
Crystal system	Monoclinic
Space group	P 2_1/c
Unit cell dimensions	a = 18.6542(6) Å b = 13.7070(4) Å β = 96.4240(10)° c = 9.2529(3) Å
Volume	2351.05(13) $Å^3$
Z	4
Density (calculated)	1.771 Mg/m^3
Absorption coefficient	1.230 mm^{-1}
F(000)	1268
Crystal size	0.40 × 0.12 × 0.09 mm^3
θ range for data collection	1.098 to 26.394°
Index ranges	−23 < =h < =23, −17 < =k < =17, −11 < =l < =11
Reflections collected	42,766
Independent reflections	4816 [R(int) = 0.0274]
Completeness to theta = 25.242	100.0%
Absorption correction	Multi-scan
Max. and min. Transmission	0.7454 and 0.6596
Refinement method	Full-matrix least-squares on F^2
Data/restraints/parameters	4816/14/381
Goodness-of-fit on F^2	1.043
Final R indices [I > 2sigma (I)]	R_1 = 0.0401, wR_2 = 0.1082
R indices (all data)	R_1 = 0.0473, wR_2 = 0.1138
Extinction coefficient	n/a
Largest diff. Peak and hole	0.687 and −0.547 e.$Å^{-3}$

(0.09 g, 0.25 mmol) with 0.25 mmol of hydrazide dissolved in a minimum amount of methanol. The mixture was stirred for 2 h, followed by the addition of *N,N*-donor heterocyclic ligand (0.25 mmol) previously dissolved in methanol. After 48 h, the compound was filtered, washed with methanol and dried under reduced pressure.

a. $[Cu(4\text{-}FH)(phen)(ClO_4)_2]$ **I.**

M.M.: 626.82 g mol^{-1}. Yield: 75%. Color: Blue. Anal. Calc. for ($CuC_{20}H_{17}FN_4O_{10}Cl_2$): C, 38.32; H, 2.73; N, 8.94%. Found: C, 38.68; H, 2.77; N, 8.90%. (+)-HRESIMS (methanol), *m/z*: 426.0555 [M – $2ClO_4$ – H]$^+$ (calc. For $C_{20}H_{16}CuFN_4O_2$, 426.0548 (Δ 1.6 ppm)). IR (ATR) ν (cm^{-1}): 3262, 3204, 3069, 1661, 1588, 1525, 1511, 1434, 1371, 1250, 1221, 1138, 1100, 1088, 1049, 927, 878, 854, 830, 780, 742, 721, 652, 615. UV–Vis (methanol), λ_{max} (nm) = 293 ($1.1 \times 10^4\ M^{-1}\ cm^{-1}$), 272 ($3.5 \times 10^4\ M^{-1}\ cm^{-1}$), 220 ($3.7 \times 10^4\ M^{-1}\ cm^{-1}$), 640 ($2.9 \times 10^1\ M^{-1}\ cm^{-1}$), 610 (solid). EPR parameters (in methanol frozen solution): $g_\perp$ 2.063; $g_{//}$ 2.255; $A_{//}$ $185 \times 10^{-4}\ cm^{-1}$. Molar conductivity, ΛM (methanol) = 188.45 μS cm^{-1}.

b. $[Cu(4\text{-}FH)(dmb)(ClO_4)_2]\cdot H_2O$ **II**

M.M.: 680.86 g mol^{-1}. Yield: 51%. Color: Blue. Anal. Calc. for ($CuC_{20}H_{23}FN_4O_{13}Cl_2$): C, 35.28; H, 3.40; N, 8.23%. Found: C, 34.85; H, 3.56; N, 7.81%. (+)-HRESIMS (methanol), *m/z*: 462.0760 [M–$2ClO_4$–H]$^+$ (calc. for $C_{20}H_{20}CuFN_4O_4$, 462.0759 (Δ 0.2 ppm)). IR (ATR) ν (cm^{-1}): 3613, 3256, 3094, 2980, 1669, 1614, 1562, 1506, 1476, 1444, 1424, 1370, 1342, 1322, 1288, 1272, 1264, 1251, 1229, 1217, 1087, 1048, 1030, 1010, 970, 920, 889, 859, 832, 778, 742. UV–Vis (methanol), λ_{max} (nm) = 299 ($1.4 \times 10^4\ M^{-1}\ cm^{-1}$), 286 ($1.7 \times 10^4\ M^{-1}\ cm^{-1}$), 277 ($1.8 \times 10^4\ M^{-1}\ cm^{-1}$), 229 ($6.4 \times 10^4\ M^{-1}\ cm^{-1}$), 635 ($2.6 \times 10^1\ M^{-1}\ cm^{-1}$), 607 (solid). EPR parameters (in methanol frozen solution): $g_\perp$ 2.058; $g_{//}$ 2.244; $A_{//}$ $188 \times 10^{-4}\ cm^{-1}$. Molar conductivity, ΛM (methanol) = 176.01 μS cm^{-1}.

c. $[Cu(4\text{-}NH)(phen)(ClO_4)_2]\cdot H_2O$ **III**

M.M.: 641.81 g mol^{-1}. Yield: 54%. Color: Blue. Anal. Calc. for ($CuC_{19}H_{17}N_5O_{12}Cl_2$): C, 35.56; H, 2.67; N, 10.91%. Found: C, 35.95; H, 2.68; N, 10.92%. (+)-HRESIMS (methanol), *m/z*: 423.0399 [M – $2ClO_4$ −H]$^+$ (calc. For $C_{19}H_{14}CuN_5O_3$, 423.0387 (Δ 2.8 ppm)). IR (ATR) ν (cm^{-1}): 3509, 3461, 3236, 3166, 3092, 3070, 2978, 2915, 1653, 1619, 1574, 1522,1493, 1431, 1368, 1350, 1322, 1236, 1160, 1133, 1101, 1088, 1054, 1011, 924, 866, 856, 826, 788, 741, 721, 710. UV–Vis (methanol), λ_{max} (nm) = 293 ($2. \times 10^4\ M^{-1}\ cm^{-1}$), 272 ($5.6 \times 10^4\ M^{-1}\ cm^{-1}$), 224 ($4.8 \times 10^4\ M^{-1}\ cm^{-1}$), 206 ($5.1 \times 10^4\ M^{-1}\ cm^{-1}$), 632 ($3.5 \times 10^1\ M^{-1}\ cm^{-1}$), 608 (solid). EPR parameters (in methanol frozen solution): $g_\perp$ 2.062; $g_{//}$ 2.254; $A_{//}$ $183 \times 10^{-4}\ cm^{-1}$. Molar conductivity, ΛM (methanol) = 168.19 μS cm^{-1}.

d. $[Cu(4\text{-}NH)(bipy)(ClO_4)_2]\cdot H_2O$ **IV**

M.M.: 617.79 g mol^{-1}. Yield: 60%. Color: Blue. Anal. Calc. for ($CuC_{17}H_{17}N_5O_{12}Cl_2$): C, 33.05; H, 2.77; N, 11.34%. Found: C, 33.43; H, 2.68; N, 11.12%. (+)-HRESIMS (methanol), *m/z*: 399.0393 [M – $2ClO_4$ – H]$^+$ (calc. For $C_{17}H_{14}CuN_5O_3$, 399.0387 (Δ 1.5 ppm)). IR (ATR) ν (cm^{-1}): 3534, 3475, 3240, 3172, 3116, 3085, 3038, 2979, 2902, 2858, 1650, 1618, 1610, 1601, 1574, 1522, 1496, 1476, 1448, 1348, 1321, 1249, 1227, 1178, 1127, 1110, 1089, 1056, 1034, 1013, 933, 909, 866, 852, 825, 778, 731, 709, 666. UV–Vis (methanol), λ_{max} (nm) = 310 ($2.4 \times 10^4\ M^{-1}\ cm^{-1}$), 298 ($2.7 \times 10^4\ M^{-1}\ cm^{-1}$), 249 ($3.0 \times 10^4\ M^{-1}\ cm^{-1}$), 206 ($3.4 \times 10^4\ M^{-1}\ cm^{-1}$), 203 ($3.6 \times 10^4\ M^{-1}\ cm^{-1}$), 625 ($1.3 \times 10^1\ M^{-1}\ cm^{-1}$), 605 (solid). Molar conductivity, ΛM (methanol) = 191.75 μS cm^{-1}.

e. $[Cu(4\text{-}NH)(dmb)(ClO_4)_2].H_2O$ **V**

M.M.: 677.84 g mol^{-1}. Yield: 73%. Color: Blue. Anal. Calc. for ($CuC_{19}H_{21}N_5O_{14}Cl_2$): C, 33.67; H, 3.12; N, 10.33%. Found: C, 33.40; H, 2.97; N, 10.00%. (+)-HRESIMS (methanol), *m/z*: 459.0606 [M – $2ClO_4$ – H]$^+$ (calc. for $C_{19}H_{18}CuN_5O_5$, 459.0598 (Δ 1.7 ppm)). IR (ATR) ν (cm^{-1}): 3610, 3257, 3180, 3125, 3090, 2972, 2912, 2848, 1652, 1609, 1573, 1558, 1533, 1499, 1474, 1440, 1417, 1347, 1323, 1283, 1251, 1222, 1128, 1093, 1063, 1044, 1013, 970, 931, 907, 871, 852, 838, 709. UV–Vis (methanol), λ_{max} (nm) = 299 ($2.7 \times 10^4\ M^{-1}\ cm^{-1}$), 287 ($3.2 \times 10^4\ M^{-1}\ cm^{-1}$), 229 ($8.4 \times 10^4\ M^{-1}\ cm^{-1}$), 622 ($7.1\ M^{-1}\ cm^{-1}$), 604 (solid). Molar conductivity, ΛM (methanol) = 214.60 μS cm^{-1}.

2.5. Cells and culture

2.5.1. K562 cells

The K562 cell line was purchased from the Rio de Janeiro Cell Bank (number CR083 of the RJCB collection). This cell line was established from pleural effusion of a 53 year-old female with chronic myelogenous leukemia in terminal blast crisis. Cells were cultured in RPMI 1640 (Sigma Chemical Co.) medium supplemented with 10% fetal calf serum (CULTILAB, São Paulo, Brazil) at 37 °C in a humidified 5% CO_2 atmosphere. Cultures grow exponentially from 10^5 cells mL^{-1} to about 8×10^5 cells mL^{-1} in three days. Cell viability was checked by Trypan Blue exclusion. The cell number was determined by Coulter counter analysis.

For cytotoxicity assessment, 1×10^5 cells mL^{-1} were cultured for 72 h in the absence and presence of a range of concentrations of tested compounds. The sensitivity to compound was evaluated by the concentration that inhibits cell growth by 50% (IC_{50}). Stock solutions were prepared in DMSO and diluted accordingly to obtain the concentrations used in the cytotoxic assays. The final concentration of

DMSO in the experiments was below 0.5% and we have checked that the solvent has no effect in cell growth at this concentration.

2.5.2. Human breast cancer cell lines

The MDA-MB-231 and MCF-7 cell lines were purchased from the Rio de Janeiro Cell Bank. MCF-7 and MDA-MB-231 cells were cultured in DMEM medium supplemented with 10% fetal bovine serum, 100 units/mL penicillin, 100 mg/mL streptomycin, pH 7.4 at 37 °C with 5% CO_2, in humid chamber, to reach ≈80% confluence for assays. Cells detachments for subculture/plating were done with a trypsin/EDTA solution for MCF-7 cells and EDTA solution for MDA-MB-231 cells, for 5 min; trypsin inactivation was carried out with BFS when applied and the cells were washed three times with medium. The cell number was determined by Neubauer chamber Counter analysis.

For cytotoxicity assessment, 5×10^4 cells mL^{-1} were cultured for 36 h in the absence and the presence of a range of concentrations of tested compounds. The sensitivity to compound was evaluated by the concentration that inhibits cell growth by 50% (IC_{50}). Stock solutions of the compounds were prepared in DMSO.

2.5.3. Determination of cell death mode – flow cytometric analysis

The Annexin V/Dead Cell kit utilizes a fluorescent dye conjugated to Annexin-V to detect phosphatidylserine on the external membrane of apoptotic cells and a cell death dye 7-AAD that provides information on the membrane integrity or cell death. 7-AAD is excluded from living healthy cells, as well as early apoptotic cells. By observing the events of graphical plots populations of cells were classified into four distinguished groups: *Viable cells*: Annexin (−) and 7-AAD (−), lower-left quadrant (Q_4); *Early apoptotic cells*: Annexin (+) and 7-AAD (−), lower right quadrant (Q_3); *Late apoptotic cells*: Annexin (+) and 7-AAD (+), upper-right quadrant (Q_2). *Cells that have died through non-apoptotic pathway*: Annexin V (−) and 7-AAD (+), upper-left quadrant (Q_1). MDA-MB-231 cells were seeded in a 24-well culture plate at a density of 3×10^5 cells/well and were cultured overnight in RPMI supplemented with 5% fetal bovine serum. In the next day cells were exposed to 50 μM of the complexes **I** and **III** for 24 h. MDA-MB-231 cells were harvested by trypsinisation and analyzed for the detection of early/late apoptosis and cell death mode using Annexin V/Dead Cell and 7-AAD.

2.6. Anti-Mycobacterium tuberculosis activity assay

The anti-MTB activity of the compounds was determined by the REMA (Resazurin Microtiter Assay) method [35]. Stock solutions of the tested compounds were prepared in DMSO at 10 mg/mL and diluted in Middlebrook 7H9 broth (Difco) supplemented with oleic acid, albumin, dextrose and catalase (OADC), performed by Precision XS (Biotek®) to obtain the final drug concentration range of 0.09–25 μg/mL. Rifampicin was dissolved in DMSO and was used as standard drugs. A suspension of the *M. tuberculosis* H37Rv ATCC 27294 was cultured in Middlebrook 7H9 broth supplemented with OADC and 0.05% Tween 80. When the culture obtained a turbidity of McFarland standard No. 1, it was adjusted by 5×10^5 CFU per mL and 100 μL of the inoculum were added to each well of a 96-well microplate (Kasvi®) together with 100 μL of the compounds. Samples were set up in triplicate. The plates were incubated for 7 days at 37 °C. Resazurin (solubilized in water) was added (30 μL of 0.01%). The fluorescence of the wells was read after 24 h with a Cytation 3 (Biotek®). The MIC was defined as the lowest concentration resulting in 90% inhibition of growth of MTB.

2.7. DNA binding

A Cary100 Varian spectrometer was used for UV and visible absorption measurements. For the interactions with CT DNA, the complex concentration used was 2.5×10^{-5} M and the DNA concentration varied from 0 to 3×10^{-4} M. The DNA concentration per nucleotide was determined by the $\varepsilon = 6600\ M^{-1}\ cm^{-1}$ at 260 nm. The ionic strength was maintained constant with 1×10^{-3} M NaCl and the pH was fixed at 7.3 with 20 mM HEPES buffer. The absorbance of DNA itself was subtracted by adding equal quantity of DNA to both the complex and the reference solutions.

CD spectra were recorded in a Jasco J-815 spectropolarimeter in HEPES buffer (20×10^{-3} M) pH 7.3. DNA concentration was 1×10^{-4} M and complex concentration varied from 0 to 3.2×10^{-5} M. The absorbance of the complexes was subtracted from that of the reaction mixture.

3. Results and discussion

Ternary complexes of copper(II) of the type [Cu(N−O)(N−N)$(ClO_4)_2$], in which N–O = 4-fluorophenoxyacetic acid hydrazide (4-FH) or 4-nitrobenzoic hydrazide (4-NH); N–*N* = 1,10-phenanthroline (phen), 4–4′-dimethoxy-2-2′-bipyridine (dmb) or 2,2-bipyridine (bipy) were synthesized. The complexes were characterized by elemental analyses, conductivity measurements and spectroscopic methods. In addition, complex **I** was analyzed by single crystal X-ray diffraction. All the copper complexes are colorful, non-hygroscopic, stable to air and light and soluble in organic solvents such as methanol, DMSO and acetonitrile.

The results of elemental analyses, which are given in experimental section, are in accordance with the proposed structures. The molar conductance measurements of the complexes were performed in methanol (1×10^{-3} M) at room temperature. The values varied between 168.19 and 214.60 μS cm^{-1}, depending of the complex, which indicates that they are 1:2 electrolytes [31]. The labilization of the axial ligands in solution (perchlorate anions) results in the generation of compounds of type $[Cu(N{-}O)(N{-}N)]^{2+}$ [17,19].

The high-resolution mass spectra of the copper complexes were recorded. The water molecules present in the molecular structures of **II–V** were dissociated from the complexes in the ionization process. The *m/z* values listed in the experimental section refer to the peak containing the most abundant isotope (^{63}Cu). For instance, mass spectrum of the complex **V** exhibited the charged ion at *m/z* 459.0606 $[M–2ClO_4–H]^+$ that was close to the calculated value for $C_{19}H_{18}CuN_5O_5$, 459.0598 (Δ 1.7 ppm), and represents the pattern observed for all compounds (Fig. 2) [36].

In the IR spectra of the complexes **II–V**, a broad band at 3550 cm^{-1} indicates the presence of one water molecule. For all complexes, a group of bands between 2900 and 3080 cm^{-1} corresponds to the νC–H stretching vibration. Two intense bands between 1085 and 1045 cm^{-1} are attributable to the presence of two unidentate perchlorate ions [37]. Hydrazides show characteristic absorptions between 3332 and 3150 cm^{-1} which are attributable to the NH_2 and NH groups [22,23]. In all complexes studied, the bands originating from NH_2 group showed considerable shift as compared to the free ligands. An absorption assigned to νC═O around 1666–1645 cm^{-1} corroborates with the proposed structures.

Electronic absorption spectra of all compounds were performed in methanol (10^{-5} M). A red shift in relation to free ligands confirms the presence of the complexes in solution [31]. The complexes possess only one broad and asymmetric d-d band centered at ≈630 nm. For example, the complex **IV** exhibits a d-d band centered at 625 nm ($\varepsilon = 13\ M^{-1}\ cm^{-1}$). These observations are consistent with a distortion from the octahedron geometry due to the Jahn-Teller effect [19]. In the solid state, all complexes exhibit the same d-d band centered at ≈608 nm, indicating that the geometry of the complexes in solution differs from that in solid state [19,20]. Moreover, in the solid state, the complexes exhibited a new band (CT) around 480 nm.

From EPR data, the corresponding parameters were determined for the studied copper(II) complexes (Table 2). The obtained values were very close, indicating a tetragonal arrangement of the ligands around the copper center, with a small tetrahedral distortion, as estimated by the empirical ratio $g_{//}/A_{//}$ [31], around 120 cm. In the solid state, all

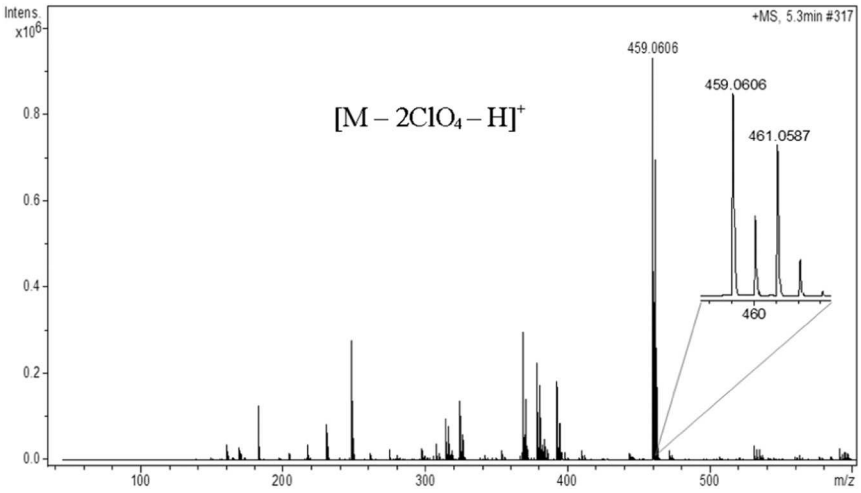

Fig. 2. (+)-HRESI-MS spectrum of complex **V** (charged complex ion observed was $[M - 2ClO_4 - H]^+$).

Table 2
EPR parameters for copper(II) complexes in solid state and in methanol frozen solution, at 77 K.

Complex	g_{iso} [#]	$g_{\perp}$	$g_{//}$	$A_{//}$ (G)	$A_{//}$ (10^{-4} cm^{-1})[§]	$g_{//}$ /$A_{//}$ (cm)
I	2.065	2.063	2.255	176	185	122
II	2.065	2.058	2.244	179	188	119
III	2.071	2.062	2.254	174	183	123

[#] In solid state.
[§] $\mathbf{A}_{//}$ (in 10^{-4} cm^{-1}) = $g_{//}$ β $A_{//}$ (in G) = 0.46686 × 10^{-4} $g_{//}$ $A_{//}$ (in G); where β = 1.39969 MHz/G.

the compounds exhibited only an isotropic g_{iso} value, 2.065 to 2.071.

3.1. Crystal structure

Blue crystals suitable for single crystal X-ray diffraction were obtained for complex **I** after slow evaporation of a methanol/toluene solution at room temperature. The crystals thereby formed were collected, washed with water and dried under reduced pressure. Single crystal X-ray analysis demonstrates that complex **I** crystallizes in the monoclinic system, space group $P2_1/c$. Fig. 3 illustrates the molecular structure of the complex **I** along with atomic labeling scheme. As it can be seen, the complex **I** exhibits a distorted octahedral geometry around Cu(II) ion, in which the ligands are coordinated in a bidentate mode. The equatorial site is occupied by two nitrogen atoms from phen (N3 and N4) and two atoms from 4-FH ligand (O1 and N2). The apical sites are occupied by two oxygen atoms (O3a and O10a) from two perchlorates weakly bonded [31]. The perchlorate anions are disordered over two sites. The solid lines (labeled a) indicate the bonds between the atoms with higher occupation factor (54.7%), whereas the dashed lines (labeled b) represent the species with the lower occupation (45.3%). Selected bond lengths and angles are reported in Table 3.

The Cu1—O bond lengths from the disordered perchlorate ions range from 2.4 to 2.8 Å. These values are considerably longer than the Cu1—O distance in the basal plane. This elongation can be explained by the Jahn-Teller effect [19]. The Cu1—N_{phen} (1.994(2) and 1.976(2)Å), Cu1—N2 (2.025(2) Å) and Cu1—O1 (1.970(2) Å) bond distances are normal and are comparable to those found for the related copper(II) complexes [31,38–41].

The basal geometry is considerably distorted from the perfect square-plane owing to the bite angle of the chelating phen ligand (83.23(9)°). The *trans* angles are 173.20(9)° and 174.52(9)°. The values of bond lengths and angles are within the values expected for this class of compounds [31,38]. The bidentate chelation to the copper(II) ion by the ligands lead to the formation of two 5-membered planar rings and the root mean square (r.m.s) deviation to the fitted atoms is 0.0154 and 0.0124 Å. The angle between the mean planes formed by these rings is 7.27(13)°. The copper atom is in the equatorial plane and the r.m.s deviations of the five fitted atoms in the CuN3O plane are 0.0368 Å. The phen ligand is approximately planar and the r.m.s deviations to the fitted non-hydrogen atoms are 0.0251 Å. The copper ion is displaced about 0.050 Å in relation to this plane.

The crystal structure is stabilized by hydrogen bonds (listed in Table 4) and weak π–π stacking interactions. Intramolecular hydrogen bonds could be observed between the donor atoms of the 4-FH ligand and the oxygen atoms of the perchlorate groups (N2⋯O8a = 2.987(8)

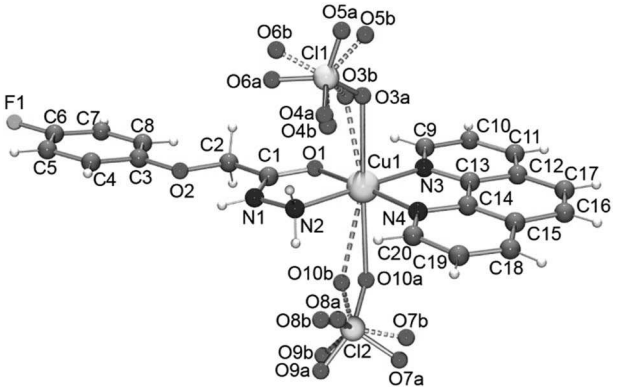

Fig. 3. Molecular structure of the complex $[Cu(4\text{-FH})(phen)(ClO_4)_2]$ **I** showing oxygen atoms from the perchlorate disordered over two sites. Major component (solid lines) with 54.7% occupation and minor component (dashed lines) with 45.3% occupation.

Table 3
Select bond lengths [Å] and angles [°] for complex **I**.

Cu1—O1	1.970(2)
Cu1—N2	2.025(2)
Cu1—N3	1.976(2)
Cu1—N4	1.994(2)
Cu1—O3a	2.489(7)
Cu1—O3b	2.412(10)
Cu1—O10a	2.601(7)
Cu1—O10b	2.769(7)
N3—Cu1—N4	83.23(9)
O1—Cu1—N2	82.49(8)
N4—Cu1—N2	100.89(9)
O1—Cu1—N3	93.04(8)
O1—Cu1—N4	173.20(9)
N3—Cu1—N2	174.52(9)

Table 4
Hydrogen bonds for complex **I** [Å and °].

D—H···A	d(D—H)	d(H···A)	d(D···A)	< (DHA)
N1—H1···O8a$^{\#1}$	0.86	2.38	2.846(7)	114.3
N1—H1···O9a$^{\#1}$	0.86	2.38	3.212(11)	163.7
N1—H1···O8b$^{\#1}$	0.86	2.14	2.723(8)	124.9
N2—H2a···O8a	0.89	2.18	2.987(8)	150.2
N2—H2a···O8b	0.89	2.07	2.881(9)	151.5
N2—H2b···O4a	0.89	2.40	3.164(12)	143.8
N2—H2b···O4b	0.89	2.20	2.955(12)	141.7

Symmetry transformations used to generate equivalent atoms: #1 x, − y + 1/2, z-1/2.

Å and N2···O4a = 3.164(12) Å) as illustrated in Fig. S1 (Supplementary Material). The N1 nitrogen atom of the 4-FH ligand is a proton donor in two hydrogen bonds of the type N—H···O, involving the O8 and O9 oxygen atoms from perchlorate groups, resulting in chains that extend along [001] direction as depicted in Fig. S2 (Supplementary Material). Using complete graph-set analysis [42] to describe patterns in the hydrogen-bond network, we find $C_1^2(7)[R_1^2(4)]$. These chains connect into a three-dimensional architecture by π–π stacking interactions among the phen moieties belonging to adjoining layers with centroid–centroid (Cg1–Cg2) distance of 3.770(1) Å for Cg1 (generated by the ring C9/C10/C11/C12/C13/N3) and Cg2 (generated by ring C12–C17) (Fig. S3, Supplementary Material).

3.2. Behavior in aqueous solution

The complexes were evaluated by UV–Vis spectroscopy at different times in a mixture containing H_2O/DMSO 0.1%. The values of absorbance and wavelength were not affected, even after 6 h. These results indicate that the species $[Cu(N—O)(N—N)]^{2+}$ remain intact in solution under the test conditions [19]. The spectra of a representative complex are reported in the Fig. 4.

3.3. Cytotoxic studies and determination of cell death mode

The cytotoxic activity of complexes is depicted in Table 5. IC_{50} values obtained for the free ligands, carboplatin and for the complex $[Cu(phen)_2](ClO_4)_2$ are also shown for the sake of comparison.

Concerning K562 cell line, phen and 4-NH exhibit high activity. However, for the phenanthroline and its derivatives, it is assumed that the sequestering of trace metals *in situ* is involved and that the resulting metallic complexes are the active species [43]. The organic compounds bipy and dmb display moderate activity. In turn, the copper complexes inhibit the growth of K562 cells with IC_{50} values between 1.6 and 28 μM. As can be seen in the Table 5, the order of cytotoxic activity is: **III** > **I** > **V** > **II** > **IV**. The copper complexes with 1,10-phenanthroline (phen) are more active than those with 4–4′-dimethoxy-2-2′-bipyridine (dmb) and 2,2-bipyridine (bipy). In the literature, several studies have shown that copper(II) complexes with phenanthroline are more reactive than similar ones with bipyridine ligands [17,31,44]. An accepted explanation for this order of reactivity is that the planar polycyclic phen ring interacts better with DNA [45]. The cytotoxic activity of complexes **I** and **III** is higher than the activity of all corresponding free ligands, carboplatin and $[Cu(Phen)_2]^{2+}$, a complex known by its nuclease action [31]. The complexes **II**, **IV** and **V** exhibit moderate to good activity against K562 cell line.

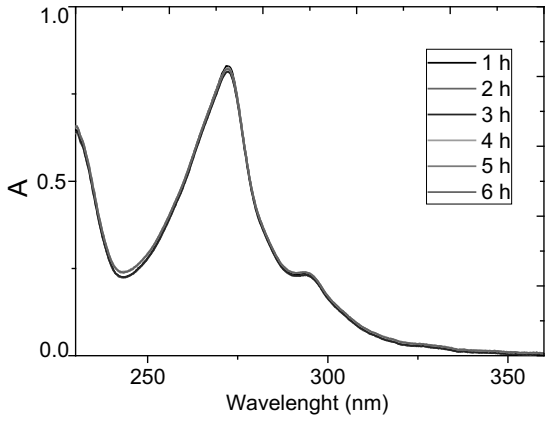

Fig. 4. Ultraviolet spectra of complex **I** as a function of time.

Table 5
IC_{50} (μM) values for ligands, complexes, $[Cu(phen)_2](ClO_4)_2$ and carboplatin.[a]

Compound	K562 (72 h)	MDA-MB-231 (36 h)	MCF-7 (36 h)
4-FH	> 100	> 100	> 100
4-NH	10.5	> 100	> 100
dmb	23.5	–	–
bipy	30.0	–	–
phen	3.2	> 100	> 100
$[Cu(4\text{-}FH)(phen)(ClO_4)_2]$ **I**	1.8	8.8	6.5
$[Cu(4\text{-}FH)(dmb)(ClO_4)_2].H_2O$ **II**	26.2	–	–
$[Cu(4\text{-}NH)(phen)(ClO_4)_2].H_2O$ **III**	1.6	5.5	4.6
$[Cu(4\text{-}NH)(bipy)(ClO_4)_2].H_2O$ **IV**	28.0	–	–
$[Cu(4\text{-}NH)(dmb)(ClO_4)_2].H_2O$ **V**	15.0	–	–
$[Cu(phen)_2](ClO_4)_2$	3.4	–	–
Carboplatin	10.0	> 100	> 100

[a] IC_{50} is the concentration required to inhibit 50% of K562 cell growth.

As it can be seen in Table 5, the complexes **I** and **III** were also very active against MDA-MB-231 and MCF-7 cells. It is worth noting that the free ligands and carboplatin exhibit IC_{50} values > 100 μM against MDA-MB-231 and MCF-7 cells. In general, the cytotoxic activity of these compounds is similar to copper complexes with *N,N*-donor heterocyclic ligands already described [46–51,17,31], although, the mode of action can be quite different [19].

We have used flow cytometric analysis to determine whether the selected complexes **I** and **III** (50 μM) are able to induce apoptosis. In accordance with our results, after 24 h incubation, the copper complexes **I** and **III** induce late apoptosis in MDA-MB-231 cell line (Fig. 5). Several copper(II) complexes were reported in literature by induce apoptosis, a form of programmed cell death that occurs in tumor cells as response to some anticancer agents [52–54].

3.4. DNA binding

We have registered the spectra of solutions of the complexes in the absence and in the presence of increasing concentrations of CT DNA. The addition of DNA induces a hypochromic effect and a minor batochromic shift, indicating that both complexes interact with calf thymus DNA. A representative experiment obtained with complexes **I** and **III** at 2.5×10^{-5} M and DNA concentration ranging from 0 a 3×10^{-4} M is shown in Figs. 6 and 7, respectively. In order to evaluate the binding strengths of the complexes, the binding constant, K, was calculated accordingly to the equation.

$$[DNA] / (\varepsilon_a - \varepsilon_f) = [DNA] / (\varepsilon_0 - \varepsilon_f) + 1/K(\varepsilon_0 - \varepsilon_f).$$

in which, [DNA] is the concentration of DNA in base pairs, ε_a is the ratio of the absorbance/[Cu], ε_f is the extinction coefficient of the free Cu^{II} complex and ε_0 is the extinction coefficient of the complex in the fully bound form. The ratio of slope to intercept in the plot of [DNA]/($\varepsilon_a - \varepsilon_f$) *versus* [DNA] gives the value of K (Figs. 6 and 7). The affinity of complex **I** to DNA is slightly higher than that complex **III** with K values of 4.38×10^4 and 2.62×10^4, respectively.

The high sensitivity of circular dichroism (CD) to conformational aspects makes this technique suitable to follow changes in DNA

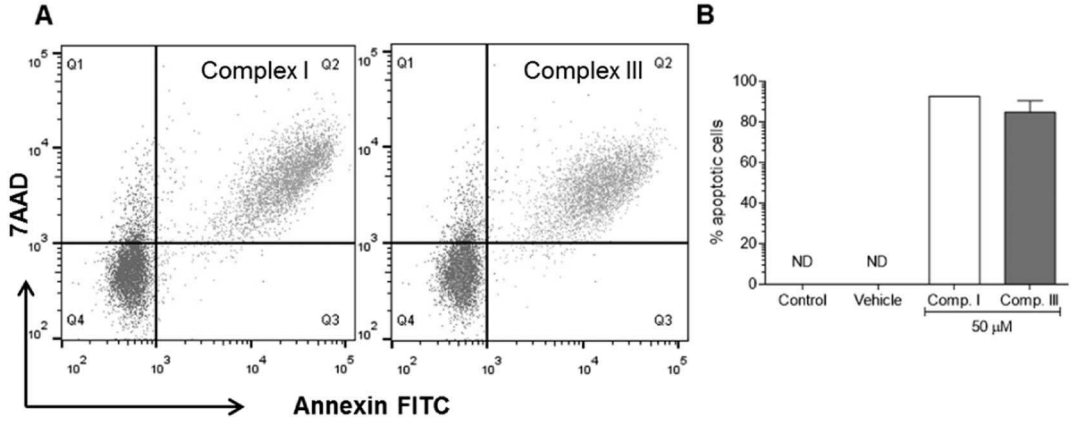

Fig. 5. Representative flow cytometry plots of MDA-MB-231 cell treated with complexes **I** and **III**.

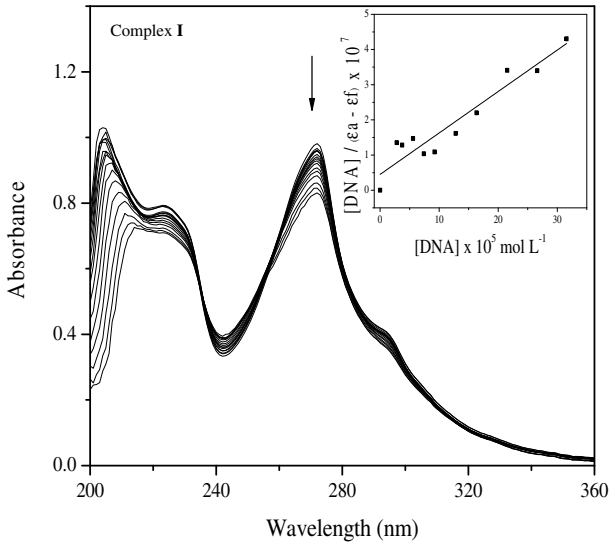

Fig. 6. Spectra of solutions containing complex **I** (2.5×10^{-5} M) and increasing concentrations of DNA in HEPES buffer pH 7.3. [DNA]: [complex **I**] ranging from 0 to 12. Inset: [DNA]/(εa - εf) *versus* [DNA].

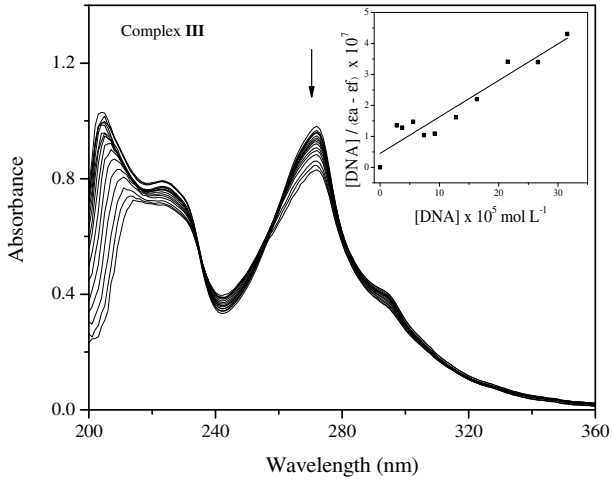

Fig. 7. Spectra of solutions containing complex **III** (2.5×10^{-5} M) and increasing concentrations of DNA in HEPES buffer pH 7.3. [DNA]: [complex **III**] ranging from 0 to 12. Inset: [DNA]/(εa - εf) *versus* [DNA].

morphology caused by interactions with drugs or small molecules. The CD spectrum of the free DNA is composed of a positive band at 275 nm, due to base stacking, and a negative one at 245 nm, due to the right-handed helicity of B-DNA [55–56]. By adding aliquots of **I** and **III** in the DNA solution the intensity of DNA bands increase (Fig. S4). This behavior is usually observed upon drug intercalation, since it enhances the base stacking and stabilizes helicity, and thus increases intensities of the bands, whereas simple groove binding and electrostatic interaction of small molecules show less or no perturbation on the base stacking and helicity bands [55–56].

3.5. Anti-M. tuberculosis activity

The antimycobacterial activity of compounds **I** and **III** were evaluated *in vitro* against MTB H37Rv (ATCC 27294) strain by the REMA method. The minimum inhibitory concentrations (MICs) found for the complexes, free ligands and rifampicin (standard drug) are shown in Table 6. The complexes **I** and **III** exhibited activity against the MTB with MIC values equal to 6.3 and 6.5 μg/mL, respectively. It is worth noting that the novel complexes possess MIC (μM) values lower than those of the corresponding free ligands. Moreover, compared to similar compounds containing aromatic diimine ligands (N—N) already described, they are among the most active [57–59]. Whereas compounds with anti-MTB activity at ≤ 10 μg/mL (or molar equivalent) are selected for subsequent tests [60], these results show that copper complexes containing hydrazides and *N,N*-donor ligands are promising agents against MTB.

4. Concluding remarks

Five new copper complexes containing hydrazides and *N,N*-donor heterocyclic ligands were prepared and characterized. The X-ray structural analysis of one representative compound indicates that the geometry around the copper ion is octahedral distorted, in which both the ligands are coordinated in a bidentate mode, (N—O) and (N—N). EPR parameters determined for the all series of complexes corroborated these data, attesting a tetragonal geometry around the copper ion in solution. The obtained results of cytotoxicity activity of the synthesized compounds are very promising, especially in the case of copper

Table 6
Anti-MTB activity (MIC) of **I**, **III**, free ligands and rifampicin.

Compound	MIC_{90} μg/mL	MIC_{90} μM
phen	2.3	12.7
4-FH	> 25	–
4-NH	> 25	–
$[Cu(4\text{-}FH)(phen)(ClO_4)_2]$ **I**	6.3	10.0
$[Cu(4\text{-}NH)(phen)(ClO_4)_2].H_2O$ **III**	6.5	10.1
Rifampicin (standard drug)	0.02	0.03

complexes with phenanthroline, with IC_{50} values in the range of a few μM. Also, the coordination to the metal ion ameliorates the ligand activity. Regarding its antitubercular activity, they are among the most active in comparison to similar compounds, with MIC ≤ 10 μg/mL. These findings are noteworthy and motivate further studies with such compounds.

Abbreviations

Phen	1,10-phenanthroline
bipy	2,2′-bipyridine
dmb	4–4′-dimethoxy-2-2′-bipyridine
DNA	Deoxyribonucleic acid
CT DNA	calf-thymus DNA
UV–Vis	ultraviolet-visible
IR	infrared
EPR	electron paramagnetic resonance
CD	circular dichroism
DMSO	dimethyl sulfoxide
K562	chronic myelogenous leukemia
MCF-7	breast adenocarcinoma
MDA-MB-231	human breast adenocarcinoma
IC_{50}	concentration required to inhibit 50% of cell growth
MIC	minimum inhibitory concentration
MTB	Mycobacterium tuberculosis
CT	charge transfer

Acknowledgements

To CNPq (Conselho Nacional de Desenvolvimento Científico e Tecnológico, Brazil) (442328/2014-1), CAPES (Coordenação de Aperfeiçoamento de Pessoal de Nível Superior, Brazil), and FAPEMIG (Fundação de Amparo à Pesquisa de Minas Gerais, Brazil) (APQ-00668-15) by financial support and fellowships. The authors are also thankful to the Grupo de Materiais Inorgânicos do Triângulo - GMIT research group supported by FAPEMIG (APQ-00330-14). This work is a collaboration research project of members of the Rede Mineira de Química (RQ-MG) supported by FAPEMIG (Project: CEX - RED-00010-14).

Appendix A. Supplementary data

CCDC 1499893 contains the supplementary crystallographic data for the complex **I**. These data can be obtained free of charge *via* http://www.ccdc.cam.ac.uk/conts/retrieving.html, or from the Cambridge Crystallographic Data Centre, 12 Union Road, Cambridge CB2 1EZ, UK; fax: (+44) 1223-336-033; or e-mail: deposit@ccdc.cam.ac.uk. Supplementary data associated with this article can be found in the online version, at http://dx.doi.org/10.1016/j.jinorgbio.2017.04.024.

References

[1] M. Chikira, C. Hee Ng, M. Palaniandavar, Int. J. Mol. Sci. 16 (2015) 22754–22780.
[2] P. Ruíz, R. Ortiz, L. Perelló, G. Alzuet, M. González-Álvarez, M. Liu-González, F. Sanz-Ruíz, J. Inorg. Biochem. 101 (2007) 831–840.
[3] P.R. Reddy, A. Shilpa, N. Raju, P. Raghavaiah, J. Inorg. Biochem. 105 (2011) 1603–1612.
[4] A.K. Patra, S. Roy, A.R. Chakravarty, Inorg. Chim. Acta 362 (2009) 1591–1599.
[5] I. Correia, S. Roy, C.P. Matos, S. Borovic, N. Butenko, I. Cavaco, F. Marques, J. Lorenzo, A. Rodríguez, V. Moreno, J.C. Pessoa, J. Inorg. Biochem. 147 (2015) 134–146.
[6] A.M. Thomas, A.D. Naik, M. Nethaji, A.R. Chakravarty Inorg, Chim. Acta 357 (2004) 2315–2323.
[7] C. Marzano, M. Pellei, F. Tisato, C. Santini, Anti Cancer Agents Med. Chem. 9 (2009) 185–211.
[8] C. Santini, M. Pellei, V. Gandin, M. Porchia, F. Tisato, C. Marzano, Chem. Rev. 114 (2014) 815–862.
[9] J.L. García-Giménez, M. González-Álvarez, M. Liu-González, B. Macías, J. Borrás, G. Alzuet, J. Inorg. Biochem. 103 (2009) 923–934.
[10] T. Kiran, V.G. Prasanth, M.M. Balamurali, C.S. Vasavi, P. Munusami, K.L. Sathiyanarayanan, M. Pathak, Inorg. Chimica Acta 433 (2015) 26–34.
[11] T. Ma, J. Xu, Yuan Wang, H. Yu, Y. Yang, Y. Liu, W. Ding, W. Zhu, R. Chen, Z. Ge, Y. Tan, L. Jia, T. Zhu, J. Inorg. Biochem. 144 (2015) 38–46.
[12] P. Gurumoorthy, D. Mahendiran, D. Prabhu, C. Arulvasu, A.K. Rahiman, J. Mol. Struct. 1080 (2015) 88–98.
[13] S. Abdolmaleki, M. Ghadermazi, A. Fattahi, S. Sheshmani, Inorg. Chimica Acta 443 (2016) 284–298.
[14] I. Castillo, M. Suwalsky, M.J. Gallardo, V. Troncoso, B.N. Sánchez-Eguía, E. Santiago-Osorio, I. Aguiñiga, A.K. González-Ugarte, J. Inorg. Biochem. 156 (2016) 98–104.
[15] J. Serment-Guerrero, P. Cano-Sanchez, E. Reyes-Perez, F. Velazquez-Garcia, M. Bravo-Gomez, L. Ruiz-Azuara, Toxicol. in Vitro 25 (2011) 1376–1384.
[16] S. Iglesias, N. Alvarez, M.H. Torre, E. Kremer, J. Ellena, R.R. Ribeiro, R.P. Barroso, A.J. Costa-Filho, M.G. Kramer, G. Facchin, J. Inorg. Biochem. 139 (2014) 117–123.
[17] P.P. Silva, W. Guerra, J.N. Silveira, A.M. Da Costa Ferreira, T. Bortolotto, F.L. Fischer, H. Terenzi, A. Neves, E.C. Pereira-Maia, Inorg. Chem. 50 (2011) 6414–6424.
[18] T. Bortolotto, P.P. Silva, A. Neves, E.C. Pereira-Maia, H. Terenzi, Inorg. Chem. 50 (2011) 10519–10521.
[19] J.C. Almeida, D.A. Paixão, I.M. Marzano, J. Ellena, M. Pivatto, N.P. Lopes, A.M. Da Costa Ferreira, E.C. Pereira-Maia, S. Guilardi, W. Guerra, Polyhedron 89 (2015) 1–8.
[20] P.S. Lopes, D.A. Paixão, F.C.S. de Paula, A.M. Da Costa Ferreira, J. Ellena, S. Guilardi, E.C. Pereira-Maia, W. Guerra, J. Mol. Struct. 1034 (2013) 84–88.
[21] S. Rollas, Ş.G. Küçükgüzel, Molecules 12 (2007) 1910–1939.
[22] L.M. Sousa, P.P. Corbi, A.L.B. Formiga, Marcelo Lancellotti, I.M. Marzano, E.C. Pereira-Maia, G. Von Poelhsitz, W. Guerra, J. Mol. Struct. 1097 (2015) 15–22.
[23] M.A. Rodrigues, I.M. Marzano, G.H. Ribeiro, L. Colina-Vegas, M. Pivatto, A.P.S. Fontes, C.M. Ribeiro, F.R. Pavan, K.J. Almeida, A.A. Batista, E.C. Pereira-Maia, W. Guerra, Polyhedron 98 (2015) 146–153.
[24] E.H.S. Sousa, F.G.M. Vieira, J.S. Butler, L.A. Basso, D.S. Santiago, I.C.N. Diógenes, L.G.F. Lopes, P.J. Sadler, J. Inorg. Biochem. 140 (2014) 236–244.
[25] E.H.S. Sousa, L.A. Basso, D.S. Santos, I.C.N. Diógenes, E. Longhinotti, L.G.F. Lopes, I.S. Moreira, J. Biol. Inorg. Chem. 17 (2012) 275–283.
[26] S.A. Galal, K.H. Hegab, A.S. Kassab, M.L. Rodriguez, S.M. Kerwin, A. Abdel-Mo'men, El-Khamry, H.I. El Diwani, Eur. J. Med. Chem. 44 (2009) 1500–1508.
[27] V. Mahalingam, N. Chitrapriya, M. Zeller, K. Natarajan, Polyhedron 28 (2009) 1532–1540.
[28] P. Sur, S.P. Chatterjee, P. Roy, B. Sur, Cancer Lett. 94 (1995) 27–32.
[29] G.D. de Souza, M. A, L.E. Fernandes, P.P. Silva, R. Ruggiero, E.C. Pereira-Maia, W. Guerra, Cent. Eur. J. Chem. 11 (2013) 290–294.
[30] N. Dodoff, K. Granharov, N. Spassovska, J. Inorg. Biochem. 60 (1995) 257–266.
[31] P.P. Silva, W. Guerra, G.C. dos Santos, N.G. Fernandes, J.N. Silveira, A.M. da Costa Ferreira, T. Bortolotto, H. Terenzi, A.J. Bortoluzzi, A. Neves, E.C. Pereira-Maia, J. Inorg. Biochem. 132 (2014) 67–76.
[32] T. Bortolotto, P.P. Silva-Caldeira, C.T. Pich, E.C. Pereira-Maia, H. Terenzi, Chem. Commun. 52 (2016) 7130–7133.
[33] G.M. Sheldrick, SHELXS97, Program for the Solution of Crystal Structures, University of Göttingen, Germany, 1997.
[34] G.M. Sheldrick, SHELXL2014.
[35] J.C. Palomino, A. Martin, M. Camacho, H. Guerra, J. Swings, F. Portaels, Antimicrob. Agents Chemother. 46 (2002) 2720–2722.
[36] K. Shin-Geol Kang, Ryu, Soo-Kyung Jung, Shang-Su Kim, Bull. Kor. Chem. Soc. 17 (1996) 331–334.
[37] S. Dey, T. Mukherjee, S. Sarkar, H.S. Evans, P. Chattopadhyay, Transit. Met. Chem. 36 (2011) 631–636.
[38] K. Kaabi, M. El Glaoui, M. Zeller, C.B. Nasr, Acta Cryst E66 (2010) m1145–m1146.
[39] T. Pivetta, F. Trudua, E. Valletta, F. Isaia, C. Castellano, F. Demartin, R. Tuveri, S. Vascellari, *A. pani.* J. Inorg. Biochem. 141 (2014) 103–113.
[40] X. Li, Z. Zhang, C. Wang, T. Zhang, K. He, F. Deng. J. Inorg. Biochem. 105 (2011) 23–30.
[41] G.A. Van Albada, I. Dominicus, I. Mutikainen, U. Turpeinen, J. Reedijk. Polyhedron 26 (2007) 3731–3736.
[42] M.C. Etter, J.C. MacDonald, J. Bernstein, Acta Cryst B46 (1990) 256–262.
[43] M. McCann, A.L.S. Santos, B.A. da Silva, M.T.V. Romanos, A.S. Pyrrho, M. Devereux, K. Kavanagh, I. Fichtner, A. Kellet, Toxicol. Res. 1 (2012) 47–54.
[44] C. Santini, M. Pellei, V. Gandin, M. Porchia, F. Tisato, C. Marzano, Chem. Rev. 114 (2014) 815–862.
[45] M. Bravo-Gomez, J.C. Garcia-Ramos, I. Gracia-Mora, L. Ruiz-Azuara, J. Inorg. Biochem. 103 (2009) 299–309.
[46] D. İnci, R. Aydın, Ö. Vatan, T. Sevgi, D. Yılmaz, Y. Zorlu, Y. Yerli, B. Çoşut, E. Demirkan, N. Çinkılıç, J. Biol. Inorg. Chem. 22 (2017) 61–85.
[47] A. Marín-Hernandez, I. Gracia-Mora, L. Ruiz-Ramírez, R. Moreno-Sanchez, Biochem. Pharmacol. 65 (2003) 1979–1989.
[48] R. Singh, R.N. Jadeja, M.C. Thounaojam, T. Patel, R.V. Devkar, D. Chakraborty, Inorg. Chem. Commun. 23 (2012) 78–84.
[49] S. Patitungkho, S. Adsule, P. Dandawate, S. Padhye, A. Ahmad, F.H. Sarkar, Bioorg. Med. Chem. Lett. 21 (2011) 1802–1806.
[50] K.M. Vyas, R.N. Jadeja, D. Patel, R.V. Devkar, V.K. Gupta, Polyhedron 80 (2014) 20–33.
[51] E.K. Efthimiadou, H. Thomadaki, Y. Sanakis, C.P. Raptopoulou, N. Katsaros, A. Scorilas, A. Karaliota, G. Psomas, J. Inorg. Biochem. 101 (2007) 64–73.
[52] C. Fernandes, A. Horn Jr., B.F. Lopes, E.S. Bull, N.F.B. Azeredo, M.M. Kanashiro, F.V. Borges, A.J. Bortoluzzi, B. Szpoganicz, A.B. Pires, R.W.A. Franco, J.C. de Almeida, L.L.F. Maciel, J.A.L.C. Resende, G. Schenk, J. Inorg. Biochem. 153 (2015) 68–87.
[53] K.G. Daniela, P. Gupta, R.H. Harbach, W.C. Guida, Q.P. Dou, Biochem. Pharmacol.

67 (2004) 1139–1151.
[54] Xue-Quan Zhou, Y. Li, Dong-Yan Zhang, Y. Nie, Zong-Jin Li, W. Gu, X. Liu, Jin-Lei Tian, Shi-Ping Yan, Eur. J. Med. Chem. 114 (2016) 244–256.
[55] Ferenc Zsila, Int. J. Biol. Macromol. 72 (2015) 1034–1040.
[56] M. Sinan, M. Panda, A. Ghosh, K. Dhara, P.E. Fanwick, D.J. Chattopadhyay, S. Goswami, J. Am. Chem. Soc. 130 (2008) 5185–5193.
[57] H.R. Dholariya, K.S. Patel, J.C. Patel, K.D. Pate, Spectrochim. Acta A Mol. Biomol. Spectrosc. 108 (2013) 319–328.
[58] A.E. Hoffman, M. DeStefano, C. Shoen, K. Gopinath, D.F. Warner, M. Cynamon, R.P. Doylea, Eur. J. Med. Chem. 70 (2013) 589–593.
[59] J.C. Almeida, I.M. Marzano, M. Pivatto, N.P. Lopes, A.M. Da Costa Ferreira, F.R. Pavan, I.C. Silva, E.C. Pereira-Maia, G. Von Poelhsitz, W. Guerra, Inorg. Chim. Acta 446 (2016) 87–92.
[60] F.R. Pavan, D.N. Sato, C. Q., F. Leite, An approach to the search for new drugs against tuberculosis, in: P.-J. Cardona (Ed.), Mycobacterium tuberculosis/book 2, Intech, 2011.